

See discussions, stats, and author profiles for this publication at: <https://www.researchgate.net/publication/326894093>

Compact and microchannel heat exchangers: A comprehensive review of air-side friction factor and heat transfer correlations

Article in Energy Conversion and Management · October 2018

DOI: 10.1016/j.enconman.2018.06.104

CITATIONS

60

READS

3,585

2 authors:



Naef A.A. Qasem

King Fahd University of Petroleum and Minerals

94 PUBLICATIONS 2,200 CITATIONS

[SEE PROFILE](#)



Syed M. Zubair

King Fahd University of Petroleum and Minerals

347 PUBLICATIONS 11,473 CITATIONS

[SEE PROFILE](#)

Some of the authors of this publication are also working on these related projects:



Heat transfer and solid mechanics [View project](#)



NF-RO hybrid system... a preliminary step towards ZLD [View project](#)

Energy Conversion and Management

Volume 173, 1 October 2018, Pages 555-601
<https://doi.org/10.1016/j.enconman.2018.06.104>

Compact and microchannel heat exchangers: A comprehensive review of air-side friction factor and heat transfer correlations

Naef A. A. Qasem, and Syed M. Zubair*

Mechanical Engineering Department, KFUPM Box# 1474

King Fahd University of Petroleum & Minerals

Dhahran 31261, Saudi Arabia

Abstract

This review focuses on the thermal-hydraulic performance correlations for the air-side of the compact and microchannel heat exchangers. These correlations are presented in tables, mainly in terms of Colburn j -factor and fanning friction factor (f), based on each type of fin arrangements with appropriate constraints including Reynolds number ranges, geometrical parameter limits, and fitting uncertainties. The correlations used for air-side arrangements of mini/micro channels, which are constructed in slabs, are the same of those used for the compact heat exchangers. In particular, these correlations are used for louver-fin, wavy-fin, offset strip-fin, and extended surfaces (plain fins and pin fins) arrangements. However, the correlations proposed for fin-and-tube (round) are only valid for the compact heat exchangers. We have also compared some correlations with the experimental data of Kays and London standard reference. Some performance correlations are generalized (as one correlation for each j - and f -factor) to represent all louver-fin types. However, other fin arrangements have distinct correlations based on their specific geometry. The most reported correlations are valid for dry fin conditions, whereas there are limited correlations devoted to wet or frost surfaces. A guideline based on this study is provided to facilitate the use of correlations for various configurations.

* Corresponding author: e-mail; smzubair@kfupm.edu.sa, Tel.: +966 13 860-3135; Fax: +966-13-860-2949

Keywords: Heat and flow correlations; j -factor; f -factor; Microchannel heat exchangers; Compact heat exchangers; Air-side fins

Nomenclature

$2A$	Two times of wavy length amplitude, mm
A_{tot}	Total heat surface area ($A_f + A_l$), m ²
A_c	Minimum flow area, m ²
A_f	Fin surface area, m ²
A_{fr}	Frontal area, m ²
A_l	Louver surface area, m ²
A_t	External tube surface area, m ²
B	Blockage ratio of offset strip-fin
C	Foam coefficient, 1/m
c_p	Specific heat capacity of the air, J/kg K
d	Pin diameter, mm
d_f	Spiral fin outside diameter, mm
D_c	Diameter of outside collar fin ($D_o + 2F_t$), mm
D_h	Hydraulic diameter of fin array, mm
D_m (or D_o)	External tube diameter, mm
E	Friction power per unit surface area, W/m ²
Eu	Euler number
F_p (or P)	Fin pitch, mm
F_d	Fin depth, mm
F_l	Fin length, mm
F_t (or t)	Fin thickness, mm
f	Fanning friction factor
G	Mass flux, kg/m ² .s
h	Height of the offset strip fin, mm
h_e	Heat transfer coefficient, W/m ² .K
j	Colburn factor
H	Height, m
K	Permeability, m ²
K_c	Abrupt contraction pressure loss coefficient at inlet
K_e	Abrupt contraction pressure loss coefficient at outlet
k	Thermal conductivity, W/m.K
k_f	Fin thermal conductivity, W/m.K
l	Length, mm / Length of the offset strip, mm
L	Wavelength of wavy fin, mm
L_d	Flow Length, mm
L_h	Louver height, mm
L_l	Louver length, mm
L_p	Louver pitch, mm

\dot{m}	Mass flow rate, kg/s
N_{row}	No. of rows
N_l	No. of louvers over flow direction
P_d	Pore density, PPI
Pr	Prandtl number
P_l	Longitudinal spacing, mm
P_t	Transverse spacing, mm
Re_{Dh}	Reynolds number based on hydraulic diameter (GD_h/μ)
Re_{Do}	Reynolds number based on outer tube diameter (GD_o/μ)
Re_H	Reynolds number based on the metal foam height (GH/μ)
Re_{Lp}	Reynolds number based on louver pitch (GD_{Lp}/μ)
s	Pin spacing in streamwise direction/spacing of the offset strip fin, mm
S_1	Non-louvered inlet and exit fin regions, mm
S_2	Re-directed length, mm
S_h	Slot/slit height, mm
S_l	Longitudinal spacing, mm
S_r	Stanton number/ transverse spacing, mm
S_w	Slot/slit width, mm
T_p	Tube pitch, mm
T_d	Tube depth, mm
V_c	Maximum air velocity, m/s
V_h	Height of vortex generator, mm
V_l	Length of vortex generator, mm
U	Average velocity in a channel, m/s
W	Width, mm

Greek symbols

α	Attack angle, rad.
β	Surface area density – compactness, m^2/m^3
Γ	Frost thickness over the fin pitch, mm
Φ	f - or j -factor
θ	Louver angle, deg.
θ_A	Advancing contact angle, rad.
θ_R	Receding contact angle, rad.
ε	A_{tot}/A_t , finning factor / foam porosity / void fraction
ε_I	A_f/A_{tot}
μ	Dynamic viscosity, Pa.s
ν	Kinematic viscosity, m^2/s
η_f	Fin efficiency
η_o	Overall heat transfer efficiency (air-side)
σ	Ratio of minimum free flow area to frontal area
ρ_e	Outlet air density, kg/m^3
ρ_i	Intlet air density, kg/m^3
ρ_m	Mean air density, kg/m^3

Subscripts

l	Louvered zones
2	Unlouvered zones
f	Fin
o	External tube
w	Water

Abbreviations

CFD	Computational fluid dynamics
FPI	Fins per inch
HVAC	Heating, ventilation and air conditioning
PPI	Pores per inch

1. Introduction

Heat exchangers are a vital component of many applications including power generation [1], chemical reactors, petrochemical industry [2], solar water heater, food engineering, transportation, air conditioning and refrigeration [3], electronics [4], and process industry [5]. The energy efficiency of heat exchangers contributes enormously to the overall efficiency of a system [6]. However, interrupting the flow path by using different fins leads to increase the friction power [7, 8].

The gas-to-liquid heat exchangers are said to be compact heat exchangers if they have a high surface area density above $700 \text{ m}^2/\text{m}^3$ on the air-side; human lungs are the best example to present one of the most compact heat exchangers, having an area density of about $17,500 \text{ m}^2/\text{m}^3$ [9]. Different types of compact heat exchangers, which are augmented by heat transfer surfaces including plain-fin, wavy-fins, offset strip-fin, louver-fin, and fin-tubes, are made of different materials such as aluminum, stainless steels, nickel, copper, etc., depending upon the operating temperatures and pressures. They are used in various fields such as aerospace, automobile, and cryogenic industries because of their compactness, good thermal performance, small space and weight, robust structure, and most importantly low energy requirement and cost [10].

On the other hand, mini/micro channel heat exchangers were designed to have a flow passage less than 1 mm in diameter, in which the heat transfer surface density reaches more than $10,000 \text{ m}^2/\text{m}^3$ [11-13]. Because the microchannel heat exchangers have higher heat transfer rate, lower weight and space, higher energy savings potentials, and less materials than the conventional compact heat exchangers (for the main fluid passage such refrigerants and nanofluids), microchannels can solve a lot of thermal-hydraulic challenges [12]. Having small sizes, mini/micro channels could be arranged in non-circular heat sink [14-21] or put together in flat

slabs [22-28] for heat exchangers, as shown in Figure 1 [12]. The slabs contain some mini/micro channels in different geometries, as shown in Figure 2.

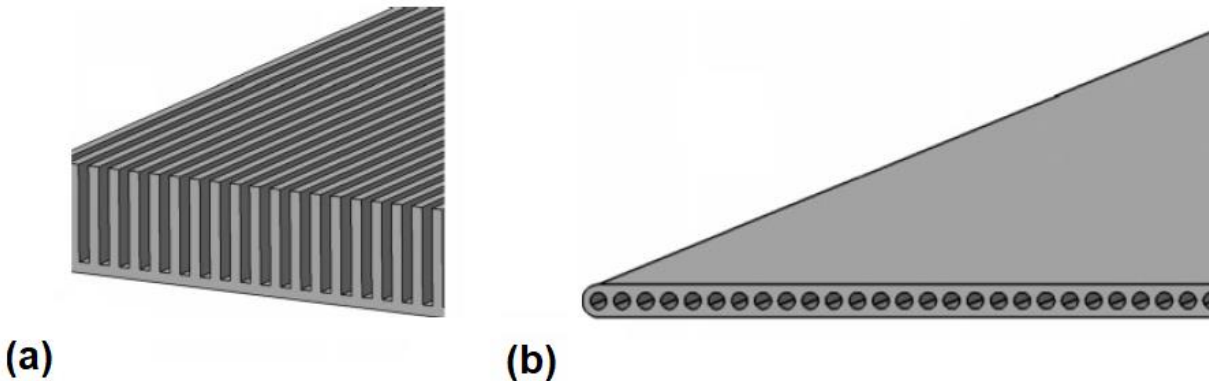


Figure 1. Microchannel heat exchangers used for (a) heat sink electronic cooling (non-circular) and (b) thermal heat exchangers (slab) [12].

For a gas-to-liquid microchannel heat exchangers, the air-side can be constructed between the microchannel slabs, similar to the air-side of compact heat exchangers; thus, the louver-fin, wavy-fin, strip-fin, plain fins and pins are augmented heat transfer surface used on the air-side of both microchannels and compact heat exchangers [23-34]. Conversely, the finned tube (round) is only used for compact heat exchangers because the tubes have typically high diameters – greater than 6 mm. The thermal-hydraulic performance characteristics of the microchannels were comprehensively reviewed [11, 12, 35-37] to discuss flow, heat transfer, and design aspects. Moreover, Siddiqui and Zubair [38] reviewed the manifolds of microchannels.

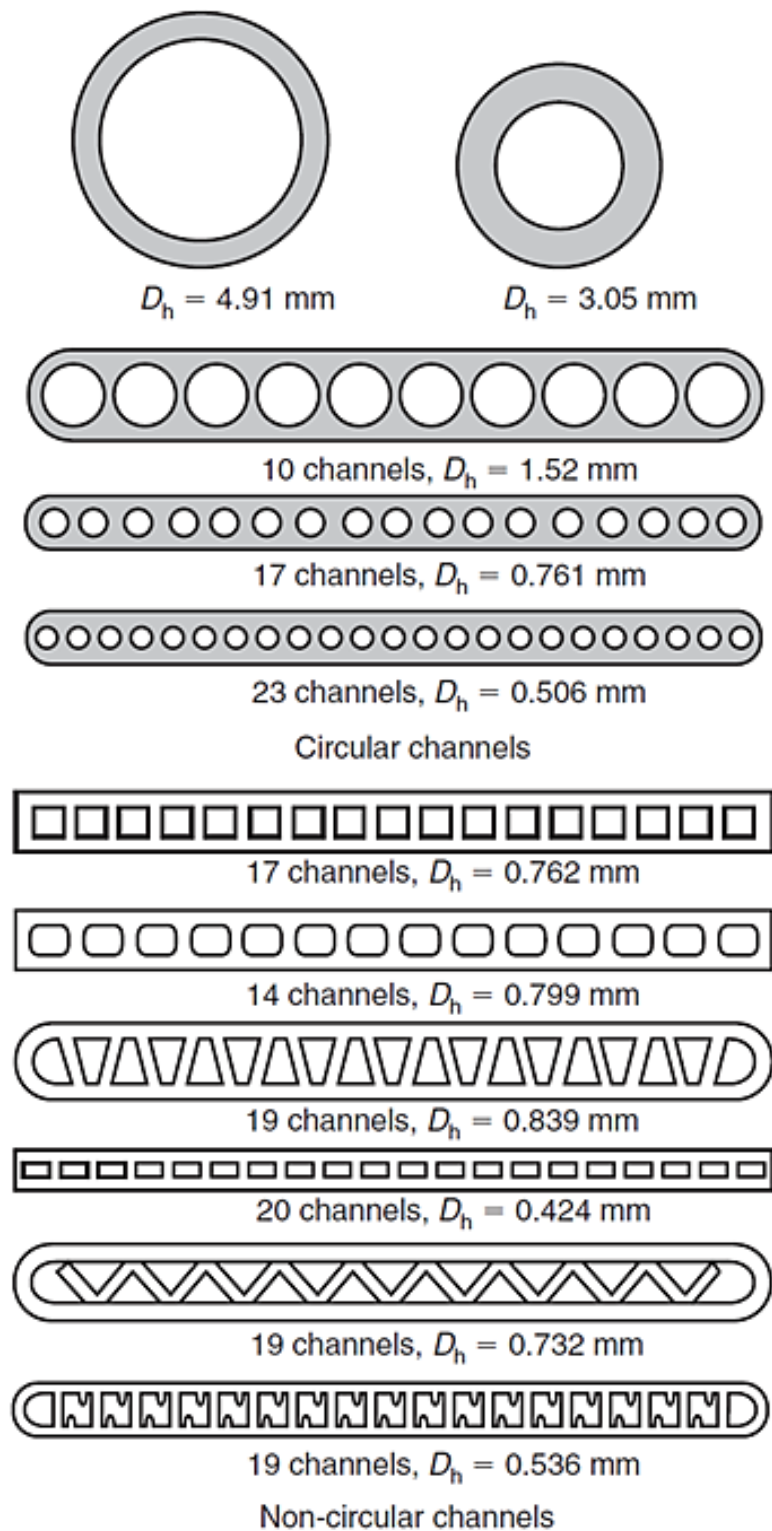


Figure 2. Different geometries of mini/micro channel heat exchangers [39].

The thermal-hydraulic designs of the air-side of microchannels and compact heat exchanger crucially depend upon the performance of heat transfer surfaces. On account of the complexity of the air-side geometries, the heat and fluid flow are usually characterized by experimental studies; thus, the relevant correlations (mostly in terms of Colburn – j factor and fanning friction factor f vs. Reynolds number, and geometrical parameters) can be fitted from the experimental data.

The most cited reference which is used to study heat and flow performance characteristics for the air-side of the compact heat exchangers is compact heat exchanger reference book by Kays and London [40]. However, this source is only limited to represent standardized geometries. Consequently, many experimental and numerical investigations were conducted to cover a wide range of air-side surfaces (e.g. Park and Jacobi [41] used 126 different geometries to develop f - and j -factor correlations for louvered fin heat exchangers).

This paper aims at representing the air-side thermal-hydraulic correlations (mostly in terms of j - and f -factor) that are used both for compact and microchannel heat exchangers, including those having louver-fin, wavy-fin, strip-fin, plain fins and pins arrangements as well as those only used for compact heat exchangers such as finned circular tubes. In this regard, the study provides the state-of-the-art extensive reference source for air-side thermal-hydraulic performance correlations for both microchannels and compact heat exchangers. The correlations are examined with respect to the experimental data for use in a typical microchannel and compact heat exchangers. A comparison between different air-side arrangements is also investigated.

2. Flow and heat transfer performance correlations

2.1. Background and approach

Many thermal-hydraulic performance correlations were fitted from experimental data to represent heat transfer and pressure drop characteristics of the air-side of heat exchangers. Some flow and heat transfer performance characteristics for various types of louvered fin surfaces were investigated in 1950 by Kays and London [42]. In 1963, some correlations for heat and pressure drop were suggested for staggered finned tubes [43], while in (1966), additional pressure drop correlations were formulated [44]. Also, some heat and flow correlations for smooth plate fin-and-

tube heat exchangers were obtained in 1973 and 1975 [45, 46]. The offset strip-fin exchangers correlations were presented in 1975 [47], while some correlations of the louver-fin were proposed in 1983 [48].

Kays and London [40] in 1984 published Compact Heat Exchanger book, which includes comprehensive experimental data of existing types of compact heat exchangers. The book also suggested interpolations for j - and f -factors as functions of Reynolds numbers. Since the publications of this book until today, many heat and fluid-flow correlations were obtained, mostly from experimental data. Recently, some correlations were also formulated from numerical simulations. The most accurate and efficient methods to represent thermal-hydraulic characteristics is by fanning friction factor (f) and Colburn j -factor. The experimental j - and f -values were generally calculated based on the following equations (Eqs. (1-2)) [40].

$$j = \frac{Nu}{Re \ Pr^{1/3}} = \frac{h_e}{\rho_m V_c c_p} Pr^{2/3} \quad (1)$$

$$f = \frac{A_c \rho_m}{A_{tot} \rho_i} \left[\frac{2\rho_i \Delta P}{(\rho_m V_c)^2} - (K_c + 1 - \sigma^2) - 2 \left(\frac{\rho_i}{\rho_e} - 1 \right) + (1 - \sigma^2 - K_e) \frac{\rho_i}{\rho_e} \right] \quad (2)$$

Here, Nu is the Nusselt number, Re is the Reynolds number, Pr is the Prandtl number, h_e (in $\text{W}/\text{m}^2 \text{ K}$) is the heat transfer coefficient, ρ_m , ρ_i , and ρ_e (in kg/m^3) are the mean average, inlet and outlet air densities, respectively, V_c (in m/s) is the maximum air velocity, c_p (in $\text{J}/\text{kg K}$) is the specific heat of the air, A_c (in m^2) is the minimum flow area, A_{tot} (in m^2) is the total air side area, ΔP (in Pa) is the pressure drop, K_c is the abrupt contraction pressure loss coefficient at inlet, K_e is the abrupt expansion pressure loss coefficient at outlet, and σ is the contraction ratio of the fin array (A_c/A_{fr} ; A_{fr} is frontal area (in m^2))

After obtaining experimental f and j data, they are plotted against Reynolds number values, thereby the correlations could be fitted as functions of Reynolds number and geometrical parameters. For example, a method to correlate j - and f -factor of louvered fin data is given by the following equation [49].

$$j \text{ or } f = A_1 Re^{A_2} \left(\frac{\theta}{90} \right)^{A_3} \left(\frac{F_p}{L_p} \right)^{A_4} \left(\frac{F_l}{L_p} \right)^{A_5} \left(\frac{D_m}{L_p} \right)^{A_6} \left(\frac{L_l}{L_p} \right)^{A_7} \left(\frac{F_t}{L_p} \right)^{A_8} \left(\frac{F_d}{L_p} \right)^{A_9} \quad (3)$$

Here, A1 to A9 are fitting constants, and the parameters between brackets are the geometrical parameters such as the fin pitch (F_p), the louver pitch (L_p), the louver angle (θ), the fin length (F_l), the main fluid duct/slab outer diameter (D_m), the louver length (L_l), the fin thickness (F_t), and the fin depth (F_d). All the parameters are taken in mm.

The use of the Reynolds number in the correlations should explicitly be identified by a certain flow parameter (e.g. hydraulic diameter, louver pitch, and outer diameter of a tube). Some of Reynolds numbers used in the j - and f -factor correlations are

$$Re_{D_h} = \frac{GD_h}{\mu} \quad (4)$$

$$Re_{L_p} = \frac{GL_p}{\mu}, \quad (5)$$

$$Re_H = \frac{GL_H}{\mu}, \quad (6)$$

$$Re_{D_m} = \frac{GD_m}{\mu}, \quad (7)$$

where, D_h (in m) is hydraulic diameter, L_p (in m) is the louver pitch, H (in m) is the height, D_m (or D_o) (in m) is the outer diameter of conduit/slab, G (in kg/m² s) is the mass flux, and μ (in Pa.s) is the dynamic viscosity.

The fitting constants are determined with the lowest possible uncertainty. The error values (uncertainty) are always estimated and shown in plots. For instance, a comparison of j or f -factor experimental data and those obtained from correlations is shown in Figure 3. Alternatively, the average and mean deviations between both the correlated and experimental data are calculated as

$$\text{Average deviation} = \frac{1}{N_{exp}} \left(\sum_1^{N_{exp}} \frac{\Phi_{cor} - \Phi_{exp}}{\Phi_{exp}} \right) \times 100\%, \quad (8)$$

$$\text{Mean deviation} = \frac{1}{N_{exp}} \left(\sum_1^{N_{exp}} \frac{|\Phi_{cor} - \Phi_{exp}|}{\Phi_{exp}} \right) \times 100\%, \quad (9)$$

where N_{exp} is the included experimental data, Φ is f - or j -factor and the subscript “cor” denotes from the correlation and “exp” is by experiments

To obtain a reliable correlation, large experimental data should be involved besides including all the geometrical parameters. The correlation fitting should, also, have a small uncertainty value.

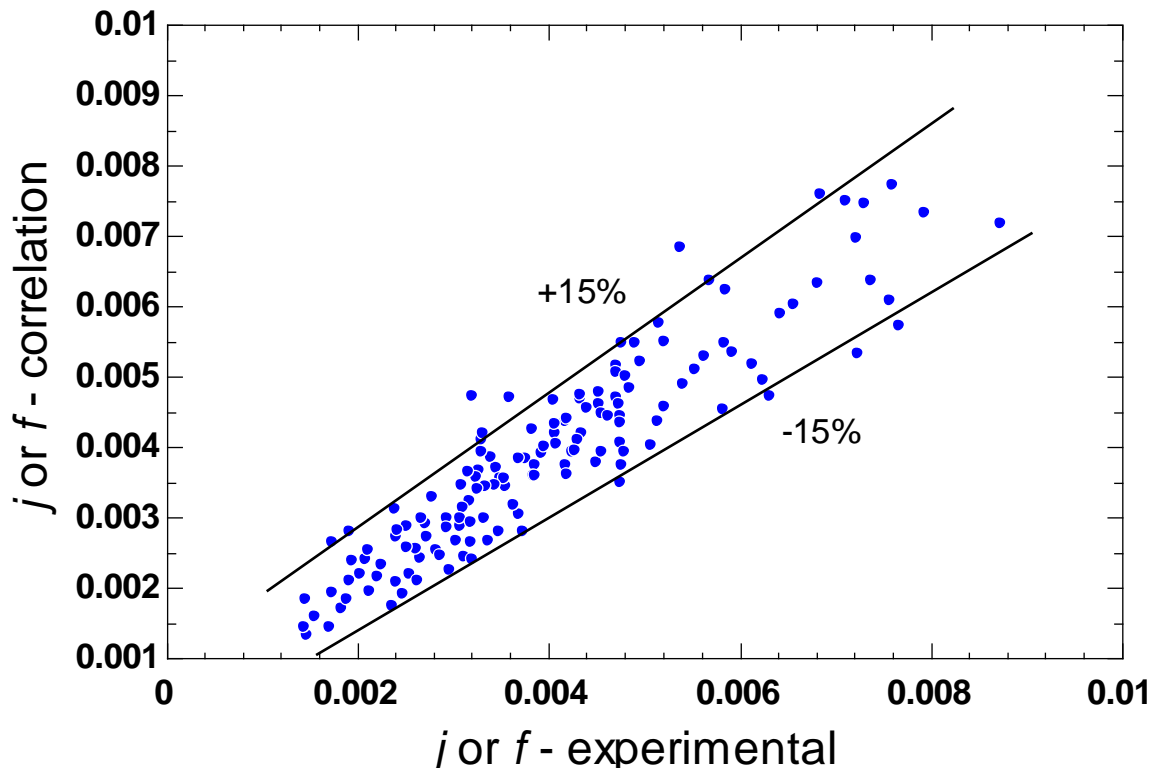


Figure 3. An example to represent the uncertainty level as a comparison of j - or f -factor experimental data and that obtained using a correlation.

2.2. Louver-fin compact and microchannel heat exchangers

Widely, the louvered fin and flat multi-channel (or microchannel slabs) heat exchangers have practically been used in many applications, such as refrigeration and air-conditioning systems, power generation, heating, cooling and evaporation, etc. These are mainly used because of their compactness, robust at high-pressure, sustainability, and low refrigerant charge (HVAC) [50]. The louver (discontinuous solid wall) interrupts air flow, generating a series of thin boundary layers by

stopping their growth, leading to improvement in the heat transfer [7, 51, 52]. Moreover, the intra-passage circulation between fins results in mixing cold and hot air, leading to enhancing the heat transfer [7]. Alternatively, the increase of flow path due to circulation of flow in passages may result in high pressure drop. Thus, the heat transfer improvements should be maximized with the minimum possible pressure drop [7, 8].

Many researchers carried out experimental and numerical investigations to enhance air-side thermal-hydraulic performances of microchannel/compact louvered fin heat exchangers. Many heat and fluid-flow correlations were formulated from different louver-fin constructions to explore the optimum parametric design. The earliest (1950) flow friction and heat transfer performance characteristics for various types of louvered fin surfaces were investigated by Kays and London [42]. Davenport [48] introduced thermal-hydraulic correlations for corrugated louver-fin having triangular channels. The correlations were fitted from experimental data as a function of Reynolds number and some geometrical parameters. Kays and London [40] published numerous experimental data about heat and fluid-flow characteristics including some for louver-fin heat exchangers. Achaichia and Cowell [53] expressed some correlations for heat and fluid-flow in terms of Stanton number (S_t) and f -factor, respectively, using 15 different geometries of louvered fin heat exchangers. Thermal-hydraulic correlations (j and f) for corrugated louver-fin having rectangular channels, were also obtained by Sunden and Svantesson [54]. Over 32 geometries of louver-fin, Dillen and Webb [55] fitted experimental heat and flow data introducing new j and f factor correlations.

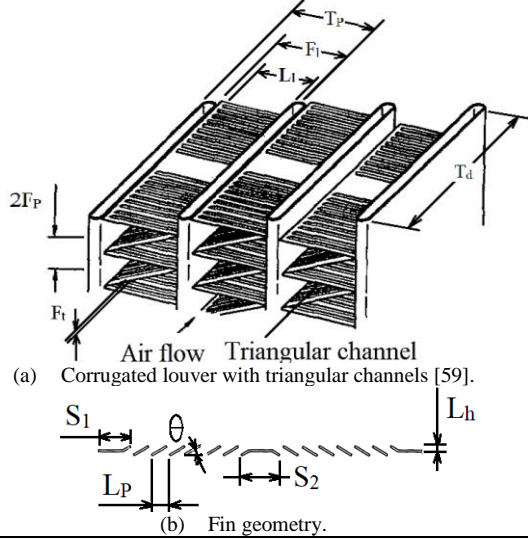
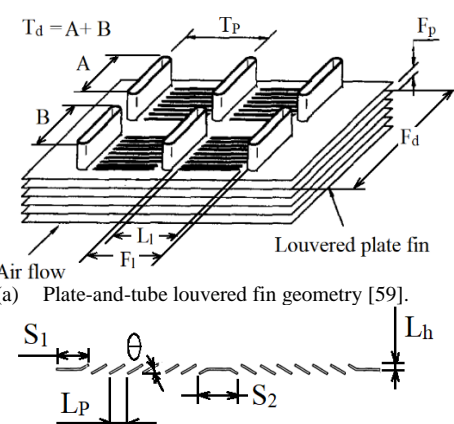
Furthermore, Webb et al. [56] obtained thermal-hydraulic correlations using 57 heat exchanger cores to represent the corrugated louver-fin that have triangular and rectangular channels. Chang and Wang [57] introduced j - and f -factor correlations for corrugated louver-fin (having rectangular channels). A combination of most previous experimental data (91 cores) for louver-fin were correlated to introduce new j - and f -factor correlations for all louvered fin constructions [58, 59]. A wet air flow was also investigated as a cooling medium in louver-fin side; the corresponding correlations for j - and f -factor were obtained from a combination of different 30 heat exchanger cores [60]. Also, Kim and Bullard [61] presented fluid-flow and heat transfer correlations for dry air using 40 configurations. Following the method of gathering most of previous data [59], Jacobi et al. [62] derived a new correlation for j -factor (using 104 cores) to be applied for all types of the

louver-fin geometries. In addition, Park and Jacobi [41] tried to generalize j and f correlations for all the louver-fin types by considering most of the previous experimental data of 126 cores. Recently, some f - and j -factor correlations were fitted from computational fluid dynamics (CFD) modeling data to characterize thermal-hydraulics data of the air-side of louver-fin heat exchangers [63].

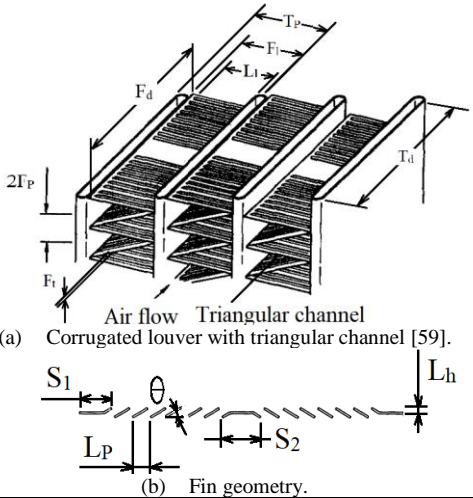
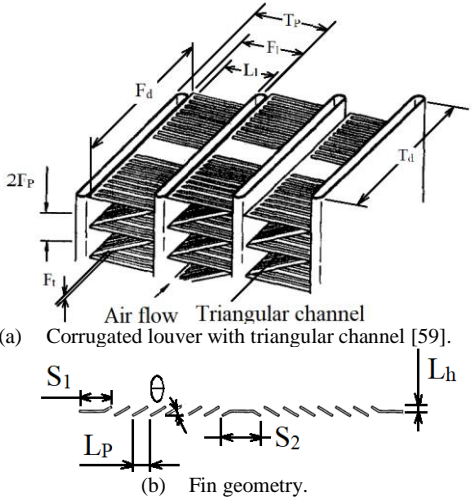
Some researchers, moreover, investigated an enhancement of heat transfer for various louvered fin heat exchangers without developing correlations. Saleem and Kim [64] investigated thermal-hydraulic performance of air-side multi-louvered fin flat-tube of microchannel heat exchanger using ANSYS Fluent 3D model. The study conducted with five geometries based on louver pitch values (0.8, 1.0, 1.4, 1.7 and 2.0 mm) in a laminar flow ($Re = 50 - 450$). The fanning f factor and Nusselt number were plotted against Reynolds number without fitting respective correlations. The 1.0 mm louver pitch configuration showed the highest average Nusselt number of 123% at the penalty of 116% pressure drop compared to louver pitch of 2.0 mm ($Re = 50$). Recently, Yin et al. [30] characterized microchannel condenser using CFD model; they relied on f - and j -factor correlations obtained from previous works [57, 59] to evaluate thermal-hydraulic performance on the air-side of louvered-fin multi-strips microchannel heat exchangers. Türkakar et al. [29] utilized some reported correlations [61] to calculate thermal-hydraulic characteristics of a microchannel-condenser using as a part of vapor compression refrigeration cycle.

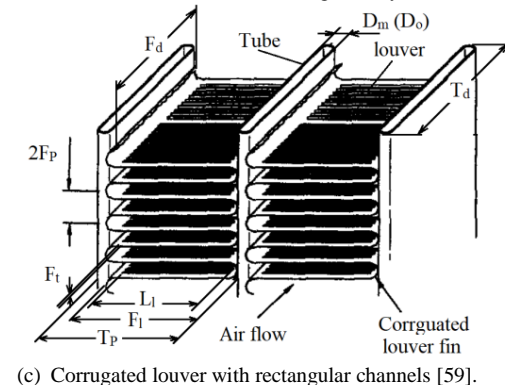
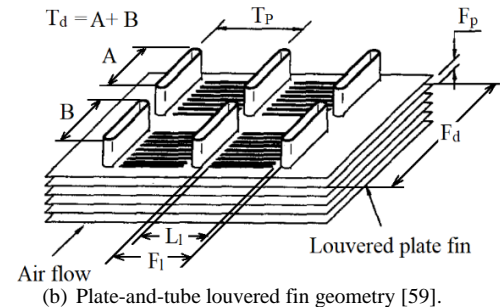
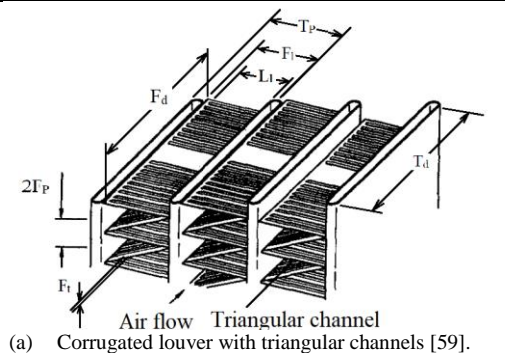
The thermal-hydraulic performance correlations of different constructions of the louver-fin are summarized in Table 1, including geometrical parameters, limitations and operating range of Reynolds number as well as the uncertainties – due to fitting the correlations from the relevant experimental/numerical data. An indication to the suitable louver-fin construction is also added to the Table 1.

Table 1. Summary of reported thermal-hydraulic performance correlations using air-side louvered fin geometries.

Geometry	Correlations	Conditions and limitations	Ref.
 <p>(a) Corrugated louver with triangular channels [59].</p> <p>(b) Fin geometry.</p>	<p>For $300 \leq Re_{D_h} \leq 4000$,</p> $j = 0.249 Re_{L_p}^{-0.42} L_h^{0.33} \left(\frac{L_l}{F_l}\right)^{1.1} F_l^{0.26}.$ <p>For $70 \leq Re_{D_h} \leq 900$,</p> $f = 5.47 Re_{L_p}^{-0.72} \left(\frac{L_l}{F_l}\right)^{0.89} F_l^{0.23} L_p^{0.2} L_h^{0.37}.$ <p>For $1000 \leq Re_{D_h} \leq 4000$,</p> $f = 0.494 Re_{L_p}^{-0.39} \left(\frac{L_h}{F_l}\right)^{0.33} \left(\frac{L_l}{F_l}\right)^{1.1} F_l^{0.46}.$	<p>Dry Geometries = 32</p> <p>$F_p = 2.01 \sim 3.35$ mm $L_p = 1.5 \sim 3.0$ mm $\theta = 8.34 \sim 30.4^\circ$ $F_l = 7.8 \sim 12.7$ mm $L_h = 0.186 \sim 0.46$ mm $L_l = 5.0 \sim 11.7$ mm $F_d(T_d) = 40$ mm $F_t = 0.075$ mm $D_h = 1.8 \sim 2.99$ mm</p> <p>Uncertainty – 95% of the experimental data were correlated within error $\pm 6\%$.</p>	[48]
 <p>(a) Plate-and-tube louvered fin geometry [59].</p> <p>(b) Fin geometry.</p>	<p>For $Re_{L_p} \geq 75$,</p> $St = 1.554 \frac{\left(0.936 - \frac{243}{Re_{L_p}} - 1.76 \frac{F_p}{L_p} + 0.995\theta\right)}{\theta} Re_{L_p}^{-0.59} \left(\frac{T_p}{L_p}\right)^{-0.09} \left(\frac{F_p}{L_p}\right)^{-0.04},$ <p>where $j = St Pr^{\frac{2}{3}}$.</p> <p>For $150 < Re_{L_p} \leq 3000$,</p> $f = 0.895 f_A^{1.07} F_p^{-0.22} L_p^{0.25} T_p^{0.26} F_l^{0.33},$ <p>where $f_A = 596 Re_{L_p}^{(0.318 \log(Re_{L_p}) - 2.25)}$.</p> <p>For $Re_{L_p} \leq 150$,</p> $f = 10.4 Re_{L_p}^{-1.17} F_p^{0.05} L_p^{1.24} T_p^{0.83} F_l^{0.25}.$	<p>Dry Geometries = 15</p> <p>$F_p = 1.65 \sim 3.33$ mm $L_p = 0.81 \sim 1.4$ mm $\theta = 20 \sim 30^\circ$ $L_h = 0.139 \sim 0.334$ mm $L_l = 5.0 \sim 11.0$ mm $F_d = 20.8$ and 41.6 mm $F_l = 6.0 \sim 12.0$ mm $T_d = 16.0$ mm $F_t = 0.05$ mm $D_h = 2.69 \sim 5.02$ mm $\sigma = 0.747 \sim 0.850$ $D_m = 2$ mm $A_c/A_{tot} < 0.023$</p> <p>Uncertainty – All the Stanton number data are within error $\pm 10\%$; the correlation coefficient of f-factor is 0.91.</p>	[53]

<p>Corrugated louver with rectangular channels,</p> <p>(a) Corrugated louver with rectangular channels [59].</p> <p>(b) Fin geometry.</p>	<p>For $100 \leq Re_{L_p} \leq 1000$,</p> $j = 0.436 Re_{L_p}^{-0.559} \varepsilon^{0.192} \varepsilon_1^{0.0956},$ $f = 0.862 Re_{L_p}^{-0.488} \varepsilon^{0.706} \varepsilon_1^{1.04}.$ <p>Here, $\varepsilon = \frac{A}{A_t}$ is finning factor, $\varepsilon_1 = \frac{A_l}{A}$ is louver surface area over the heat transfer characteristics.</p>	<p>Dry Geometries = 27</p> <p>$F_p = 1.8 \sim 2.2 \text{ mm}$ $L_p = 1.318 \sim 1.693 \text{ mm}$ $\theta = 28^\circ$ $F_l = 16.0 \sim 19.0 \text{ mm}$ $L_l = 12.15 \sim 17.18 \text{ mm}$ $F_d = 22 \sim 44 \text{ mm}$ $F_t = 0.16 \text{ mm}$ $D_h = 3.007 \sim 3.740 \text{ mm}$ $\varepsilon = 7.778 \sim 11.704$ $\varepsilon l = 0.432 \sim 0.628$</p> <p>Uncertainty – 85% of the experimental data were correlated within error $\pm 10\%$.</p> <p>[57]</p>	
<p>Multi-louvered fin with triangular channels,</p>	<p>For $100 \leq Re_{L_p} \leq 600$,</p> $j = Re_{L_p}^{-0.487} \left(\frac{\theta}{90} \right)^{0.257} \left(\frac{F_p}{L_p} \right)^{-0.13} \left(\frac{F_l}{L_p} \right)^{-0.29} \left(\frac{F_d}{L_p} \right)^{-0.235} \left(\frac{L_l}{L_p} \right)^{0.68} \left(\frac{T_p}{L_p} \right)^{-0.279} \left(\frac{F_t}{L_p} \right)^{-0.05},$ $f = Re_{L_p}^{-0.781} \left(\frac{\theta}{90} \right)^{0.444} \left(\frac{F_p}{L_p} \right)^{-1.682} \left(\frac{F_l}{L_p} \right)^{-1.22} \left(\frac{F_d}{L_p} \right)^{0.818} \left(\frac{L_l}{L_p} \right)^{1.97}.$	<p>Dry Geometries = 45</p> <p>$F_p = 1.0 \sim 1.4 \text{ mm}$ $L_p = 1.7 \text{ mm}$ $\theta = 15 \sim 29^\circ$ $F_l = 8.15 \text{ mm}$ $L_l = 6.4 \text{ mm}$ $F_d = 16.0 \sim 24.0 \text{ mm}$ $T_p = 10.15 \text{ and } 11.15 \text{ mm}$ $F_t = 0.1 \text{ mm}$</p> <p>[61]</p>	

 <p>(a) Corrugated louver with triangular channel [59].</p> <p>(b) Fin geometry.</p>		<p>Uncertainty – <i>j</i>: the data were correlated within error $\pm 14.5\%$. <i>f</i>: the data were correlated within error $\pm 7\%$.</p>	
<p>Louvered fin with triangular channels,</p>  <p>(a) Corrugated louver with triangular channel [59].</p> <p>(b) Fin geometry.</p>	<p>For $100 \leq Re_{L_p} \leq 300$,</p> $j = Re_{L_p}^{-0.512} \left(\frac{\theta}{90} \right)^{0.25} \left(\frac{F_p}{L_p} \right)^{-0.171} \left(\frac{F_l}{L_p} \right)^{-0.29} \left(\frac{T_d}{L_p} \right)^{-0.248} \left(\frac{L_l}{L_p} \right)^{0.68} \left(\frac{T_p}{L_p} \right)^{-0.275} \left(\frac{F_t}{L_p} \right)^{-0.05},$ $f = Re_{L_p}^{-0.798} \left(\frac{\theta}{90} \right)^{0.395} \left(\frac{F_p}{L_p} \right)^{-2.635} \left(\frac{F_l}{L_p} \right)^{-1.22} \left(\frac{T_d}{L_p} \right)^{0.823} \left(\frac{L_l}{L_p} \right)^{1.97}.$	<p>Wet Geometries = 30 $F_p = 1.0 \sim 1.4$ mm $L_p = 1.7$ mm $\theta = 15 \sim 29^\circ$ $F_l = 8.15 \sim 8.8$ mm $L_l = 6.4$ mm $F_d = 16.0 \sim 24.0$ mm $T_d = 16.0 \sim 25.4$ mm $T_p = 10.15 \sim 11.15$ mm $D_m = 2 \sim 2.35$ mm $F_t = 0.1$ mm Water film = 0.1 mm Inlet dry temperature = 27 °C Wet bulb temperature = 19 °C Uncertainty – <i>j</i>: the experimental data were correlated within error $\pm 16.9\%$. <i>f</i>: the experimental data were correlated within error $\pm 13.6\%$.</p>	[60]
<p>Louvered fin (all types),</p>	<p>For $100 \leq Re_{L_p} \leq 3000$,</p> $j = 1.18 Re_{L_p}^{-0.505} \left(\frac{\theta}{90} \right)^{0.26} \left(\frac{F_l}{L_p} \right)^{-0.51} \left(\frac{T_d}{L_p} \right)^{-0.26} \left(\frac{L_l}{L_p} \right)^{0.82} \left(\frac{T_p}{L_p} \right)^{-0.25} \left(\frac{F_t}{L_p} \right)^{-0.097}.$ <p>For folded fin geometry,</p>	<p>Dry Geometries = 91 $F_p = 0.51 \sim 3.33$ mm $L_p = 0.5 \sim 3.0$ mm $\theta = 8.43 \sim 35^\circ$ $F_l = 6.0 \sim 20.0$ mm</p>	[58, 59]



$$j = Re_{L_p}^{-0.49} \left(\frac{\theta}{90} \right)^{0.27} \left(\frac{F_p}{L_p} \right)^{-0.14} \left(\frac{F_l}{L_p} \right)^{-0.29} \left(\frac{T_d}{L_p} \right)^{-0.23} \left(\frac{L_l}{L_p} \right)^{0.68} \left(\frac{T_p}{L_p} \right)^{-0.28} \left(\frac{F_t}{L_p} \right)^{-0.05},$$

$$f = f_1 f_2 f_3,$$

where,

$$f_1 = \begin{cases} 14.39 Re_{L_p}^{-0.805(F_p/F_l)} \left(\ln \left(1.0 + \left(\frac{F_p}{L_p} \right) \right) \right)^{3.04} & \text{for } Re_{L_p} < 150 \\ 4.97 Re_{L_p}^{(0.6049 - \frac{1.046}{60.2})} \left(\ln \left(0.9 + \left(\frac{F_t}{F_p} \right)^{0.5} \right) \right)^{-0.527} & \text{for } 150 \leq Re_{L_p} < 5000, \end{cases}$$

$$f_2 = \begin{cases} \left(\ln \left(0.9 + \left(\frac{F_t}{F_p} \right)^{0.48} \right) \right)^{-1.435} \left(\frac{D_h}{L_p} \right)^{-3.01} \left(\ln \left(0.5 Re_{L_p} \right) \right)^{-3.01} & \text{for } Re_{L_p} < 150 \\ \left(\frac{D_h}{L_p} \right) \ln \left(0.3 Re_{L_p} \right)^{-2.966} \left(\frac{F_p}{L_l} \right)^{-0.7931(T_p/(T_p - D_m))} & \text{for } 150 \leq Re_{L_p} < 5000, \end{cases}$$

and

$$f_3 = \begin{cases} \left(\frac{F_p}{L_l} \right)^{-0.308} \left(\frac{F_d}{L_l} \right)^{-0.308} \exp(-0.1167(T_p/D_m)) \theta^{0.35} & \text{for } Re_{L_p} < 150 \\ \left(\frac{T_p}{D_m} \right)^{-0.0446} \ln \left(1.2 + \left(\frac{L_p}{F_p} \right)^{1.4} \right)^{-3.553} \theta^{-0.477} & \text{for } 150 \leq Re_{L_p} < 5000. \end{cases}$$

$$L_l = 0.94 \sim 18.5 \text{ mm}$$

$$T_d(F_d) = 15.6 \sim 57.4 \text{ mm}$$

$$T_p = 7.51 \sim 25.0 \text{ mm}$$

$$F_t = 0.0254 \sim 1.16 \text{ mm}$$

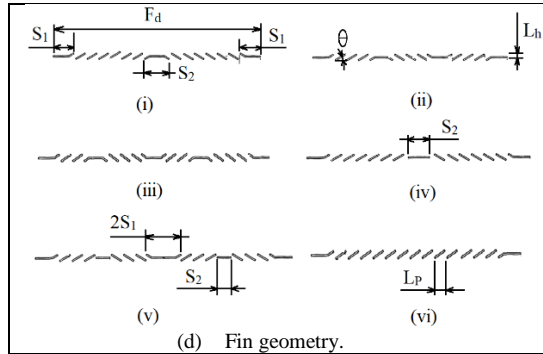
$$D_h = 0.824 \sim 5.2 \text{ mm}$$

$$D_m = 1.5 \sim 5.0 \text{ mm}$$

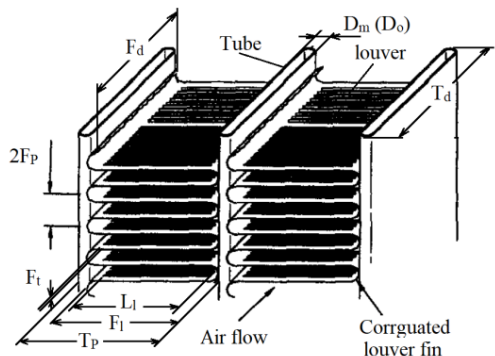
Uncertainty –

j: 89% of the data were correlated within $\pm 15\%$.

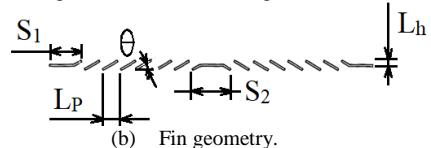
f: 83.14% of the data were correlated within $\pm 15\%$.



Corrugated louver with rectangular channels,



(a) Corrugated louver with rectangular channels [59].



For $65 \leq Re_{L_p} \leq 750$,

$$j = 3.67 Re_{L_p}^{-0.591} \left(\frac{\theta}{90} \right)^{0.239} \left(\frac{F_p}{L_p} \right)^{0.0206} \left(\frac{F_l}{L_p} \right)^{-0.285} \left(\frac{L_h}{L_p} \right)^{0.0671} \left(\frac{F_d}{L_p} \right)^{-0.243},$$

$$f = 9.2 Re_{L_p}^{-0.54} \left(\frac{F_p}{L_p} \right)^{-0.022} \left(\frac{F_l}{L_p} \right)^{-1.085} \left(\frac{L_h}{L_p} \right)^{0.067} \left(\frac{F_d}{L_p} \right)^{0.31}.$$

Dry

[54]

Geometries = 6

$F_p = 1.5 \sim 2.0$ mm
 $L_p = 0.5 \sim 1.4$ mm
 $F_l = 8.0 \sim 12.5$ mm
 $L_h = 0.16 \sim 0.39$ mm
 $L_l = 5.0 \sim 10.3$ mm
 $F_d = 37.0 \sim 57.4$ mm
 $F_t = 0.04 \sim 0.06$ mm

Uncertainty –
the equations need to be treated
with caution [65]

Corrugated louver with triangular channels,

For $400 \leq Re_{D_h} \leq 4000$,

$$St = \frac{1}{\rho_m V_c \eta_o A_o} \left(h_e A_e + 0.0874 \eta_f k L_1 \beta Re_{L_p}^{0.555} \left(\frac{\theta}{90} \right)^{0.201} \left(\frac{F_p}{F_l} \right)^{-0.139} \right),$$

where $j = St Pr^{\frac{2}{3}}$,

$$\frac{h_e D_h}{k} = 10.81 + 12.63 X - 1.61 X^2 - 18.86 X^{0.5},$$

$$Y = \frac{T_p - D_o - L_l}{F_p - F_t}, \quad X = \begin{cases} Y & \text{for } Y \leq 1 \\ \frac{1}{Y} & \text{for } Y > 1, \end{cases}$$

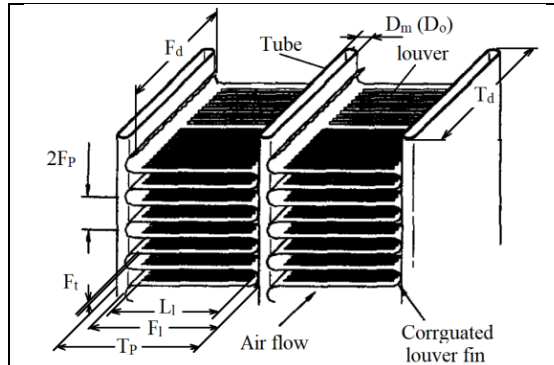
Dry

[55]

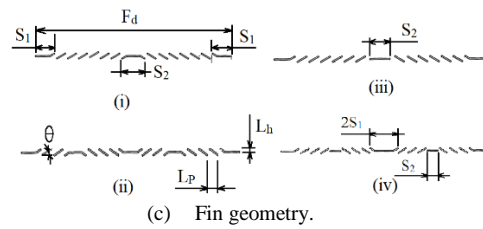
Geometries = 32, data taken
from [48]

$F_p = 2.01 \sim 3.35$ mm
 $L_p = 1.5 \sim 3.0$ mm
 $\theta = 8.34 \sim 30.4^\circ$
 $F_l = 7.8 \sim 12.7$ mm
 $L_h = 0.186 \sim 0.46$ mm
 $L_l = 5.0 \sim 11.7$ mm

<p>(a) Corrugated louver with triangular channels [59].</p> <p>(b) Fin geometry.</p>	$D_h = \frac{2(T_p - D_o - L_l)(F_p - F_t)}{(T_p - D_o - L_l + F_p - F_t)},$ $A_e = 2 F_d (T_p - D_o - L_l + F_p - F_t), \text{ and}$ $\beta = 2 \left(\frac{S_1}{L_p} \right)^{0.5} + N_1 + \left(\frac{S_2}{L_p} \right)^{0.5}.$ <p>For $400 \leq Re_{D_h} \leq 1000$,</p> $f = f_e \frac{A_e}{A_o} + Z \frac{A_D}{A_o} + 4.5 \frac{L_l L_p}{A_o} \beta Re_{L_p}^{-0.6} \left(\frac{\theta}{90} \right)^{0.31} \left(\frac{F_p}{F_l} \right)^{-0.4}.$ <p>For $1000 \leq Re_{D_h} \leq 4000$,</p> $f = f_e \frac{A_e}{A_o} + Z \frac{A_D}{A_o} + 1.14 \frac{L_l L_p}{A_o} \beta Re_{L_p}^{-0.43} \left(\frac{\theta}{90} \right)^{0.41} \left(\frac{F_p}{F_l} \right)^{-0.53},$ <p>where $\frac{f_e D_h V_c}{v} = 32.72 + 18.73 X - 37.04 X^{0.5} - \frac{0.164}{X}$,</p> $A_D = N_l L_l F_t, \text{ and}$ $Z = \begin{cases} \frac{2\pi \sin(\theta)}{0.8} & \text{for } \theta < 8^\circ \\ \frac{\cos(\theta)}{0.222 + 0.283/\sin(\theta)} & \text{for } 8^\circ \leq \theta \leq 12^\circ \\ \frac{\cos(\theta)}{0.222 + 0.283/\sin(\theta)} & \text{for } \theta \geq 12^\circ. \end{cases}$	$F_d = 40 \text{ mm}$ $F_t = 0.075 \text{ mm}$ $D_h = 1.8 \sim 2.99 \text{ mm}$ $D_o = 1.5 \text{ mm}$ Uncertainty – 81% of the data were correlated within error $\pm 10\%$.
<p>(a) Corrugated louver with triangular and rectangular channels [59].</p> <p>(b) Fin geometry.</p>	<p>For $400 \leq Re_{D_h} \leq 4000$,</p> $St = \frac{1}{\rho_m V_c \eta_o A_o} \left(h_e A_e + 0.744 \eta_f k L_1 \beta Re_{L_p}^{0.581} \left(\frac{\theta}{90} \right)^{0.195} \left(\frac{F_p}{F_l} \right)^{-0.0522} \right),$ <p>where $j = St Pr^{\frac{2}{3}}$,</p> $\frac{h_e D_h}{k} = 10.81 + 12.63 X - 1.61 X^2 - 18.86 X^{0.5},$ $X = \begin{cases} Y & \text{for } Y \leq 1 \\ \frac{1}{Y} & \text{for } Y > 1 \end{cases}, \text{ and } Y = \frac{T_p - D_o - L_l}{F_p - F_t},$ $D_h = \frac{2(T_p - D_o - L_l)(F_p - F_t)}{(T_p - D_o - L_l + F_p - F_t)},$ $A_e = 2 F_d (T_p - D_o - L_l + F_p - F_t), \text{ and}$ $\beta = 2 \left(\frac{S_1}{L_p} \right)^{0.5} + N_l + \left(\frac{S_2}{L_p} \right)^{0.5}.$ <p>For $400 \leq Re_{D_h} \leq 1000$,</p> $f = f_e \frac{A_e}{A_o} + Z \frac{A_D}{A_o} + 6.242 \frac{L_l L_p}{A_o} \beta Re_{L_p}^{-0.759} \left(\frac{\theta}{90} \right)^{0.233} \left(\frac{F_p}{F_l} \right)^{-0.628}.$ <p>For $1000 < Re_{D_h} \leq 4000$,</p> $f = f_e \frac{A_e}{A_o} + Z \frac{A_D}{A_o} + 0.876 \frac{L_l L_p}{A_o} \beta Re_{L_p}^{-0.555} \left(\frac{\theta}{90} \right)^{0.521} \left(\frac{F_p}{F_l} \right)^{-0.0772},$ <p>where $\frac{f_e D_h V_c}{v} = 32.72 + 18.73 X - 37.04 X^{0.5} - \frac{0.164}{X}$,</p> $A_D = N_l L_l F_t, \text{ and}$	<p>Dry For data taken from [48, 57]</p> <p>[56]</p> <p>Geometries = 57</p> <p>$F_p = 1.80 \sim 3.35 \text{ mm}$ $L_p = 1.318 \sim 3.0 \text{ mm}$ $\theta = 8.34 \sim 30.4^\circ$ $F_l = 7.8 \sim 19.0 \text{ mm}$ $L_h = 0.186 \sim 0.663 \text{ mm}$ $L_l = 5.0 \sim 17.18 \text{ mm}$ $F_d = 22 \sim 44 \text{ mm}$ $F_t = 0.075 \text{ and } 0.16 \text{ mm}$ $D_h = 1.8 \sim 3.74 \text{ mm}$ $D_o = 1.5 \text{ and } 5.0 \text{ mm}$</p> <p>Uncertainty – 81% of the data were correlated within error $\pm 10\%$.</p>



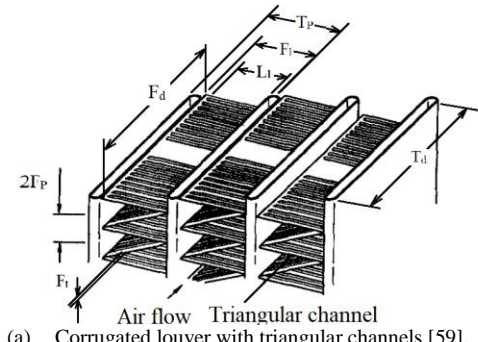
(b) Corrugated louver with rectangular channels [59].



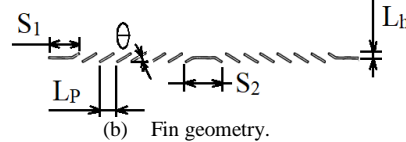
(c) Fin geometry.

$$Z = \begin{cases} \frac{2\pi \sin(\theta)}{0.8} & \text{for } \theta < 8^\circ \\ 0.8 & \text{for } 8^\circ \leq \theta \leq 12^\circ \\ \frac{\cos(\theta)}{0.222 + 0.283/\sin(\theta)} & \text{for } \theta \geq 12^\circ. \end{cases}$$

Louvered-fin flat-tube,



(a) Corrugated louver with triangular channels [59].



(b) Fin geometry.

For $70 \leq Re_{L_p} \leq 1000$

$$\frac{j}{j_0} = 1.0 - 3.020\Gamma + 2.719\Gamma^2,$$

$$\frac{j}{j_0} = 1.0 - 6.870\Gamma + 14.336\Gamma^2,$$

$$\frac{j}{j_0} = 1.0 - 2.804\Gamma + 4.233\Gamma^2,$$

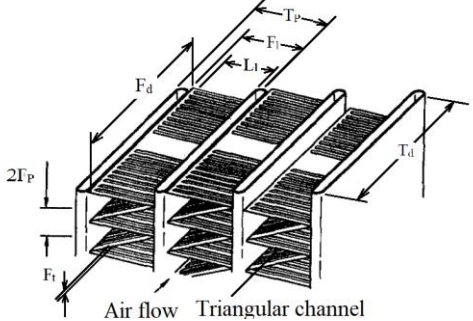
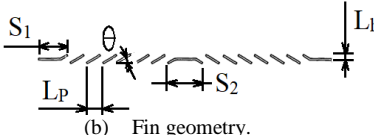
Frost

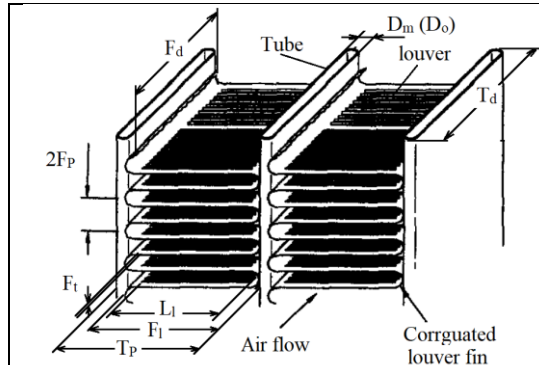
$F_p = 1.40 \sim 2.12 \text{ mm}$
 $\Gamma < 0.30$ (Γ is a frost thickness over the fin pitch)
 $T_a = -1^\circ\text{C}$, $RH = 80\%$, face velocity = 1 m/s, $T_c = -10^\circ\text{C}$
Uncertainty –
 $R^2 = 0.91$

$F_p = 1.06 \text{ mm}$
 $\Gamma < 0.3$
 $T_a = -1^\circ\text{C}$, $RH = 80\%$, face velocity = 1 m/s, $T_c = -10^\circ\text{C}$
Uncertainty –
 $R^2 = 0.99$

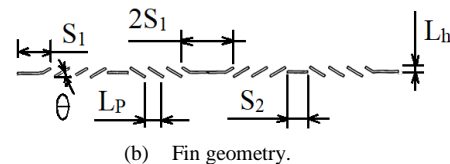
$F_p = 1.40 \sim 2.12 \text{ mm}$
 $\Gamma < 0.3$
 $T_a = -1^\circ\text{C}$, $RH = 80\%$, face velocity = 2 m/s, $T_c = -15^\circ\text{C}$
Uncertainty –
 $R^2 = 0.89$

[66]

	$\frac{j}{j_0} = 1.0 - 4.612\Gamma + 11.343\Gamma^2,$ $\frac{j}{j_0} = 1.0 - 5.527\Gamma + 12.093\Gamma^2,$ <p>where $j_0 = Re_{L_p}^{-0.49} \left(\frac{\theta}{90}\right)^{0.27} \left(\frac{F_p}{L_p}\right)^{-0.14} \left(\frac{F_t}{L_p}\right)^{-0.29} \left(\frac{T_d}{L_p}\right)^{-0.23} \left(\frac{L_l}{L_p}\right)^{0.68} \left(\frac{T_p}{L_p}\right)^{-0.28} \left(\frac{F_t}{L_p}\right)^{-0.05}$</p> $f = 5.47 Re_{L_p}^{-0.72} (L_p \sin \theta)^{0.37} (L_p)^{0.2} \left(\frac{L_l}{F_t}\right)^{0.89}.$	$F_p = 1.40 \sim 2.12 \text{ mm}$ $\Gamma < 0.2$ $T_a = -1^\circ\text{C}, RH = 80\%, \text{face velocity} = 2 \text{ m/s}, T_c = -10^\circ\text{C}$ $\text{Uncertainty} - R^2 = 0.93$ $F_p = 1.40 \sim 2.12 \text{ mm}$ $\Gamma < 0.2$ $T_a = -1^\circ\text{C}, RH = 70\%, \text{face velocity} = 2 \text{ m/s}, T_c = -10^\circ\text{C}$ $\text{Uncertainty} - R^2 = 0.96$ $\text{Uncertainty} - \text{poor (no value mentioned)}$
<p>Multi-louvered fin with triangular channels,</p>  <p>(a) Corrugated louver with triangular channels [59].</p>  <p>(b) Fin geometry.</p>	<p>For $200 \leq Re_{L_p} \leq 5000$,</p> $j = 0.26712 Re_{L_p}^{-0.1944} \left(\frac{\theta}{90}\right)^{0.257} \left(\frac{F_p}{L_p}\right)^{-0.5177} \left(\frac{F_t}{L_p}\right)^{-1.9045} \left(\frac{L_l}{L_p}\right)^{1.7159} \left(\frac{F_d}{L_p}\right)^{-0.2147} \left(\frac{F_t}{L_p}\right)^{-0.05},$ $f = 0.54486 Re_{L_p}^{-0.3068} \left(\frac{\theta}{90}\right)^{0.444} \left(\frac{F_p}{L_p}\right)^{-0.9925} \left(\frac{F_t}{L_p}\right)^{0.5458} \left(\frac{L_l}{L_p}\right)^{-0.2003} \left(\frac{F_d}{L_p}\right)^{0.0688}.$	<p>Dry Geometries = 20</p> <p>$F_p = 2.0 \sim 2.75 \text{ mm}$ $L_p = 1.2 \text{ mm}$ $\theta = 22 \sim 28^\circ$ $F_d = 36.6 \sim 65 \text{ mm}$ $F_t = 0.15 \text{ and } 0.2 \text{ mm}$</p> <p>Uncertainty – j: 95% of experimental data were correlated within error 10%. f: 95% of the experimental data were correlated within $\pm 12\%$.</p>
<p>Corrugated louver with rectangular channels,</p>	<p>For $20 < Re_{L_p} \leq 80$,</p> $j = Re_{L_p}^{-0.324} \left(\frac{\theta}{90}\right)^{1.1} \left(\frac{F_p}{L_p}\right)^{-0.2} \left(\frac{F_t}{L_p}\right)^{-2.3} \left(\frac{D_m}{L_p}\right)^{1.88} \left(\frac{L_l}{L_p}\right)^{1.72} \left(\frac{F_t}{L_p}\right)^{-0.001} \left(\frac{F_d}{L_p}\right)^{-0.195},$ $f = Re_{L_p}^{-0.87} \left(\frac{\theta}{90}\right)^{0.67} \left(\frac{F_p}{L_p}\right)^{-0.06} \left(\frac{F_t}{L_p}\right)^{-0.014} \left(\frac{D_m}{L_p}\right)^{0.83} \left(\frac{L_l}{L_p}\right)^{0.007} \left(\frac{F_t}{L_p}\right)^{-1.35} \left(\frac{F_d}{L_p}\right)^{0.019}.$ <p>For $80 < Re_{L_p} \leq 200$,</p>	<p>Dry Geometries = 26</p> <p>$F_p = 7 \sim 21.17 \text{ mm}$ $L_p = 0.9 \sim 2.44 \text{ mm}$ $\theta = 20.0 \sim 34.0^\circ$ $F_l = 5.6 \sim 10 \text{ mm}$ $L_l = 5.97 \sim 7.87 \text{ mm}$ $F_d = 12.0 \sim 30.0 \text{ mm}$ $T_d = 12.0 \sim 30.0 \text{ mm}$</p>



(a) Corrugated louver with rectangular channels [59].



(b) Fin geometry.

$$j = Re_{L_p}^{-0.4} \left(\frac{\theta}{90} \right)^{0.09} \left(\frac{F_p}{L_p} \right)^{-0.07} \left(\frac{F_l}{L_p} \right)^{-2.48} \left(\frac{D_m}{L_p} \right)^{1.65} \left(\frac{L_l}{L_p} \right)^{1.83} \left(\frac{F_t}{L_p} \right)^{-0.006} \left(\frac{F_d}{L_p} \right)^{-0.012},$$

$$f = Re_{L_p}^{-0.856} \left(\frac{\theta}{90} \right)^{0.74} \left(\frac{F_p}{L_p} \right)^{-0.016} \left(\frac{F_l}{L_p} \right)^{-0.01} \left(\frac{D_m}{L_p} \right)^{0.53} \left(\frac{L_l}{L_p} \right)^{0.31} \left(\frac{F_t}{L_p} \right)^{-1.1121} \left(\frac{F_d}{L_p} \right)^{0.053},$$

$D_m = 1.5 \sim 4.19 \text{ mm}$

Uncertainty –

j : 85.3 % of experimental data were correlated within error $\pm 19.69\%$ for $20 < Re_{L_p} \leq 80$, and 84.8 % of experimental data were correlated within error $\pm 22.12\%$ for $80 < Re_{L_p} < 200$.

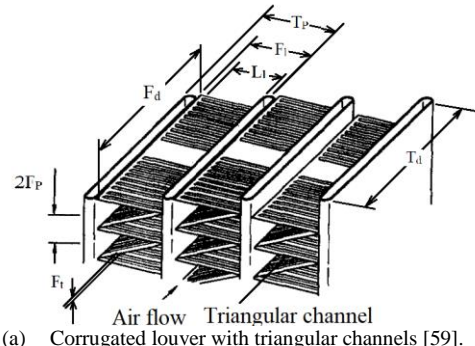
f : 85.3 % of experimental data were correlated within error $\pm 13.53\%$ for $20 < Re_{L_p} \leq 80$, and 85.6 % of experimental data were correlated within error $\pm 10.68\%$ for $80 < Re_{L_p} < 200$.

Multi-louvered fin with triangular channels,

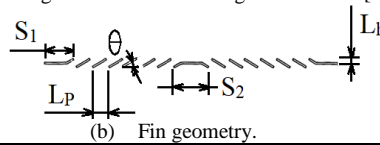
For $192 \leq Re_{L_p} \leq 536$,

$$j = 2.96196 Re_{L_p}^{-0.635645},$$

$$f = 6.31383 Re_{L_p}^{0.486849}.$$



(a) Corrugated louver with triangular channels [59].



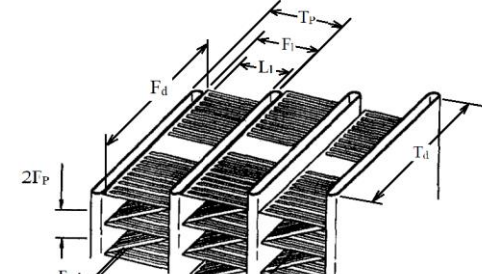
(b) Fin geometry.

Dry
Geometries = 1
 $F_p = 1.35 \text{ mm}$
 $F_l = 8.0 \text{ mm}$
 $L_p = 1.2 \text{ mm}$
 $L_t = 6.0 \text{ mm}$
 $T_p = 1.35 \text{ mm}$
 $\theta = 23^\circ$
 $F_d = 7.5 \text{ mm}$

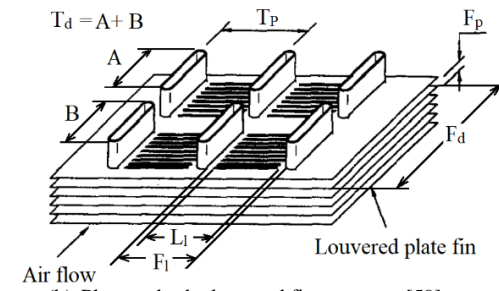
[28]

Uncertainty –
 j : average error $\pm 0.95\%$.
 f : average error $\pm 0.73\%$.

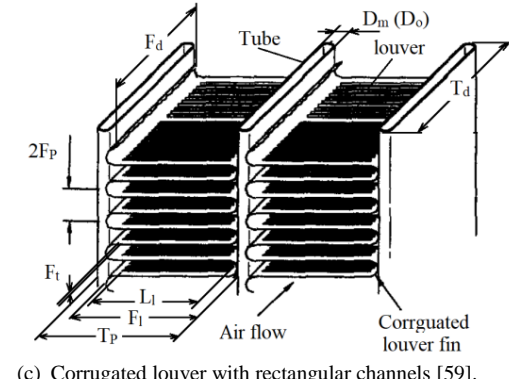
Louvered-fin flat-tube (all types),



(a) Corrugated louver with triangular channels [59].



(b) Plate-and-tube louvered fin geometry [59].



(c) Corrugated louver with rectangular channels [59].

For $27 \leq Re_{L_p} \leq 4132$,

j

$$= 1.43 A B C \left(\theta * \frac{\pi}{180} \right)^{0.247} \left(\frac{F_l}{L_p} \right)^{-0.201} \left(\frac{F_l}{F_d} \right)^{0.306} \left(\frac{L_l}{F_l} \right)^{0.801} \left(\frac{F_l}{T_p} \right)^{-0.0162} \left(\frac{L_p}{F_p} \right)^{0.226} \left(1 - \frac{F_t}{L_p} \right)^{2.32},$$

where

$$A = Re_{L_p}^{\left(-0.435 - 0.0286 \cosh\left(\frac{F_p}{L_p} - 2.14\right) \right)},$$

$$B = 1 - \frac{\sin\left(\frac{L_p}{F_p} \theta\right)}{\cosh\left(0.0482 Re_{L_p} - 0.0763 \frac{F_d}{F_p}\right)}, \text{ and}$$

$$C = 1 + 0.00245 \left(\frac{F_d}{F_p} \right) \tan(\theta) \cos\left(2\pi \left(\frac{F_p}{L_p} \cot(\theta) - 1.77 \right) \right).$$

Dry

Geometries = 104 including those studied before [48, 53, 57, 61, 68, 69]

$F_p = 0.51 \sim 5.08 \text{ mm}$

$L_p = 0.81 \sim 3.0 \text{ mm}$

$\theta = 8.34 \sim 35.92^\circ$

$F_l = 2.84 \sim 19.0 \text{ mm}$

$L_l = 2.13 \sim 17.18 \text{ mm}$

$F_d = 15.6 \sim 44.0 \text{ mm}$

$F_t = 0.0254 \sim 0.16 \text{ mm}$

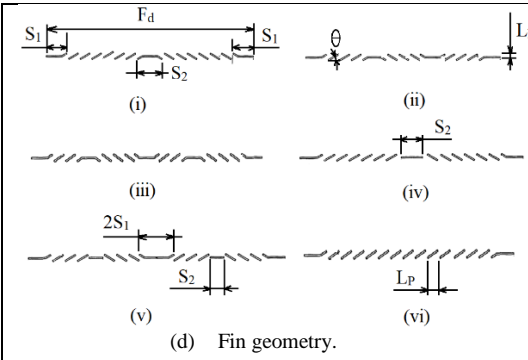
$T_d = 13.54 \sim 44.0 \text{ mm}$

$T_p = 7.51 \sim 24.0 \text{ mm}$

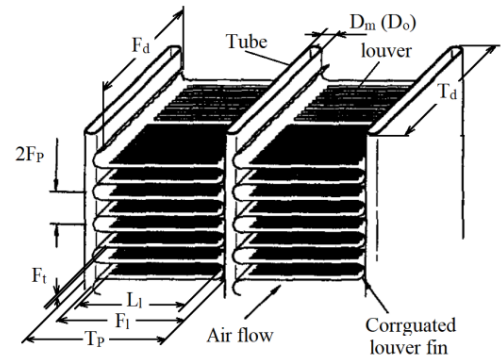
Uncertainty –

The entire experimental data were correlated within error $\pm 11.1\%$.

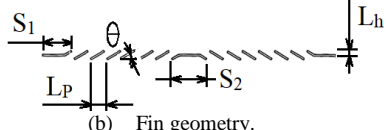
[62]



Multi-louvered fin with triangular channels,



(a) Corrugated louver with triangular channels [59].



For $2850 < Re_{L_p} \leq 11000$,

$$j = 0.065842 \left(\frac{F_d}{L_p Re_{L_p} Pr} \right)^{0.6317} \left(\frac{L_p}{F_p} \right)^{-0.4825} \left(\frac{F_d \tan \theta}{F_p} \right)^{-0.433} \left(\frac{\delta}{F_t} \right)^{-1.1902} \left(\frac{L_l}{F_t} \right)^{-0.2074},$$

$$f = 0.07667 \left(\frac{F_d}{L_p Re_{L_p} Pr} \right)^{0.3211} \left(\frac{L_p}{F_p} \right)^{-2.0217} (\tan \theta)^{-2.3501} \left(\frac{\delta}{F_t} \right)^{-2.5343} \left(\frac{L_l}{F_t} \right)^{-0.7862}.$$

Dry Geometries = more than 12

$$L_p / F_p > 0.56 / \tan(\theta)$$

$$\theta = 20.0 \sim 34.0^\circ$$

$$F_t = 0.15 \sim 1 \text{ mm}$$

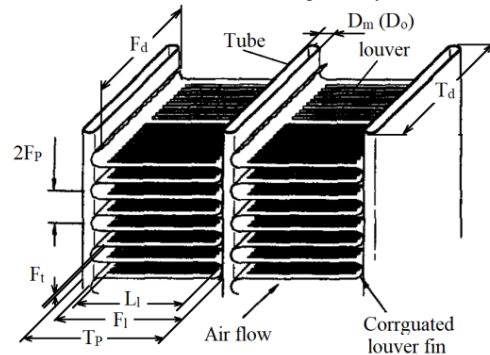
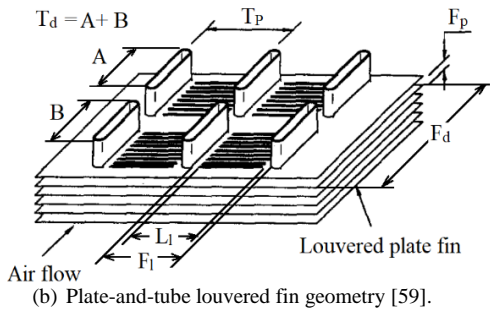
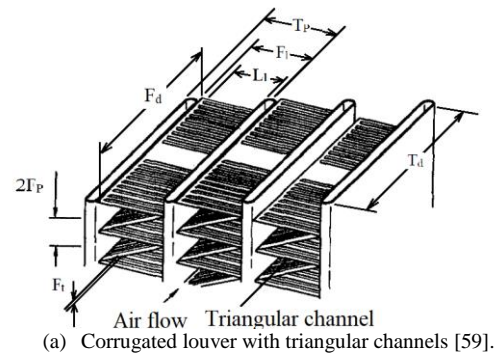
$$\delta \geq 1.5 F_t \text{ mm}$$

$$L_p \tan(\theta) / F_p = 0.75 \sim 0.858$$

Uncertainty –
95 % of the data were correlated within error $\pm 5 \%$.

[63]

Louvered-fin flat-tube (all types),



For $27 \leq Re_{Lp} \leq 4132$,

j

$$= 0.872 ABC \left(\theta * \frac{\pi}{180} \right)^{0.219} N_{lb}^{-0.0881} \left(\frac{F_t}{L_p} \right)^{0.149} \left(\frac{F_d}{F_t} \right)^{-0.259} \left(\frac{L_l}{F_t} \right)^{0.540} \left(\frac{F_t}{T_p} \right)^{-0.902} \left(1 - \frac{F_t}{L_p} \right)^{2.62} \left(\frac{L_p}{F_p} \right)^{0.301}, \quad (1)$$

where

$$A = Re_{Lp}^{\left(-0.458 - 0.00874 \cosh\left(\frac{F_p}{L_p} - 1 \right) \right)},$$

$$B = 1 - \frac{\sin\left(\frac{L_p}{F_p} \theta \right)}{\cosh\left(0.0490 Re_{Lp} - 0.142 \frac{F_d}{N_{lb} F_p} \right)}, \text{ and}$$

$$C = 1 + 0.0065 \left(\frac{F_d}{N_{lb} F_p} \right) \tan(\theta) \cos\left(2\pi \left(\frac{F_p}{L_p} \cot(\theta) - 1.8 \right) \right).$$

Dry

Geometries = 126 including those studied before [3, 48, 53, 54, 59, 61, 62, 68, 69]

$F_p = 0.51 \sim 5.08 \text{ mm}$

$L_p = 0.5 \sim 3.0 \text{ mm}$

$\theta = 8.34 \sim 35.9^\circ$

$F_t = 2.84 \sim 20.0 \text{ mm}$

$L_l = 2.13 \sim 18.5 \text{ mm}$

$F_d = 15.6 \sim 57.4 \text{ mm}$

$F_t = 0.0254 \sim 0.16 \text{ mm}$

$N_{lb} = 1 \sim 4$

$T_p = 3.76 \sim 25.0 \text{ mm}$

[41]

Uncertainty –

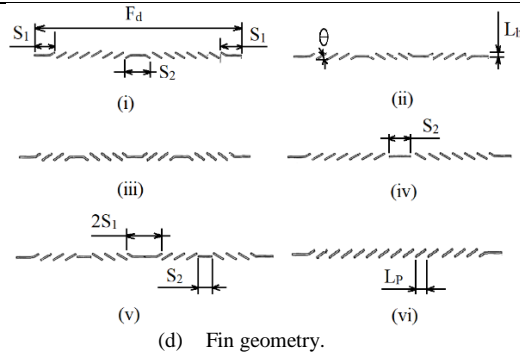
j : the experimental data were correlated within error $\pm 11.5\%$.

f : the experimental data were correlated within error $\pm 16.1\%$.

$$f = 3.69 A1 N_{lb}^{-0.256} \left(\frac{F_p}{L_p} \right)^{0.904} \left(\theta * \frac{\pi}{180} + 0.20 \right)^t \left(1 - \frac{F_t}{T_p} \right)^{0.733} \left(\frac{L_l}{F_t} \right)^{0.648} \left(\frac{F_t}{L_p} \right)^{-0.647} \left(\frac{F_t}{F_p} \right)^{0.799},$$

where

$$A1 = \left(Re_{Lp} \frac{F_p}{L_p} \right)^{-0.845} + 0.0013 Re_{Lp}^{\left(1.26 \left(\frac{F_t}{F_p} \right) \right)},$$



† A correction has been made to the louver angle term.

Amongst the correlations listed in Table 1, Chang and Wang [59] and Chang et al. [58] introduced air-side f - and j -factor correlations for all types of louvered fin heat exchangers using 91 different designs, including those of previous experimental data [48, 53, 55, 57-59, 68-70]. The percentage of including the experimental data in the correlations was higher and showed a smaller error than those of the previous works, as shown in Figure 4. For example, with error of $\pm 15\%$, Chang and Wang [59] and Chang et al. [58] included more than 90% of the experimental data to obtain both j - and f -factor correlations, whereas the other previous works included less than 70% of the total available experimental data, this is also shown in Figure 4. Later, Jacobi et al. [62] formulated a j -factor correlation from data studied by [53, 57, 59, 61, 68, 69] in addition to some new cores to represent a total of 104 different louver-fin cores. They claimed that the entire experimental data were correlated within error of $\pm 11.1\%$. Wider range of geometries (126 cores) to obtain f - and j -factor correlations were conducted by Park and Jacobi [41]. They gathered the experimental data from previous works [3, 48, 53, 54, 58, 59, 61, 62, 68, 69] in addition to their new heat exchanger cores. These newly formulated correlations were claimed to have small errors in comparison to those reported by Chang and Wang [59], Chang et al. [58], and Kim and Bullard [61]. However, Figure 5 shows that the correlation error differences among studies (Park and Jacobi [41], Chang and Wang [59], Chang et al. [58], and Kim and Bullard [61]) were not significant except the errors associated with f -factor introduced by Kim and Bullard [61].

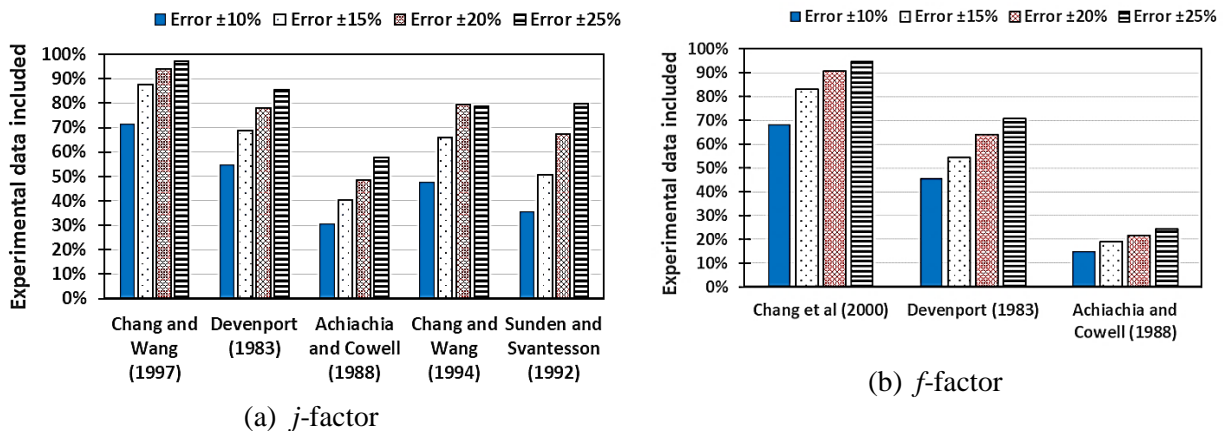


Figure 4. Comparison among experimental data inclusions to obtain j - and f -factor correlations. The charts (a) and (b) are plotted based on the data reported by Chang and Wang [59] and Chang et al. [58].

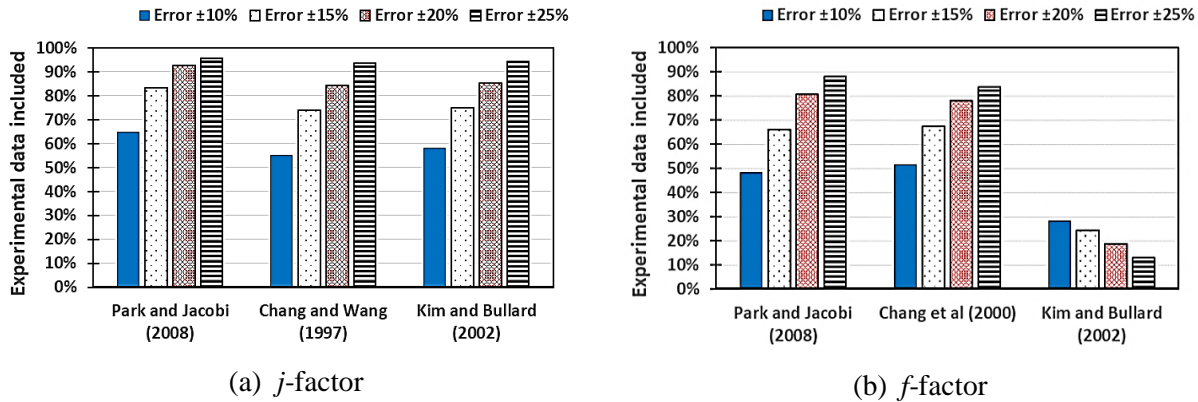


Figure 5. Comparison of experimental data inclusions to obtain *j*- and *f*-factor correlations. The charts (a) and (b) are plotted based on the data reported by Park and Jacobi [41].

To compare these generalized correlations [41, 58, 59, 62], in particular, we have plotted Figure 6 to represent both *j*- and *f*- factor correlations of these studies against experimental values reported by Kays and London [40] for ‘1/4(b)-11.1’ core, in which the geometrical parameters are the closest to the design limitations of the correlations (as described in Table 1). Practically, these correlations show an excellent agreement with those reported by Kays and London [40], as shown in Figure 6. Therefore, we recommend the use of such correlations for the air-side of louver-fin microchannel and compact heat exchangers. This recommendation is drawn based upon the closeness of the correlation values with the experimental data, and considering the previous experimental data. These correlations are actually used for air-side in dry conditions while the wet and frost fin surfaces still need massive experimental investigations to obtain generalized *f*- and *j*-factor correlations.

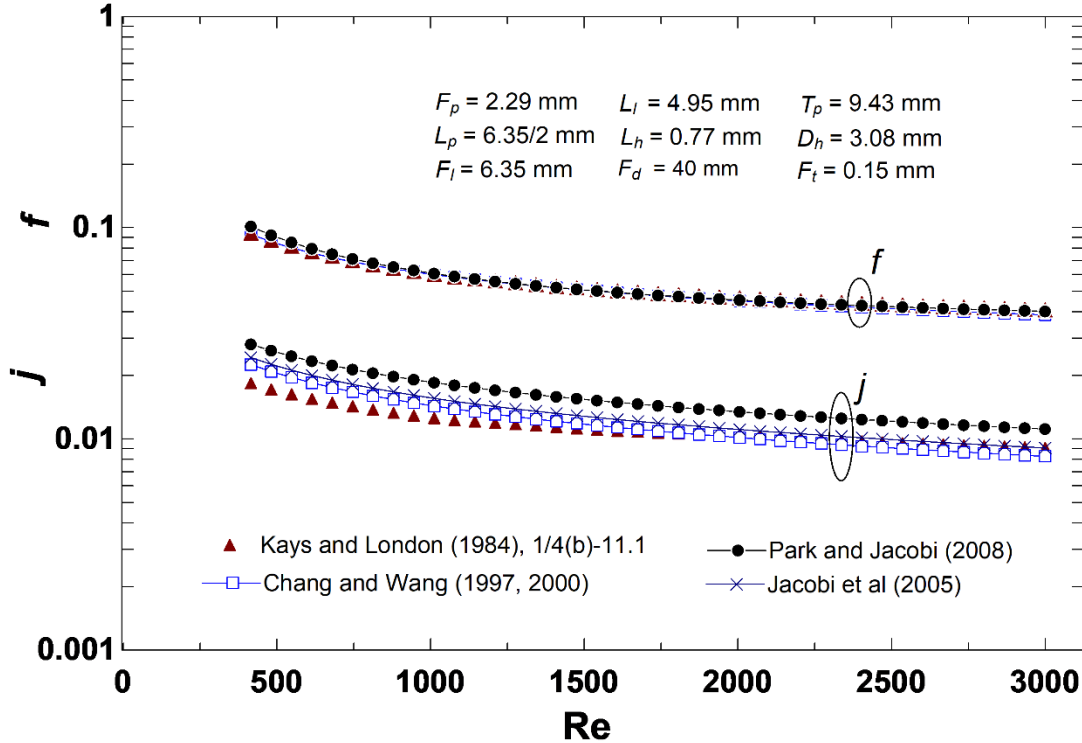


Figure 6. An example to demonstrate the accuracy of some reported j - and f -factor correlations [41, 58, 59, 62] by comparing to the experimental data [40].

2.3. Wavy-fin compact and microchannel heat exchangers

This section discusses the air-side heat and fluid-flow correlations of the wavy-fin arrangements that are constructed between flat tubes (in case of compact heat exchangers) or between microchannel slabs (in case of microchannel heat exchangers). Wavy-fin arrangements are particularly attractive because of the simplicity of their manufacturing and the potential to enhance heat transfer area. Recently, they are widely used because of their good heat transfer and lower pressure drop performances. Additionally, they demonstrate a good resistance to dust accumulation and blockage under different environmental conditions [71]. The wavy-fin enlarges the flow path resulting in better air mixing [72]. It is important to emphasize that heat transfer performance of the louver-fin is better than that of wavy-fin under clean conditions; the dust accumulation and air blockage over time result in lower heat and fluid-flow performances. In this case, the wavy-fin is recommended in off-road vehicles and engineering machinery [71]. The

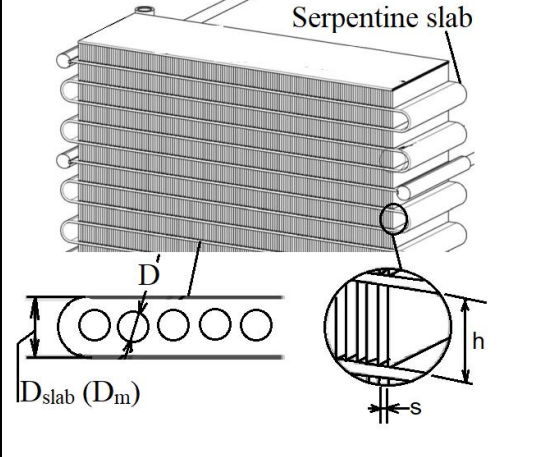
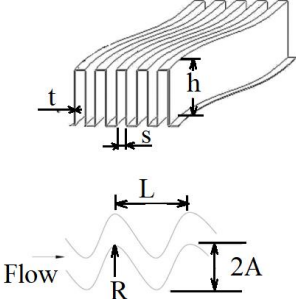
wavy-path of airflow may result in a high pressure drop; so that, a good geometry that achieves a high heat transfer and a low pressure drop.

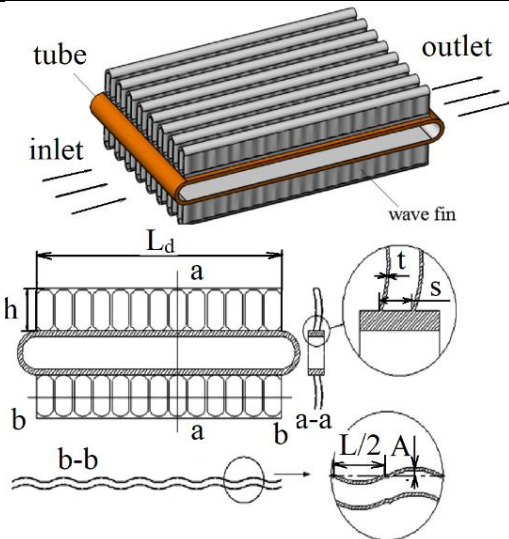
The air-side thermal-hydraulic characteristics of wavy-fin heat exchangers are influenced by wavy-fin construction geometry such as the channel corrugation ratio ($2A/L$), fin-spacing ratio ($F_p/2A$), flow length ratio (L_d/L), and flow cross-section aspect ratio (F_p/h) [73]. Dong et al. [71] evaluated the significance of this geometrical performance on the heat transfer and fluid-flow performance in term of $j/f^{d/3}$. About 39% of the performance was influenced by variation of wavy amplitude to the wavelength ($2A/L$). Independently, fin length (L_d) and fin height (F_h) contributed by about 20%. And about 18% was the effect of fin pitch (F_p) on the performance.

The published investigations on these type of fins on heat and fluid-flow performance characteristics are very limited [71]. Kays and London [40] introduced j - and f -factor experimental data for three different surface geometries (115-3/8W, 178-3/8W, and 1144-3/8W) of wavy-fin heat exchangers. Junqi et al. [74] obtained thermal-hydraulic characteristics using eleven wavy-fin geometries. The flow cross-sectional area of used wavy-fin was non-perfect rectangular (the fins corrugate almost in sinusoidal shape). A CFD modeling was carried [75] to obtain j - and f -factor correlation using 18 cores for wavy-fin, having a rectangular cross-section of flow path. Siddiqui et al. [33], also, tried to correlate heat and fluid-flow characteristics of wavy-fin mesochannel heat exchangers. The study was limited to one construction. The correlations for wavy-fin having rectangular flow path were also obtained using 15 [76] and 25 [77] different geometries by CFD models. An experimental investigation to obtain Nusselt number and f -factor correlation was carried out using 16 cores of rectangular flow cross-sectional area [71]. The most recent study [78], to formulate thermal-hydraulic performance characteristics, was a CFD modeling using 16 intermittent wavy-fin cores of non-rectangular flow path. A multiport slabs heat exchanger was experimentally investigated by Dasgupta et al. [79]. The relevant Nusselt number and f -factor correlations were obtained based on only one geometry, whereas the detailed specifications of air-side were not described. In this regard, the reported thermal-hydraulic performance correlations of wavy-fin are listed in Table 2.

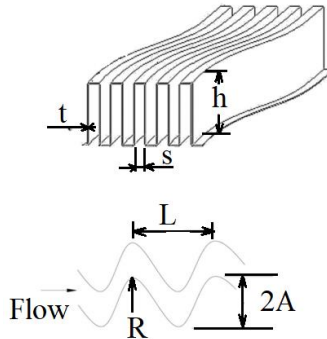
Table 2. Summary of reported heat and flow performance correlations using wavy fin geometries.

Geometry	Correlations	Conditions and limitations	Ref.
Wavy fin geometry having non- perfect flow cross-sectional area,	<p>For $600 \leq Re_{D_h} \leq 6500$,</p> $j = 0.0836 Re_{D_h}^{-0.2309} \left(\frac{F_p}{h}\right)^{0.1284} \left(\frac{F_p}{2A}\right)^{-0.153} \left(\frac{L_d}{L}\right)^{-0.326},$ $f = 1.16 Re_{D_h}^{-0.309} \left(\frac{F_p}{h}\right)^{0.3703} \left(\frac{F_p}{2A}\right)^{-0.25} \left(\frac{L_d}{L}\right)^{-0.1152},$ <p>where D_h is the hydraulic diameter of the fin entrance.</p>	<p>Dry Geometries = 11 $F_p = 2.0 \sim 2.5$ mm $L_d = 43 \sim 65$ mm $h = 7 \sim 10$ mm $t = 0.2$ mm $2A = 1.5$ mm $L = 10.8$ mm</p> <p>Uncertainty – 95% of experimental data were correlated within error $\pm 10\%$.</p>	[74]
Wavy fin geometry having non- perfect rectangular flow cross-sectional area,	<p>For $600 \leq Re_{D_h} \leq 6500$,</p> $Nu = 0.0864 Re_{D_h}^{0.914} \left(\frac{F_p}{h}\right)^{-0.301} \left(\frac{2A}{L}\right)^{0.7875} \left(\frac{L_d}{L}\right)^{-0.254} \left(\frac{2A}{L_d}\right)^{-0.226},$ $j = \frac{Nu}{Re_{D_h} Pr^{\frac{1}{3}}},$ $f = 15.46 Re_{D_h}^{-0.416} \left(\frac{F_p}{h}\right)^{-0.138} \left(\frac{2A}{L}\right)^{1.098} \left(\frac{L_d}{L}\right)^{-0.45} \left(\frac{2A}{L_d}\right)^{-0.506},$ <p>where D_h is the hydraulic diameter of the fin entrance.</p>	<p>Dry Geometries = 16</p> <p>$F_p = 4 \sim 8$ mm $L_d = 55 \sim 145$ mm $h = 7.5 \sim 10.3$ mm $t = 0.2$ mm $2A = 0.75 \sim 2.4$ mm $L = 10.8 \sim 20$ mm</p> <p>Uncertainty – Nu: 91.5% of experimental data were correlated within error $\pm 15\%$. f: 93.2% of experimental data were correlated within error $\pm 15\%$.</p>	[71]
Wavy fin multi-port serpentine cross-flow,	<p>For $752 \leq Re_{D_h} \leq 3165$,</p> $j = 0.874 Re_{D_h}^{-0.716},$ $f = 0.778 Re_{D_h}^{-0.375}.$	<p>Dry Geometries = 1</p> <p>$s = 2.11$ mm $h = 15.77$ mm $D_h = 3.49$ mm $A_{min} = 70.92$ mm2</p>	[33]

		<p>$D_m = 2 \text{ mm}$</p> <p>Uncertainty – the experimental data were correlated within error $\pm 10\%$.</p>	
<p>Wavy fin geometry having rectangular flow cross-sectional area,</p> 	<p>For $600 \leq Re_{D_h} \leq 800$ (laminar),</p> $j = 2.348 Re_{D_h}^{-0.786} \left(\frac{h}{s}\right)^{0.312} \left(\frac{2A}{s}\right)^{-0.192} \left(\frac{L}{2A}\right)^{-0.432},$ $f = 9.827 Re_{D_h}^{-0.705} \left(\frac{h}{s}\right)^{0.322} \left(\frac{2A}{s}\right)^{-0.394} \left(\frac{L}{2A}\right)^{-0.603}.$ <p>For $1000 \leq Re_{D_h} \leq 15000$ (turbulent),</p> $j = 0.242 Re_{D_h}^{-0.375} \left(\frac{h}{s}\right)^{0.235} \left(\frac{2A}{s}\right)^{-0.288} \left(\frac{L}{2A}\right)^{-0.553},$ $f = 10.628 Re_{D_h}^{-0.359} \left(\frac{h}{s}\right)^{0.264} \left(\frac{2A}{s}\right)^{-0.848} \left(\frac{L}{2A}\right)^{-1.931},$ <p>where</p> $D_h = \frac{2(s-t)h}{((s-t)+h)}.$	<p>Dry Geometries = 18</p> $1.178 \leq \frac{s}{h} \leq 20.8$ $0.636 \leq \frac{2A}{s} \leq 2.6$ $3.85 \leq \frac{L}{2A} \leq 7.65$ <p>Uncertainty – 75% and 99% of data were correlated for f and j-factor, respectively, for laminar flow. Also, 86% and 98% of data were correlated for f and j-factor, respectively, for turbulent flow. The maximum error of f correlation is $\pm 20\%$, and that of j is $\pm 10\%$.</p>	[75]
<p>Intermittent wavy finned flat tube,</p>	<p>For $215 \leq Re_{D_h} \leq 1290$,</p> $Nu = 1.5437 Re_{D_h}^{0.4057} \left(\frac{S}{d}\right)^{-0.3309} \left(\frac{A}{d}\right)^{0.4714} \left(\frac{L}{2d}\right)^{0.0988},$ $j = \frac{Nu}{Re_{D_h} Pr^{\frac{1}{3}}},$ $f = 25.469 Re_{D_h}^{-0.5204} \left(\frac{S}{d}\right)^{-0.9079} \left(\frac{A}{d}\right)^{0.9647} \left(\frac{L}{2d}\right)^{0.9428}.$ <p>Here, A is the wavy length amplitude, and</p> $D_h = \frac{2(s-t)h}{((s-t)+h)}.$	<p>Dry Geometries = 11</p> $0.12 \leq \frac{s}{d} \leq 0.16$ $0.055 \leq \frac{A}{d} \leq 0.135$ $0.455 \leq \frac{L}{2d} \leq 0.55$ <p>Uncertainty – j: the data were correlated within error $\pm 8\%$. f: the data were correlated within error $\pm 6\%$.</p>	[78]



Wavy fin geometry having rectangular flow cross-sectional area,



For $Re_{D_h} < 1900$ (laminar),

$$j = 0.2951 Re_{D_h}^{-0.1908} \left(\frac{F_p}{D_h}\right)^{0.7356} \left(\frac{h}{D_h}\right)^{0.1378} \left(\frac{L}{D_h}\right)^{-0.3171} \left(\frac{t}{D_h}\right)^{0.0485} \left(\frac{2A}{D_h}\right)^{0.2467} \left(\frac{L_d}{D_h}\right)^{-0.4976},$$

$$f = 38.7488 Re_{D_h}^{-0.3840} \left(\frac{F_p}{D_h}\right)^{-1.479} \left(\frac{h}{D_h}\right)^{-0.3696} \left(\frac{L}{D_h}\right)^{-1.4542} \left(\frac{t}{D_h}\right)^{0.1016} \left(\frac{2A}{D_h}\right)^{1.0903} \left(\frac{L_d}{D_h}\right)^{-0.1549}.$$

For $Re_{D_h} \geq 1900$ (turbulent),

$$j = 0.7293 Re_{D_h}^{-0.3637} \left(\frac{F_p}{D_h}\right)^{0.7966} \left(\frac{h}{D_h}\right)^{0.2398} \left(\frac{L}{D_h}\right)^{-0.4979} \left(\frac{t}{D_h}\right)^{0.0402} \left(\frac{2A}{D_h}\right)^{0.2012} \left(\frac{L_d}{D_h}\right)^{-0.3026},$$

$$f = 52.2375 Re_{D_h}^{-0.3524} \left(\frac{F_p}{D_h}\right)^{-1.6277} \left(\frac{h}{D_h}\right)^{-0.3529} \left(\frac{L}{D_h}\right)^{-1.7484} \left(\frac{t}{D_h}\right)^{0.1034} \left(\frac{2A}{D_h}\right)^{1.2294} \left(\frac{L_d}{D_h}\right)^{-0.2371},$$

where D_h is the hydraulic diameter of the fin entrance.

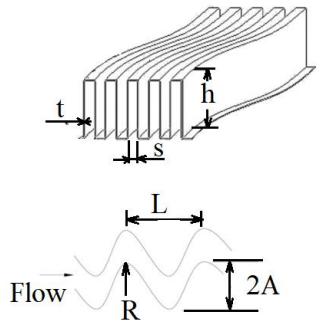
Dry Geometries = 25

$F_p = 1.5 \sim 3.5$ mm
 $h = 6.0 \sim 10.0$ mm
 $L = 7.0 \sim 11.0$ mm
 $L_d = 35 \sim 99$ mm
 $t = 0.1 \sim 0.15$ mm
 $2A = 0.5 \sim 2.5$ mm

Uncertainty –
 j : 98.0% of the experimental data were correlated within error $\pm 10\%$.
 f : 98.0% of the experimental data were correlated within error $\pm 10\%$.

[77]

Wavy fin geometry having rectangular flow cross-sectional area,



For $600 \leq Re_{D_h} \leq 7000$,

$$j = 0.0482 Re_{D_h}^{-0.23725} \left(\frac{F_p}{h}\right)^{-0.1230} \left(\frac{L_d}{L}\right)^{-0.21835},$$

$$f = 0.4006 Re_{D_h}^{-0.28666} \left(\frac{F_p}{h}\right)^{-0.09879} \left(\frac{L_d}{L}\right)^{0.072543},$$

where D_h is the hydraulic diameter of the fin entrance.

Dry Geometries = 15

$$F_p = 2 \sim 2.5 \text{ mm}$$

$$h = 7.0 \sim 10.0 \text{ mm}$$

$$L = 10.8 \text{ mm}$$

$$L_d = 43 \sim 65 \text{ mm}$$

$$t = 0.1 \sim 0.3 \text{ mm}$$

$$2A = 1.0 \sim 2.0 \text{ mm}$$

Uncertainty –
 j : average deviation is 3.22%.
 f : average deviation is 3.68%..

[76]

In the present study we selected some of the listed correlations in Table 2 to compare with the three well-known wavy-fin experimental designs of Kays and London [40] (115-3/8W, 178-3/8W, and 1144-3/8W). The selection is based on the parametric limitation of the validity of these correlations. Figure 7 shows the heat and fluid-flow correlations of the rectangular (Ismail and Velraj [75] and Aliabadi et al. [77]) and non-perfect rectangular (Junqi et al. [74]) cross-sectional area flow-path of the wavy-fin cores against Reynolds number values. Despite all the three experimental data [40] sets were mainly obtained from using a rectangular cross-section flow-path, the j - and f -factor correlations of non-perfect rectangular flow-path arrangement (Figure 7(a)) show a fair agreement with those of experimental data. A small discrepancy shown in the j -factor values might be arising by the variation of wavy-fin construction from that of the experimental data. For rectangular cross-section flow-path of wavy-fin arrangements (Figure 7(b) and (c)), the correlations values match well with those of the experimental data [40]. Notably, the correlations represented in Figure 7(b) and 8(c) are obtained from CFD simulation data. This demonstrates that CFD modeling is a good tool to obtain thermal-hydraulic correlations for different type of heat exchangers.

2.4. Offset strip-fin compact and microchannel heat exchangers

Offset-strip fins are usually used for enhancing heat transfer rate by increasing the air-side surface area and by regenerating thermal boundary layers in each channel [80]. The pressure drop due to enhancing the heat transfer by strip-fins should be reasonably low. Numerous researches investigated offset strip-fin heat exchangers. Sheik Ismail et al. [10] reviewed heat and flow performances of the offset strip-fin heat exchangers. One of the first determinations of the geometrical parameters effect on the heat transfer coefficient of offset strip-fin was by Norris and Spofford [81]. Briggs and London [82] studied the effect of fin pitch on thermal performance of offset-fin surfaces. By testing 22 different strip-fin arrangements, Wieting [47] obtained empirical correlations for heat and fluid-flow performances. Thermal-hydraulic characteristics for several designs of such types of heat exchangers were reported by Kays and London [40]. Joshi and Webb [83] obtained j - and f -factor correlation testing about 21 strip-fin heat exchangers. Mochizuki et

al. [84] attempted to modify the correlations obtained by Wieting [47] to formulate more accurate correlations.

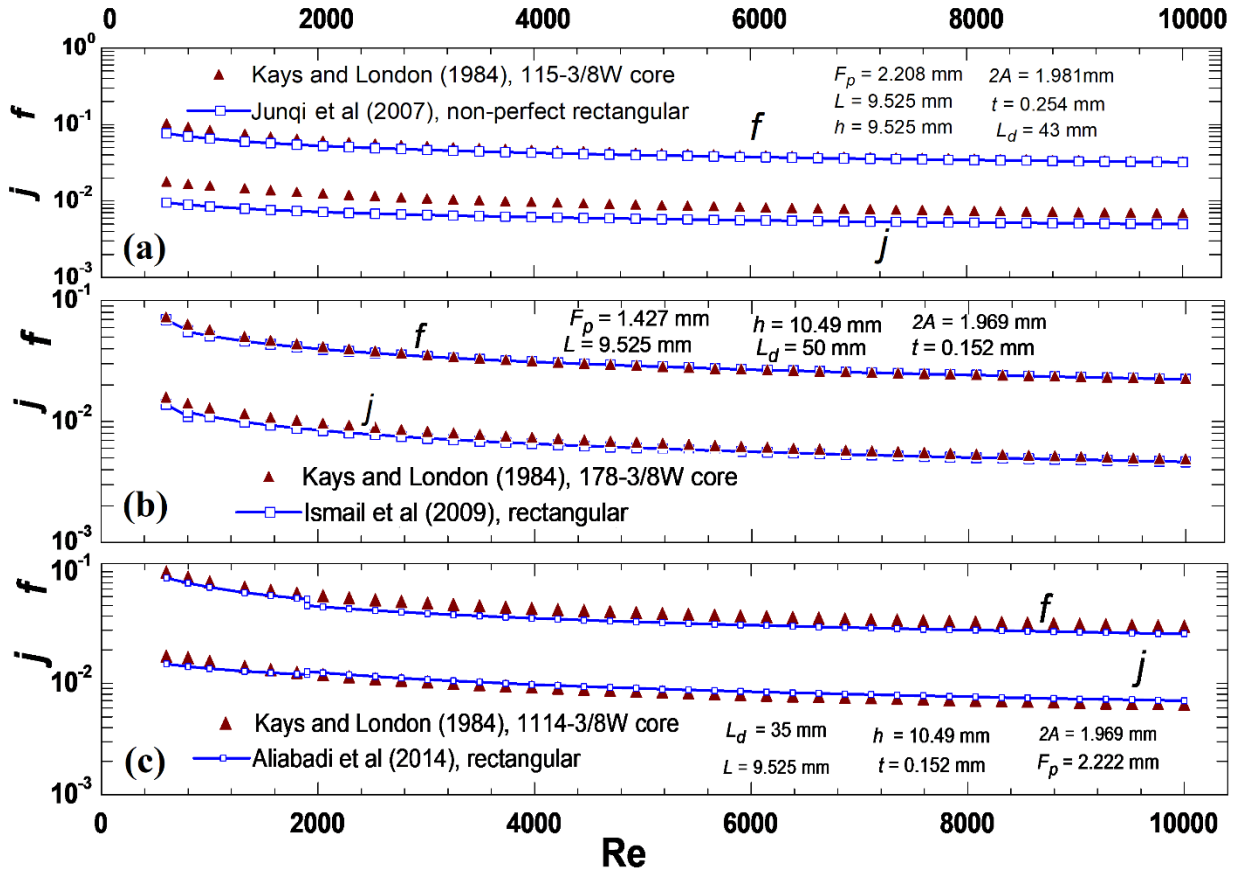


Figure 7. Comparison of j - and f -factor correlations of different wavy-fin heat exchangers with the experimental data of Kays and London [40]: (a) non-perfect rectangular (experimental based) by Junqi et al. [74], (b) rectangular (CFD simulation based) [75], and (c) rectangular (CFD simulation based) (Aliabadi et al. [77]).

The most commonly used correlations in literature are those obtained by Manglik and Bergles [85]. Also, Dong et al. [86] formulated empirical correlations of heat and flow performances by considering 16 strip-fin cores focusing on the effect of fin space, fin height, fin thickness, fin length and flow length on the heat transfer rate. For more involved designs (39 cores), Kim et al. [87] developed new correlations for thermal-hydraulic performances. Moreover, a CFD simulation was used to obtain j - and f -factor correlations by testing about 15 offset-strip-fin heat exchangers [88]. A generalized j - and f -factor correlations were recently formulated [89] by using numerical simulation by testing 55 strip-fin cores; the results were in excellent agreement with those of

experimental data [40, 86, 90]. Song et al. [2] formulated the most recent j - and f -factor correlations by simulating 7 geometries of offset-fin strip heat exchangers. As a function of Reynolds number, Bhowmik and Lee [91] only developed a limited f - and j -factor correlation by studying one offset strip-fin geometry. Upon one set of geometrical parameters, kuchhadiya and Rathod [92] developed a j -factor correlation. Thermal-hydraulic performances of a cross-flow plate-fin heat exchanger, having offset strip-fin, were also conducted [93-95].

The developed j - and f -factor correlations to evaluate thermal-hydraulic performances of offset strip-fin heat exchangers are listed in Table 3 in accordance to geometries shown in Figure 8. In this regard, the correlations are presented along with their limitations over the operating Reynolds number range and geometrical parameters as well as their fitting accuracy.

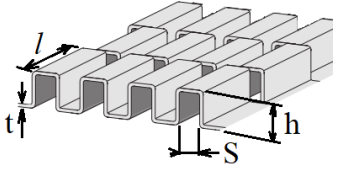
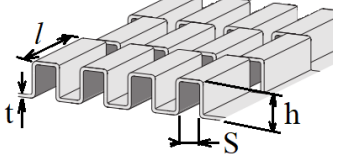
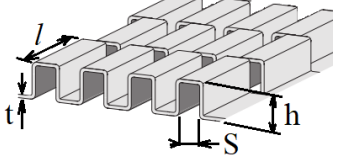


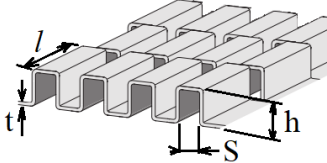
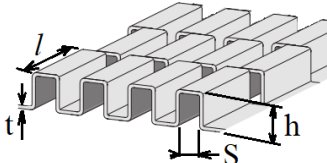
Figure 8. Offset strip fin picture [88].

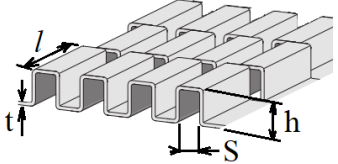
Table 3. Summary of reported thermal-hydraulic performance correlations using offset strip-fin geometries.

Geometry	Correlations	Conditions and limitations	Ref.
Offset strip-fin,	<p>For $300 \leq Re_{D_h} \leq 800$,</p> $j = 0.661 Re_{D_h}^{-0.651} \left(\frac{S}{h}\right)^{-0.313} \left(\frac{t}{S}\right)^{-0.538} \left(\frac{t}{l}\right)^{0.305},$ $f = 10.882 Re_{D_h}^{-0.79} \left(\frac{S}{h}\right)^{-0.359} \left(\frac{t}{S}\right)^{-0.187} \left(\frac{t}{l}\right)^{0.284}.$ <p>For $1000 \leq Re_{D_h} \leq 15000$,</p> $j = 0.185 Re_{D_h}^{-0.396} \left(\frac{S}{h}\right)^{-0.178} \left(\frac{t}{S}\right)^{-0.403} \left(\frac{t}{l}\right)^{0.29},$ $f = 2.237 Re_{D_h}^{-0.236} \left(\frac{S}{h}\right)^{-0.347} \left(\frac{t}{S}\right)^{0.151} \left(\frac{t}{l}\right)^{0.639},$ <p>where</p> $D_h = \frac{2(s-t)hl}{(sl+hl+th)}.$	<p>Dry Geometries = 15</p> <p>$0.254 \leq \frac{s}{h} \leq 1.693$</p> <p>$0.1 \leq \frac{t}{s} \leq 0.2$</p> <p>$0.023 \leq \frac{t}{l} \leq 0.0714$</p> <p>Uncertainty – 96% and 99% of the data have correctly predicted j- and f-factor, respectively, for laminar flow, while 96% of the data was correlated for both j- and f-factor for turbulent flow.</p>	[88]
Offset strip-fin,	<p>For $100 \leq Re_{D_h} \leq 6000$,</p> <p>and for $B < 20\%$,</p> $j = 0.655 Re_{D_h}^{(0.015 \ln Re_{D_h} - 0.623)} \left(\frac{S}{h}\right)^{-0.136} \left(\frac{t}{l}\right)^{0.236} \left(\frac{t}{S}\right)^{-0.158},$ $f = 2724.39 Re_{D_h}^{(0.126 \ln Re_{D_h} - 2.3)} \left(\frac{S}{h}\right)^{-0.159} \left(\frac{t}{l}\right)^{0.358} \left(\frac{t}{S}\right)^{-0.033}.$ <p>For $20\% \leq B < 25\%$,</p> $j = 1.18 Re_{D_h}^{(0.0445 \ln Re_{D_h} - 0.982)} \left(\frac{S}{h}\right)^{-0.134} \left(\frac{t}{l}\right)^{0.0373} \left(\frac{t}{S}\right)^{0.118},$ $f = 11614.389 Re_{D_h}^{(0.142 \ln Re_{D_h} - 2.39)} \left(\frac{S}{h}\right)^{-0.0025} \left(\frac{t}{l}\right)^{-0.0373} \left(\frac{t}{S}\right)^{1.58}.$ <p>For $25\% \leq B < 30\%$,</p> $j = 0.49 Re_{D_h}^{(0.049 \ln Re_{D_h} - 0.971)} \left(\frac{S}{h}\right)^{-0.23} \left(\frac{t}{l}\right)^{0.245} \left(\frac{t}{S}\right)^{-0.733},$ $f = 252.144 Re_{D_h}^{(0.111 \ln Re_{D_h} - 1.87)} \left(\frac{S}{h}\right)^{-0.36} \left(\frac{t}{l}\right)^{0.552} \left(\frac{t}{S}\right)^{-0.521}.$ <p>For $30\% \leq B < 35\%$,</p> $j = 0.22 Re_{D_h}^{(0.0313 \ln Re_{D_h} - 0.729)} \left(\frac{S}{h}\right)^{-0.315} \left(\frac{t}{l}\right)^{0.235} \left(\frac{t}{S}\right)^{-0.727},$	<p>Dry Geometries = 39</p> <p>$0.1 \leq \frac{s}{h} \leq 2$</p> <p>$0.042 \leq \frac{t}{s} \leq 0.4$</p> <p>$0.01 \leq \frac{t}{l} \leq 0.4$</p> <p>$0.648 \leq D_h \leq 5.494$ mm</p> <p>Blockage ratio;</p> $B = \frac{A_{total} - A_{vacancy}}{A_{total}} = \frac{(2s+2t)(h+t) - 2sh}{(2s+2t)(h+t)}$ <p>Uncertainty – $R^2 = 0.98$.</p>	[87]

	$f = 126.469 Re_{D_h}^{(0.089 \ln Re_{D_h} - 1.49)} \left(\frac{S}{h}\right)^{-0.48} \left(\frac{t}{l}\right)^{0.374} \left(\frac{t}{s}\right)^{0.511},$ <p>where</p> $D_h = \frac{2shl}{(sl + hl + th) + 0.50 ts}.$		
Offset strip-fin,	<p>For $Re_{D_h} \leq Re^*$ (laminar flow),</p> $j = 0.6522 Re_{D_h}^{-0.5403} \left(\frac{S}{h}\right)^{-0.1541} \left(\frac{t}{l}\right)^{0.1499} \left(\frac{t}{s}\right)^{-0.0678},$ $f = 9.6243 Re_{D_h}^{-0.7422} \left(\frac{S}{h}\right)^{-0.1856} \left(\frac{t}{l}\right)^{0.3053} \left(\frac{t}{s}\right)^{-0.2659}.$ <p>For $Re_{D_h} \geq Re^*$ (turbulent flow),</p> $j = 0.2435 Re_{D_h}^{-0.4063} \left(\frac{S}{h}\right)^{-0.1037} \left(\frac{t}{l}\right)^{0.1955} \left(\frac{t}{s}\right)^{-0.1733},$ $f = 1.8699 Re_{D_h}^{-0.2993} \left(\frac{S}{h}\right)^{-0.0936} \left(\frac{t}{l}\right)^{0.6820} \left(\frac{t}{s}\right)^{-0.2423}.$ <p>For both laminar and turbulent,</p> $j = 0.6522 Re_{D_h}^{-0.5403} \left(\frac{S}{h}\right)^{-0.1541} \left(\frac{t}{l}\right)^{0.1499} \left(\frac{t}{s}\right)^{-0.0678} \left[1 + 5.269 \times 10^{-5} Re_{D_h}^{1.340} \left(\frac{S}{h}\right)^{0.504} \left(\frac{t}{l}\right)^{0.456} \left(\frac{t}{s}\right)^{-1.055} \right]^{0.1},$ $f = 9.6243 Re_{D_h}^{-0.7422} \left(\frac{S}{h}\right)^{-0.1856} \left(\frac{t}{l}\right)^{0.3053} \left(\frac{t}{s}\right)^{-0.2659} \left[1 + 7.669 \times 10^{-8} Re_{D_h}^{4.429} \left(\frac{S}{h}\right)^{0.920} \left(\frac{t}{l}\right)^{3.767} \left(\frac{t}{s}\right)^{0.236} \right]^{0.1},$ <p>where</p> $Re^* = 257 \left(\frac{l}{s}\right)^{1.23} \left(\frac{t}{l}\right)^{0.58} D_h \left[t + 1.328 \left(\frac{Re_{D_h}}{l D_h}\right)^{-0.5} \right]^{-1},$ <p>and</p> $D_h = \frac{2shl}{(sl + hl + th) + 0.50 ts}.$	<p>Dry Geometries = 18</p> <p>$0.134 \leq \frac{s}{h} \leq 1.034$ $0.012 \leq \frac{t}{l} \leq 0.060$ $0.038 \leq \frac{t}{s} \leq 0.195$ $0.646 \leq D_h \leq 3.414 \text{ mm}$</p> <p>Uncertainty – $R^2 = 0.987$ for f laminar; $R^2 = 0.942$ for j laminar; $R^2 = 0.923$ for f turbulent; $R^2 = 0.972$ for j turbulent, at 99% level of confidence. For both laminar and turbulent, the experimental data were correlated within error $\pm 20\%$.</p>	[85]
Offset strip-fin,	<p>For $Re_{D_h} \leq Re^*$ (laminar flow),</p>	<p>Dry Geometries = 21</p> <p>$0.134 \leq \frac{s}{h} \leq 1.0$</p>	[83]

	$j = 0.53 Re_{D_h}^{-0.50} \left(\frac{l}{D_h} \right)^{-0.15} \left(\frac{s}{h} \right)^{-0.14},$ $f = 8.12 Re_{D_h}^{-0.74} \left(\frac{l}{D_h} \right)^{-0.41} \left(\frac{s}{h} \right)^{-0.02}.$ <p>For $Re_{D_h} \geq (Re^* + 1000)$ (turbulent flow),</p> $j = 0.21 Re_{D_h}^{-0.40} \left(\frac{l}{D_h} \right)^{-0.24} \left(\frac{t}{D_h} \right)^{0.02},$ $f = 1.12 Re_{D_h}^{-0.36} \left(\frac{l}{D_h} \right)^{-0.65} \left(\frac{t}{D_h} \right)^{0.17},$ <p>where</p> $Re^* = 257 \left(\frac{l}{s} \right)^{1.23} \left(\frac{t}{l} \right)^{0.58} D_h \left[t + 1.328 \left(\frac{Re_{D_h}}{l D_h} \right)^{-0.5} \right]^{-1},$ <p>and</p> $D_h = \frac{2(s-t)hl}{(sl + hl + th)}.$	$0.012 \leq \frac{t}{l} \leq 0.06$ $0.038 \leq \frac{t}{s} \leq 0.202$ $0.632 \leq D_h \leq 3.124 \text{ mm}$ <p>Uncertainty – 80% of the f data and 75 % of the j data were correlated within error $\pm 10\%$ for the laminar flow; and 88 % of the f data and 97 % of the j data are predicted within error $\pm 20\%$ for the turbulent flow.</p>	
Offset strip-fin, 	<p>For $Re_{D_h} \leq 1000$,</p> $j = 0.483 Re_{D_h}^{-0.536} \left(\frac{l}{D_h} \right)^{-0.162} \left(\frac{s}{h} \right)^{-0.184},$ $f = 7.661 Re_{D_h}^{-0.712} \left(\frac{l}{D_h} \right)^{-0.384} \left(\frac{s}{h} \right)^{-0.092}.$ <p>For $Re_{D_h} \geq 2000$,</p> $j = 0.242 Re_{D_h}^{-0.368} \left(\frac{l}{D_h} \right)^{-0.322} \left(\frac{t}{D_h} \right)^{0.089},$ $f = 1.136 Re_{D_h}^{-0.198} \left(\frac{l}{D_h} \right)^{-0.781} \left(\frac{t}{D_h} \right)^{0.534},$ <p>where</p> $D_h = \frac{2sh}{s+h}.$	Dry Geometries = 22 $0.7 \leq \frac{l}{D_h} \leq 5.6$ $0.126 \leq \frac{s}{h} \leq 1.196$ $0.03 \leq \frac{t}{D_h} \leq 0.166$ <p>Uncertainty – j: 85% of the experimental data were correlated within error $\pm 10\%$ f: 85% of the experimental data were correlated within error $\pm 15\%$</p>	[47]
Offset strip-fin, 	<p>For $Re_{D_h} < 2000$,</p> $j = 1.37 Re_{D_h}^{-0.67} \left(\frac{l}{D_h} \right)^{-0.25} \left(\frac{s}{h} \right)^{-0.184},$ $f = 5.55 Re_{D_h}^{-0.67} \left(\frac{l}{D_h} \right)^{-0.32} \left(\frac{s}{h} \right)^{-0.092}.$ <p>For $Re_{D_h} \geq 2000$,</p>	Dry Geometries = 18 $9.84 \leq \frac{l}{D_h} \leq 10.4$ $1 \leq \frac{L}{F_p} \leq 15$ $0.938 \leq \frac{s}{t} \leq 15$ $0.75 \leq \frac{c}{F_p} \leq 15$ $0.5 \leq \frac{c}{l} \leq 0.89$ $F_p = s+t$	[84]

	$j = 1.17 Re_{D_h}^{-0.36} \left(\frac{l}{D_h} + 3.75 \right)^{-1} \left(\frac{t}{D_h} \right)^{0.089},$ $f = 0.83 Re_{D_h}^{-0.20} \left(\frac{l}{D_h} + 0.33 \right)^{-0.5} \left(\frac{t}{D_h} \right)^{0.534},$ <p>where</p> $D_h = \frac{2sh}{s+h}.$	Uncertainty – just mentioned as excellent accuracy.	
Offset strip-fin,	 <p>For $300 \leq Re_{D_h} \leq 8000$,</p> $j = 2.34812 X \left(\frac{l}{D_h} \right)^{0.19411} Y^{0.00656} \left(\frac{t}{h} \right)^{-0.35987} \left(\frac{t}{s} \right)^{0.10391} \left(\frac{t}{l} \right)^{0.45337},$ <p>where</p> $X = \exp \left(-1.01546 \ln(Re_{D_h}) + 0.05633 \left(\ln(Re_{D_h}) \right)^2 - 0.00064 \left(\frac{h}{D_h} \right)^{0.49317} \left(\frac{t}{s} \right)^{-0.16019} \left(\ln(Re_{D_h}) \right)^3 \right),$ $Y = \left(\frac{h}{t} + \frac{s}{2t} - 2 \right)^{\left(\frac{2t}{s} \left(1 - \frac{t}{h} \right) + \frac{t}{h} \left(1 - \frac{2t}{s} \right) \right)} + \frac{4t \left(1 - \frac{t}{h} \right) + \frac{t}{h} \left(1 - \frac{2t}{s} \right)}{4 \left(\frac{t}{s} + \frac{t}{h} - 2 \frac{t^2}{s h} \right)},$ <p>and</p> $f = 2300.24 Z \left(\frac{l}{D_h} \right)^{-1.42491} Y^{0.26188} \left(\frac{1}{1-2\frac{t}{h}} \right)^{2.04570} \left(\frac{1}{1-2\frac{t}{s}} \right)^{2.16338} \left(\frac{t}{l} \right)^{-0.93414},$ <p>where</p> $Z = \exp \left(-4.52412 \ln(Re_{D_h}) + 0.49785 \left(\ln(Re_{D_h}) \right)^2 - 0.01580 \left(\frac{h}{D_h} \right)^{0.00222} \left(\frac{t}{s} \right)^{-0.08664} \left(\ln(Re_{D_h}) \right)^3 \right),$ $D_h = \frac{2sh}{s+h}.$	Dry Geometries = 55 0.021 $\leq \frac{t}{h} \leq 0.149$ 0.067 $\leq \frac{t}{s} \leq 0.30$ 0.033 $\leq \frac{t}{l} \leq 0.167$ 10% $\leq B$ (blockage) \leq 60% 1.735 $\leq D_h \leq$ 4.182 mm	[89]
Offset strip-fin,	 <p>For $500 \leq Re_{D_h} \leq 7500$,</p> $j = 0.101 Re_{D_h}^{-0.189} \left(\frac{S}{h} \right)^{-0.488} \left(\frac{t}{l} \right)^{0.479} \left(\frac{t}{s} \right)^{-0.297} \left(\frac{L_d}{l} \right)^{-0.315},$ $f = 2.092 Re_{D_h}^{-0.281} \left(\frac{S}{h} \right)^{-0.739} \left(\frac{t}{l} \right)^{0.972} \left(\frac{t}{s} \right)^{-0.780} \left(\frac{L_d}{l} \right)^{-0.497}.$ $D_h = \frac{2sh}{s+h}.$	Dry Geometries = 16 0.184 $\leq \frac{s}{h} \leq 0.338$ 0.02 $\leq \frac{t}{l} \leq 0.04$ 0.071 $\leq \frac{t}{s} \leq 0.111$ 4.5 $\leq \frac{L_d}{l} \leq 14.3$ Uncertainty –	[86]

		<i>j</i> : 95% of the experimental data were correlated within error $\pm 10\%$. <i>f</i> : 90% of the experimental data were correlated within error $\pm 10\%$.	
Offset strip-fin,	 <p>For $300 \leq Re_{D_h} \leq 10000$,</p> $j = 0.6522 Re_{D_h}^{-0.5403} \left(\frac{S}{h}\right)^{-0.1541} \left(\frac{t}{l}\right)^{0.1499} \left(\frac{t}{s}\right)^{-0.0678} \left[1 + 5.269 \times 10^{-5} Re_{D_h}^{1.340} \left(\frac{S}{h}\right)^{0.504} \left(\frac{t}{l}\right)^{0.456} \left(\frac{t}{s}\right)^{-1.055}\right]^{0.1},$ $f = 9.6243 Re_{D_h}^{-0.7422} \left(\frac{S}{h}\right)^{-0.1856} \left(\frac{t}{l}\right)^{0.3053} \left(\frac{t}{s}\right)^{-0.2659} \left[1 + 7.669 \times 10^{-8} Re_{D_h}^{4.429} \left(\frac{S}{h}\right)^{0.920} \left(\frac{t}{l}\right)^{3.767} \left(\frac{t}{s}\right)^{0.236}\right]^{0.1},$ <p>where</p> $D_h = \frac{2shl}{(sl+hl+th)+0.50ts}.$ <p>Also, for the same conditions except that $0.195 \leq \frac{t}{s} \leq 0.214$,</p> $f = \exp \left[0.132856 (\ln Re_{D_h})^2 - 2.28042 (\ln Re_{D_h}) + 6.79634 \right],$ <p>where</p> $D_h = \frac{2sh}{s+h}.$	Dry Geometries = 7 (valid in the range of correlations of [85, 96]) $0.129 \leq \frac{s}{h} \leq 1.185$ $0.012 \leq \frac{t}{l} \leq 0.060$ $0.038 \leq \frac{t}{s} \leq 0.195$ Uncertainty – <i>j</i> : the data were correlated within error $\pm 13\%$. <i>f</i> : the experimental data were within error $\pm 8\%$.	[2]

Because the experimental j - and f -factor data of 1/8-19.86 surface (Kays and London [40]) were obtained based on strip-fin design parameters that agree with the limitations of tabulated correlations (Table 3) (except those of Mochizuki et al. [84] and Dong et al. [86]), we compare the j - and f -factor values of all the correlations with this experimental data [40], as shown in Figure 9. Obviously, some correlations exhibit an excellent agreement with the experimental data including those of Manglik and Bergles [85], which are frequently taken as a reference for strip-fin compact heat exchangers. Moreover, the correlations obtained by Wieting [47], Kim et al. [87], and Song et al. [2] are matching excellent with the experimental data, and so that for those obtained by Chennu and Paturu [88], except some discrepancy for f -factor in the laminar region. Another excellent matching between experimental data and correlation is achieved by the recently generalized heat and fluid-flow correlations, by Yang and Li [89]. Even with the fact that the plotted experimental data are out of the correlation limitations of Mochizuki et al. [84], Figure 9 shows a good agreement between them leading to low caution when using these correlations. Simulation-based correlations were represented by Chennu and Paturu [88], Kim et al. [87], and Song et al. [2] showing a remarkable accuracy with those of experimental data. The discrepancy shown by using Dong et al. [86] correlations is because the geometrical ratio s/h is about 0.47, which is out of the correlation limitations ($s/h < 0.34$). Regardless of this disagreement, the f - and j -factor, at high Re values, show an acceptable matching with the experimental data.

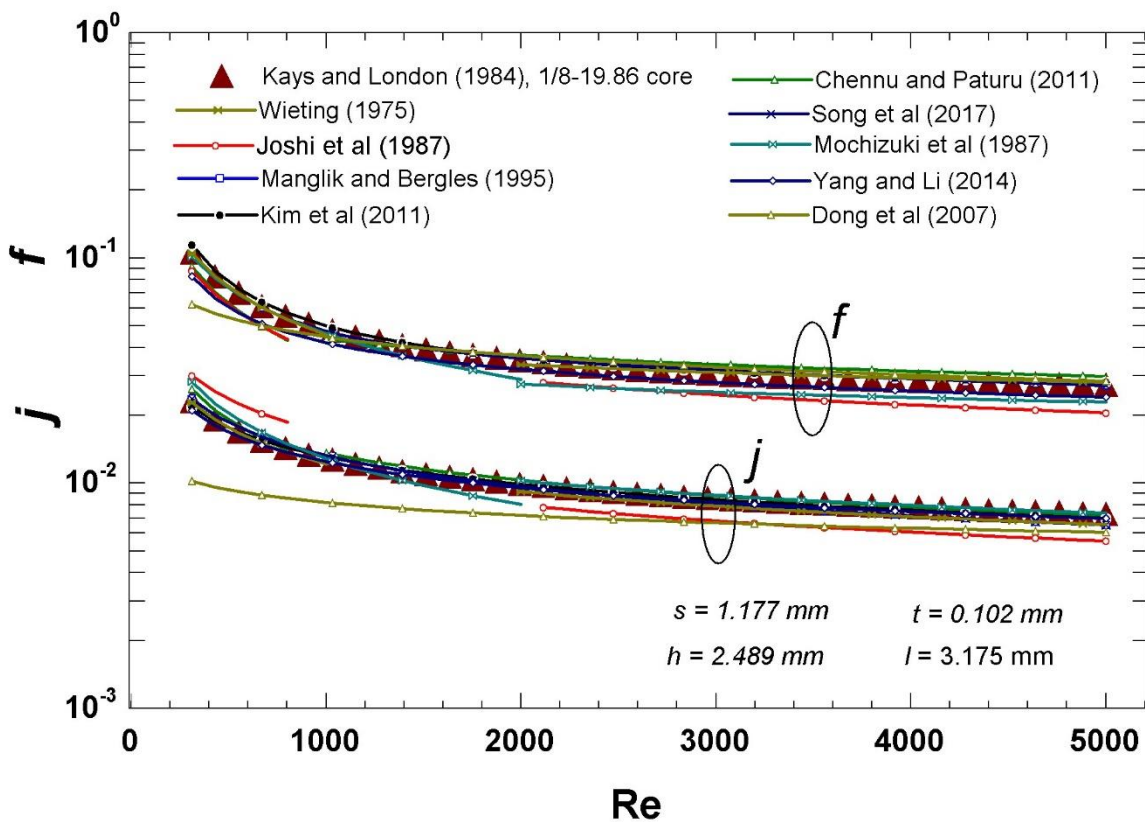


Figure 9. Comparison of j - and f -factor correlations of air-side strip-fin heat exchangers with the experimental data of Kays and London [40]. Some correlations are experimental-based (Wieting [47], Joshi and Webb [83], Mochizuki et al. [84], Manglik and Bergles [85], and Dong et al. [86]) and others are CFD simulation-based (Chennu and Paturu [88], Yang and Li [89], Kim et al. [87], and Song et al. [2]).

2.5. Fin and tube (round) compact heat exchangers

Fin and tube heat exchangers are only available for the compact heat exchangers; the tube diameter is much larger (> 6 mm) to be considered for the microchannel heat exchangers. Most heat exchangers designed for heating, ventilation, air conditioning and refrigeration use fin-and-tube geometries. Many fin patterns are constructed to enhance heat transfer performance on the air-side [97]. The comment geometries of fin and tube compact heat exchangers are shown in Figure 10. The conventionally existed fin-and-tube heat exchangers have plane-fins and round tubes. However, the fins can be plane plates, corrugated plates, spiral around tubes, H-type plates,

slit plates, louvered plates, and plates with vortex generators. The selection of these surfaces should be primarily based on a maximum heat transfer and a minimum friction power.

Because the fin-and-tube heat exchangers are widely used, many thermal-hydraulic performance correlations were obtained from both experimental (the majority) and simulation data. In an early study, Briggs and Young [43] developed a fanning friction factor for spiral fin-tube having a staggered arrangement, and Robinson and Briggs [44] proposed a heat transfer characteristic correlation for the same type of fin-and-tube heat exchangers. Wang et al. [98] obtained empirical correlations in terms of f and j factors for a wavy fin-plate (Figure 10(a-iv)) by testing 18 geometries. Abu Madi et al. [99] carried out some experiments to obtain thermal-hydraulic correlations for wavy-plate staggered-tube heat exchangers by testing fifteen different geometries. A slit-plate as a fin was also tested to formulate the performance correlations [100, 101]. For the reason that the flat-plate fins are usually used in such heat exchangers, thermal-hydraulic performance correlations were obtained using a good number of geometries (such as experimental 47 geometries [102] and 74 geometries [103] as well as numerical several geometries [104]). A louver-fin plate was also tested by using 49 different designs of staggered tube heat exchangers [105]. The study ended up with formulating proposed j - and f -factor correlations. Tang et al. [106] carried out some experimental and numerical studies about the effects of vortex generators on improving turbulence and heat transfer rate. The study proposed j and f factor correlations for the vortex-generator fins. The thermal-hydraulic performance correlations of individual fin-tube were also obtained for H-type-fin [107], welded spiral-fin [108], L-footed spiral-fin [109], and crimped spiral-fin [110].

The thermal-hydraulic performance correlations for a humid air-side of finned tube heat exchangers are represented for many types of compact heat exchangers. Wang et al. [111] reported j - and f -factor correlations for a plane plate-fin and staggered tube by studying nine geometries. Wang et al. [112] obtained thermal-hydraulic correlations under wet conditions for herringbone wavy plate-fin using eighteen geometries. Kim and Jacobi [100] investigated condensation effect on the air-side surfaces using coated/uncoated slit-plate fins. They derived j - and f -factor correlations for both coated and uncoated surfaces. Other slotted finned tube correlations were obtained by Kong et al. [113] and compared to some newly obtained correlations for flat-plate fins. More slots arrangements were investigated by Kong et al. [114]. They also developed the

correlations for plain fin by testing 25 different geometries including the effect of the plain plate angle with the tubes [1]. The wet louvered fin and staggered tubes were also tested [115] using ten different geometries to obtain thermal-hydraulic performance correlations. The correlation of j -factor was, moreover, obtained by Kim and Kim [116] under humid conditions using 22 cores of plate-fin inline and staggered tube heat exchangers.

Thermal-hydraulic performance correlations of different finned tube (round) arrangements, representing the airside of compact heat exchangers, are summarized in Table 4. The table also describes the geometrical parameter limitations, the operation range of Reynolds number and fitting uncertainties. Additional performance correlations for some (limited) fin-and-tube geometries were tabulated in recent review papers [117, 118].

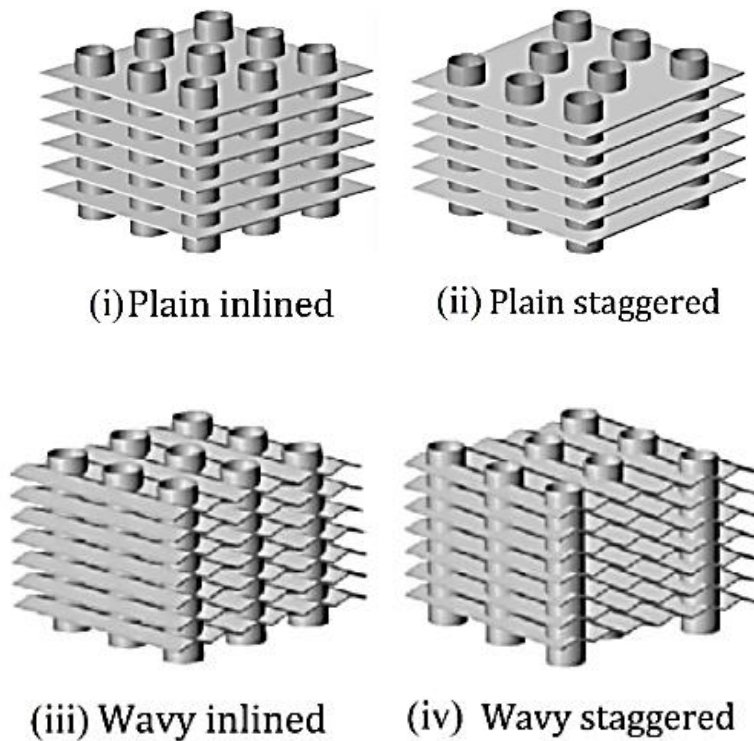
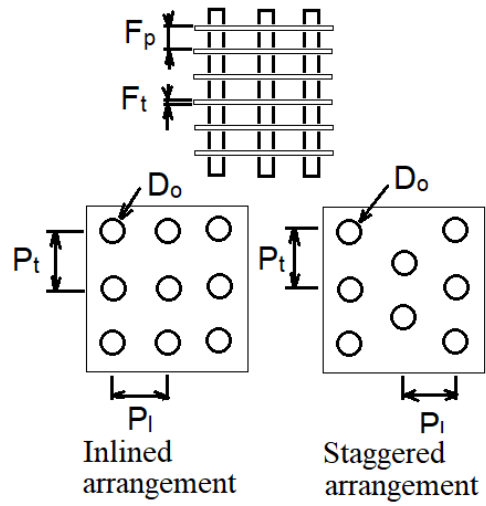
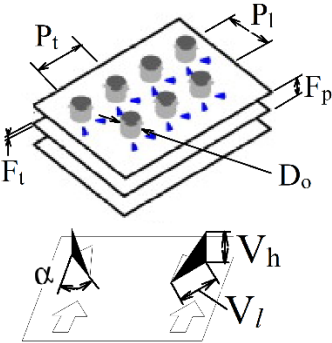
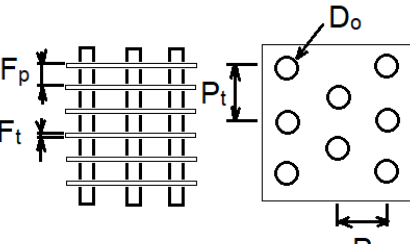
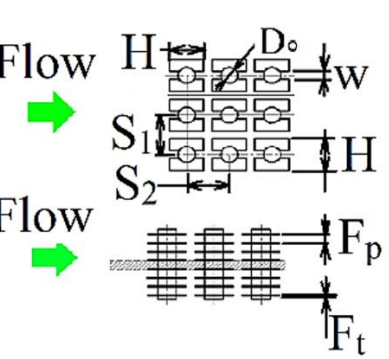
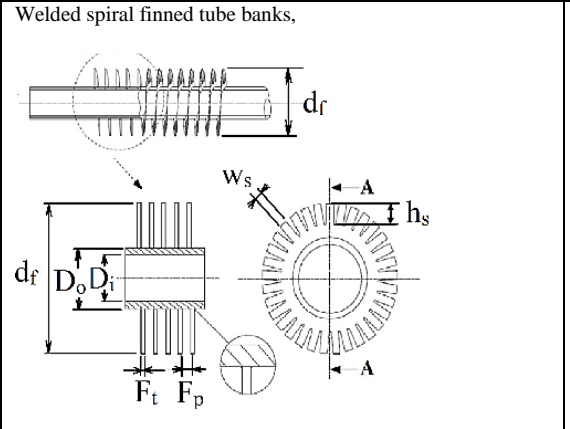
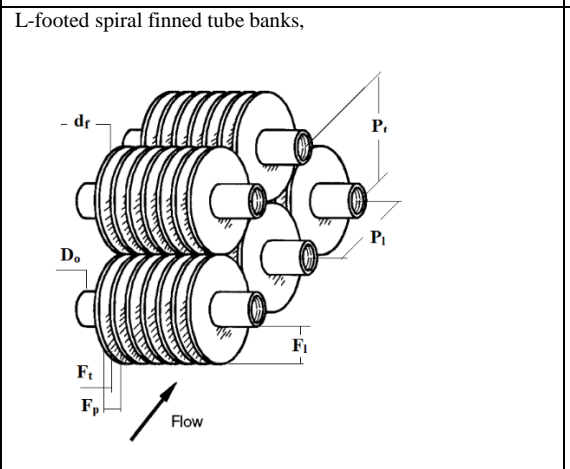
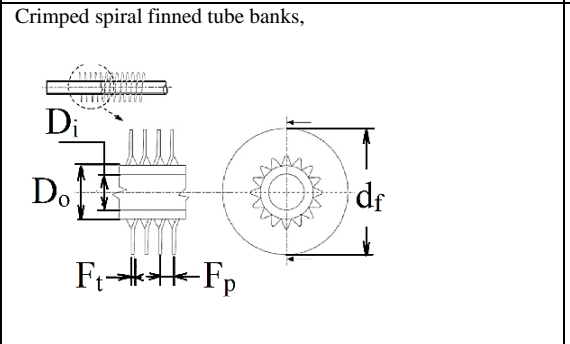


Figure 10. Types of fin and tube arrangement [117].

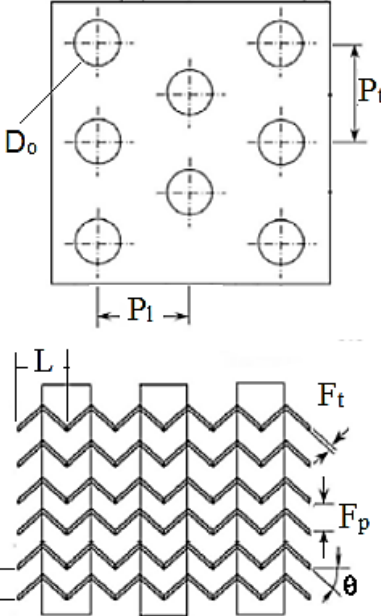
Table 4. Summary of reported thermal-hydraulic performance correlations using fin-and-tube (round) heat exchangers.

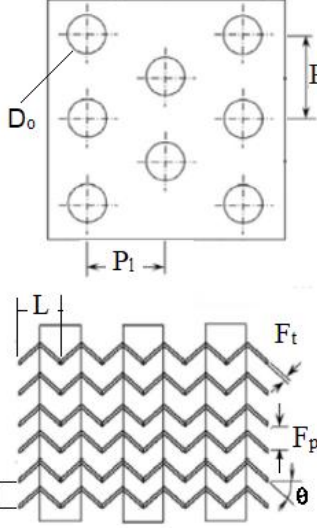
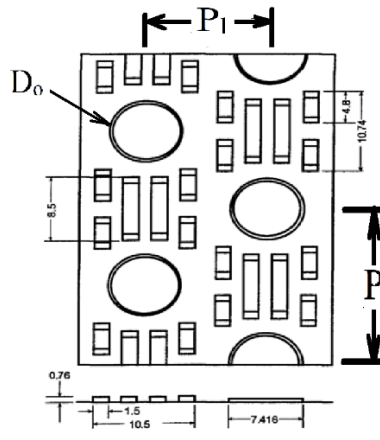
Geometry	Correlations	Conditions and limitations	Ref.
plain fin-tube heat exchangers,  Inlined arrangement Staggered arrangement	<p>For $300 \leq Re_{D_c} \leq 11000$, and for No. of rows $N_{row} = 1$,</p> $j = 0.108 Re_{D_c}^{-0.29} \left(\frac{P_t}{P_l} \right)^{(1.9-0.23\ln(Re_{D_c}))} \left(\frac{F_p}{D_c} \right)^{-1.084} \left(\frac{F_p}{D_h} \right)^{-0.768} \left(\frac{F_p}{P_t} \right)^{(-0.236+0.126\ln(Re_{D_c}))}.$ <p>For $N_{row} \geq 2$,</p> $j = 0.086 Re_{D_c}^X N_{row}^Y \left(\frac{F_p}{D_c} \right)^Z \left(\frac{F_p}{D_h} \right)^M \left(\frac{F_p}{P_t} \right)^{-0.93},$ <p>where</p> $X = -0.361 - 0.042 \frac{N_{row}}{\ln(Re_{D_c})} + 0.1581 \ln \left(N_{row} \left(\frac{F_p}{D_h} \right)^{0.41} \right),$ $Y = -1.224 - 0.076 \frac{\left(\frac{P_t}{D_h} \right)^{1.42}}{\ln(Re_{D_c})},$ $Z = -0.083 + 0.058 \frac{N_{row}}{\ln(Re_{D_c})},$ $M = -5.735 + 1.21 \ln \left(\frac{Re_{D_c}}{N_{row}} \right).$ <p>For all N_{row} values,</p> $f = 0.0267 Re_{D_c}^{X_1} \left(\frac{P_t}{P_l} \right)^{Y_1} \left(\frac{F_p}{D_c} \right)^{Z_1},$ <p>where</p> $X_1 = -0.764 + 0.739 \left(\frac{P_t}{P_l} \right) + 0.177 \left(\frac{F_p}{D_c} \right) - \frac{0.00758}{N_{row}},$ $Y_1 = -15.689 + \frac{64.021}{\ln(Re_{D_c})},$ $Z_1 = 1.696 - \frac{15.695}{\ln(Re_{D_c})},$ $D_c = D_o + 2F_t,$ $D_h = \frac{4A_c L_d}{A_o}, \text{ and } L_d \text{ is the core depth.}$	<p>Dry Geometries = 74 (including geometries of [45, 46, 119-123])</p> <p>$F_p = 1.19 \sim 8.7 \text{ mm}$ $D_o = 6.35 \sim 12.7 \text{ mm}$ $D_c = 6.9 \sim 13.6 \text{ mm}$ $D_h = 1.3 \sim 9.37 \text{ mm}$ $P_t = 12.4 \sim 27.5 \text{ mm}$ $P_f = 17.7 \sim 31.75 \text{ mm}$ $F_t = 0.115 \sim 0.2 \text{ mm}$ $N_{row} = 1 \sim 6$</p> <p>Uncertainty – j: 88.6% of the data were correlated within error $\pm 15\%$. f: 85.1% of the data were correlated within error $\pm 15\%$.</p>	[103]
Fin-tube with vortex generator fins,	<p>For $4000 \leq Re_{D_c} \leq 10000$,</p> $j = 0.9856 Re_{D_o}^{0.571} (\sin(\alpha))^{0.0086} \left(\frac{V_h}{V_t} \right)^{0.0014},$ $f = 43.28 Re_{D_o}^{-0.501} (\sin(\alpha))^{0.0143} \left(\frac{V_h}{V_t} \right)^{0.04}.$	<p>Dry Geometries = 3 $\alpha = 30 \sim 60^\circ$ $V_t = 4 \sim 6 \text{ mm}$ $V_h = 1.7 \sim 2.5 \text{ mm}$ $P_t = 42 \text{ mm}$ $F_p = 3.1 \text{ mm}$ $D_o = 18 \text{ mm}$</p>	[106]

	<p>$P_t = 34 \text{ mm}$ $N_{\text{row}} = 12$ $F_t = 0.3 \text{ mm}$</p> <p>Uncertainty – j: all data were correlated within error $\pm 10\%$. f: all data were correlated within error $\pm 2.2\%$.</p>	
<p>Plain fin-tube heat exchangers,</p> 	<p>For $1000 \leq Re_{D_c} \leq 6000$,</p> $Nu = 1.565 Re_{D_c}^{0.3414} \left(N_{\text{row}} \frac{F_p}{D_c} \right)^{-0.165} \left(\frac{P_t}{P_l} \right)^{0.0558},$ $j = \frac{Nu}{Re_{D_c} Pr^{\frac{1}{3}}},$ $f = 20.713 Re_{D_c}^{-0.3498} \left(N_{\text{row}} \frac{F_p}{D_c} \right)^{-0.1678} \left(\frac{P_t}{P_l} \right)^{0.6265},$ <p>where $D_c = D_o + 2F_t$.</p>	<p>Dry Geometries = not mentioned</p> <p>$F_p = 2.0 \sim 4.0 \text{ mm}$ $D_o = 16.0 \sim 20.0 \text{ mm}$ $P_t = 32.0 \sim 36.0 \text{ mm}$ $P_l = 38.0 \sim 46.0 \text{ mm}$ $F_t = 0.115 \sim 0.2 \text{ mm}$ $N_{\text{row}} = 2 \sim 7$</p> <p>Uncertainty – the data were correlated within deviation $\pm 10\%$.</p>
<p>H-type finned tube banks,</p> 	<p>For $2100 \leq Re_{D_o} \leq 21000$,</p> $Nu = 1.66 Re_{D_o}^{0.585} \left(\frac{F_p}{D_o} \right)^{0.389} \left(\frac{F_t}{D_o} \right)^{0.165} \left(\frac{S_1}{D_o} \right)^{-1.108} \left(\frac{S_2}{D_o} \right)^{0.293} \left(\frac{H}{D_o} \right)^{-0.624} \left(\frac{W}{D_o} \right)^{0.029},$ $j = \frac{Nu}{Re_{D_o} Pr^{\frac{1}{3}}}.$ <p>The pressure drop here calculated from Euler number $Eu =$</p> $11.63 Re_{D_o}^{-0.157} \left(\frac{F_p}{D_o} \right)^{-0.693} \left(\frac{F_t}{D_o} \right)^{0.375} \left(\frac{S_1}{D_o} \right)^{-3.026} \left(\frac{S_2}{D_o} \right)^{-0.388} \left(\frac{H}{D_o} \right)^{1.835} \left(\frac{W}{D_o} \right)^{-0.002}.$	<p>Dry Geometries = 7</p> <p>$0.158 \leq \frac{F_p}{D_o} \leq 0.474$ $0.026 \leq \frac{F_t}{D_o} \leq 0.105$ $2.24 \leq \frac{S_1}{D_o} \leq 3.42$ $2.37 \leq \frac{S_2}{D_o} \leq 3.95$ $1.32 \leq \frac{H}{D_o} \leq 2.36$ $0.158 \leq \frac{W}{D_o} \leq 0.632$ $D_o = 38 \text{ mm}$</p> <p>Uncertainty – the data were correlated within error $\pm 10\%$.</p>

Welded spiral finned tube banks, 	For $3000 \leq Re_{D_o} \leq 15000$, $j = 0.09246 Re_{D_o}^{-0.22583}$, $f = 0.76833 Re_{D_o}^{-0.11243} \left(\frac{F_p}{D_o}\right)^{0.33662}$.	Dry Geometries = 3 $F_p = 3.6 \sim 6.2 \text{ mm}$ $D_o = 25.4 \text{ mm}$ $d_f = 50 \text{ mm}$ $P_t = 66 \text{ mm}$ $P_l = 68.5 \text{ mm}$ $F_t = 1 \text{ mm}$ $N_{tube} = 5$ $N_{row} = 2$ Uncertainty – 100% of the experimental data were correlated within error $\pm 10\%$.	[108]
L-footed spiral finned tube banks, 	For $4000 \leq Re_{D_c} \leq 15000$, $j = 0.2150 Re_{D_c}^{-0.4059}$, $f = 0.4852 Re_{D_c}^{-0.2156} \left(\frac{F_p}{D_c}\right)^{0.4771}$, where $D_c = D_o + 2F_t$.	Dry Geometries = 3 $F_p = 2.4 \sim 4.2 \text{ mm}$ $D_o = 13.5 \text{ mm}$ $d_f = 34.8 \text{ mm}$ $P_t = 39 \text{ mm}$ $P_l = 35 \text{ mm}$ $F_t = 0.25 \text{ mm}$ $N_{tube} = 9$ $N_{row} = 2$ Uncertainty – 100% and 95% of the experimental data were correlated for j - and f -factor, respectively, within error $\pm 10\%$.	[109]
Crimped spiral finned tube banks, 	For $3000 \leq Re_{D_o} \leq 13000$, $j = 0.4132 Re_{D_o}^{-0.4287}$, $f = 0.3775 Re_{D_o}^{-0.1485} \left(\frac{F_p}{D_o}\right)^{0.4321}$.	Dry Geometries = 4 $F_p = 3.2 \sim 6.3 \text{ mm}$ $D_o = 16.35 \text{ mm}$ $d_f = 35 \text{ mm}$ $P_t = 40 \text{ mm}$ $P_l = 35 \text{ mm}$ $F_t = 0.5 \text{ mm}$ $N_{tube} = 9$ $N_{row} = 2 - 5$ Uncertainty – 95.04% and 91.07% of the experimental data were	[110]

		correlated for j - and f -factor, respectively, within error $\pm 10\%$.	
Plain fin-tube heat exchangers,	<p>For $505 \leq Re_{D_c} \leq 24707$,</p> $j_{N_{row}=3} = 0.163 Re_{D_c}^{-0.369} \left(\frac{S_t}{S_l}\right)^{0.106} \left(\frac{s}{D_c}\right)^{0.0138} \left(\frac{S_t}{D_c}\right)^{0.13}$ <p>For $591 \leq Re_{D_c} \leq 14430$,</p> $\frac{j_{N_{row}=1,2}}{j_{N_{row}=3}} = 1.043 \left[Re_{D_c}^{-0.14} \left(\frac{S_t}{S_l}\right)^{-0.564} \left(\frac{s}{D_c}\right)^{-0.123} \left(\frac{S_t}{D_c}\right)^{1.17} \right]^{(3-N_{row})}$ <p>For $505 < Re_{D_c} < 19766$,</p> $f = f_f \frac{A_f}{A} + f_m \left(1 - \frac{A_f}{A}\right) \left(1 - \frac{t}{F_p}\right),$ <p>where</p> $f_m = \frac{4}{\pi} \left(0.25 + \frac{0.118}{\left[\frac{S_t}{D_c} - 1\right]^{1.08}} Re_{D_c}^{-0.16} \right) \left[\frac{S_t}{D_c} - 1\right],$ $f_f = 1.455 Re_{D_c}^{-0.656} \left(\frac{S_t}{S_l}\right)^{-0.347} \left(\frac{s}{D_c}\right)^{-0.134} \left(\frac{S_t}{D_c}\right)^{1.23},$ $D_c = D_o + 2F_t.$	<p>Dry/Wet Geometries = 47</p> <p>For $N_{row} \geq 3$ for j-factor and all N_{row} for f-factor</p> $0.857 \leq \frac{S_t}{S_l} \leq 1.654$ $1.996 \leq \frac{s}{D_c} \leq 2.881$ $0.081 \leq \frac{s}{D_c} \leq 0.641$ <p>For $N_{row} = 1,2$ (j-factor)</p> $1.154 \leq \frac{S_t}{S_l} \leq 1.654$ $2.399 \leq \frac{s}{D_c} \leq 2.877$ $0.135 \leq \frac{s}{D_c} \leq 0.300$ <p>Uncertainty – 94% and 90% of the experimental data were correlated for j- and f-factor, respectively, within error $\pm 20\%$.</p>	[102]
Plain fin-tube heat exchangers,	<p>For $600 \leq Re_{D_h} \leq 2000$,</p> $j = 0.17 Re_{D_h} (N_{row})^{-0.141} \left(\frac{F_p}{D_o}\right)^{0.384},$ <p>where</p> $D_h = \frac{4A_c L_d}{A_o}$, and L_d is the core depth.	<p>Wet Geometries = 22</p> $7.5 \leq F_p \leq 15 \text{ mm}$ $1 \leq N_{row} \leq 4$ <p>Uncertainty – 90% of the experimental data were correlated, within error $\pm 10\%$.</p>	[116]
Herringbone wavy fin-tube heat exchangers,	For $300 \leq Re_{D_c} \leq 3500$,	Wet Geometries = 18	[112]

	$j = 0.472293 Re_{D_c}^X (N_{row})^{-0.4933} \left(\frac{P_t}{P_l}\right)^Y \left(\frac{2(2A)}{L}\right)^Z \left(\frac{2A}{2A-F_t}\right)^M,$ <p>where</p> $X = -0.5836 + 0.2371 \left(\frac{2A - F_t}{D_c}\right)^{0.55} (N_{row})^{0.34} \left(\frac{P_t}{P_l}\right)^{1.2},$ $Y = 1.1873 - 3.0219 \left(\frac{F_p - F_t}{D_c}\right)^{1.5} \left(\frac{2(2A)}{L}\right)^{0.9} \left(\ln(Re_{D_c})\right)^{1.22},$ $Z = 0.006672 (N_{row})^{1.96} \left(\frac{P_t}{P_l}\right),$ $M = -0.1157 \left(\frac{F_p - F_t}{D_c}\right)^{0.9} \ln\left(\frac{50}{Re_{D_c}}\right),$ <p>and</p> $f = 0.149001 Re_{D_c}^{X1} \left(\frac{P_t}{P_l}\right)^{Y1} (N_{row})^{Z1} \left(3.1 - \frac{2A}{D_c}\right)^{M1} \left(\frac{F_p}{D_c}\right)^{N1} \left(\frac{2\varphi}{\mu_w}\right)^{0.0769},$ <p>where</p> $X1 = -0.067 + \left(\frac{2A}{F_p - F_t}\right) \left(\frac{1.35}{\ln Re_{D_c}}\right) - 0.15 \left(\frac{N_{row}}{\ln(Re_{D_c})}\right) + 0.0153 \left(\frac{F_p - F_t}{D_c}\right),$ $Y1 = 2.981 - 0.082 \ln(Re_{D_c}) + \frac{0.127(N_{row})}{4.605 - \ln(Re_{D_c})},$ $Z1 = 0.53 - 0.0491 \ln(Re_{D_c}),$ $M1 = 11.91 \left(\frac{(N_{row})}{\ln(Re_{D_c})}\right)^{0.7}$ $N1 = -1.32 + 0.287 \ln(Re_{D_c}),$ $\varphi = \text{condensate flow rate per tube row}, \frac{\dot{m}}{W(N_{row})},$ $D_c = D_o + 2F_t.$	$F_p = 1.7 \sim 3.1 \text{ mm}$ $D_c = 8.62 \sim 10.38 \text{ mm}$ $P_t = 25.4 \text{ mm}$ $2A = 1.18 \sim 1.58 \text{ mm}$ $P_l = 19.0 \sim 22.0 \text{ mm}$ $F_t = 0.12 \text{ mm}$ $N_{row} = 9$ <p>Uncertainty – 93.8% and 84.1% of the experimental data were correlated for j- and f-factor, respectively, within error $\pm 10\%$.</p>	
Herringbone wavy fin-tube heat exchangers,	For $350 \leq Re_{D_c} \leq 3500$, $j = \frac{1.201}{\left(\ln\left(\frac{A_{min}/A_{face}}{Re_{D_c}}\right)\right)^{2.921}},$ $f = \frac{16.67}{\left(\ln(Re_{D_c})\right)^{2.64}} \left(\frac{A_{tot}}{A_{tube}}\right)^{-0.096} (N_{row})^{0.098},$ <p>where</p> $D_c = D_o + 2F_t.$	Dry Geometries = 18 $F_p = 1.69 \sim 3.53 \text{ mm}$ $D_c = 10.3 \text{ mm}$ $P_t = 25.4 \text{ mm}$ $P_l = 19.05 \text{ mm}$ $F_t = 0.12 \text{ mm}$ $N_{row} = 1 \sim 4$ <p>Uncertainty – j: 94.0% of the data were correlated within error $\pm 10\%$. f: 95.0% of the data were correlated within error $\pm 15\%$.</p>	[98]

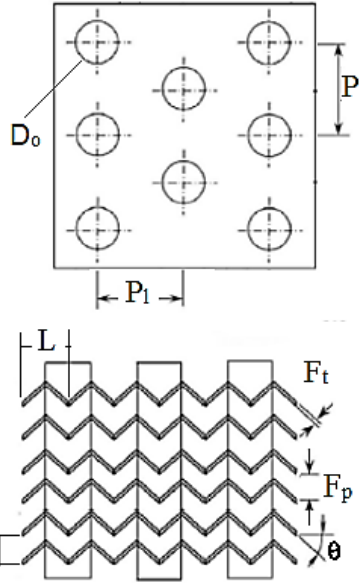
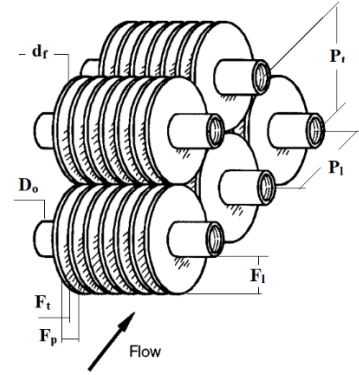
		
<p>Slit fin-tube heat exchangers,</p>  <p>For $550 \leq Re_{D_c} \leq 2000$,</p> $j_{uncoated} = 0.3647 Re_{D_c}^{0.1457} \left(\frac{F_p}{D_c}\right)^{1.21} \left(\frac{F_l N_{row}}{D_c}\right)^{-0.3181}$ $j_{coated} = 0.4559 Re_{D_c}^{-0.2383} \left(\frac{F_p}{D_c}\right)^{0.7139} \left(\frac{F_l N_{row}}{D_c}\right)^{-0.6768}$ $f_{uncoated} = 1.265 Re_{D_c}^{0.2991} \left(\frac{F_p}{D_c}\right)^{-0.2918} \left(\frac{F_l N_{row}}{D_c}\right)^{-0.1985}$ $f_{coated} = 0.502 Re_{D_c}^{-0.2593} \left(\frac{F_p}{D_c}\right)^{0.1516} \left(\frac{F_l N_{row}}{D_c}\right)^{0.5522}$	<p>Wet Geometries = 22 $F_p = 1.3 \sim 1.7 \text{ mm}$ $D_o = 7.264 \text{ mm}$ $P_t = 21.65 \text{ mm}$ $P_l = 12.7 \text{ mm}$ $F_l = 0.076 \text{ mm}$ $N_{row} \leq 3$ Wet contact angle: $\theta_{A, uncoated} = 87.5^\circ$ $\theta_{R, uncoated} = 40.4^\circ$ $\theta_{A, coated} = 9.6^\circ$ $\theta_{R, coated} = 4.3^\circ$ Uncertainty – $j_{uncoated}$: 90.0% of the experimental data were correlated within error $\pm 15\%$. j_{coated}: 95.0% of the experimental data were correlated within error $\pm 15\%$. $f_{uncoated}$: 92.0% of the experimental data were correlated within error $\pm 20\%$. f_{coated}: 94.0% of the experimental data were correlated within error $\pm 20\%$.</p>	[100]

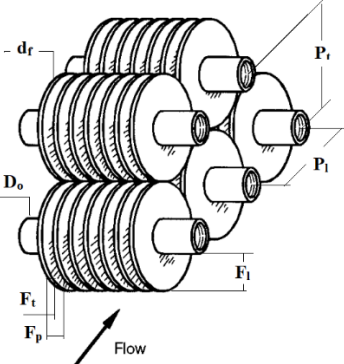
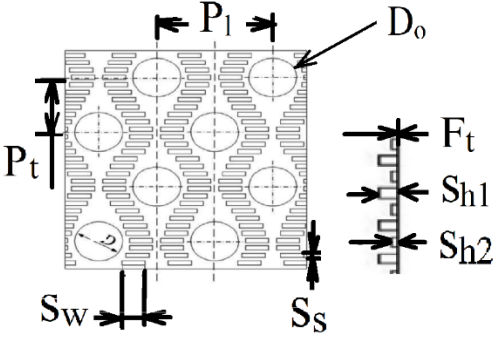
<p>Slit fin-tube heat exchangers,</p>	<p>For $550 \leq Re_{D_c} \leq 2000$,</p> $j_{uncoated} = 0.2476 Re_{D_c}^{-0.209} \left(\frac{F_p}{D_c}\right)^{0.4325} \left(\frac{F_l N_{row}}{D_c}\right)^{-0.3792},$ $j_{coated} = 0.4813 Re_{D_c}^{-0.1329} \left(\frac{F_p}{D_c}\right)^{1.001} \left(\frac{F_l N_{row}}{D_c}\right)^{-0.4967},$ $f_{uncoated} = 1.024 Re_{D_c}^{-0.5123} \left(\frac{F_p}{D_c}\right)^{-0.7315} \left(\frac{F_l N_{row}}{D_c}\right)^{-0.1666},$ $f_{coated} = 3.826 Re_{D_c}^{-0.5959} \left(\frac{F_p}{D_c}\right)^{-0.2392} \left(\frac{F_l N_{row}}{D_c}\right)^{0.04879},$	<p>Dry Geometries = 22 $F_p = 1.3 \sim 1.7$ mm $D_o = 7.264$ mm $P_t = 21.65$ mm $P_l = 12.7$ mm $F_l = 0.076$ mm $N_{row} \leq 3$</p> <p>Uncertainty – $j_{uncoated}$: 88.0% of the experimental data were correlated within error $\pm 15\%$. j_{coated}: 87.0% of the experimental data were correlated within error $\pm 15\%$. $f_{uncoated}$: 82.0% of the experimental data were correlated within error $\pm 20\%$. f_{coated}: 92.0% of the experimental data were correlated within error $\pm 10\%$.</p> <p>[100]</p>
<p>Slit fin-tube heat exchangers,</p>	<p>For $400 \leq Re_{D_c} \leq 7000$,</p> $j = 1.6409 Re_{D_c}^X \left(\frac{S_p}{S_h}\right)^{1.16} \left(\frac{P_t}{P_l}\right)^{1.37} \left(\frac{F_p}{D_c}\right)^Y N_{row}^Z,$ <p>where</p> $X = -0.674 + \frac{0.1316 N_{row}}{\ln(Re_{D_c})} - 0.3769 \left(\frac{F_p}{D_c}\right)^{1.2} - \frac{1.8857 N_{row}}{Re_{D_c}},$ $Y = -0.0178 + \frac{0.996 N_{row}}{\ln(Re_{D_c})} + \frac{26.7 N_{row}}{Re_{D_c}},$ $Z = 1.865 - \frac{14.37}{\ln(Re_{D_c})} + \frac{1244.03 F_p}{Re_{D_c} D_c},$ <p>and</p> $f = 0.3929 Re_{D_c}^{X1} \left(\frac{S_p}{S_h}\right)^{-2.48} \left(\frac{F_p}{D_c}\right)^{Y1} N_{row}^{Z1},$ <p>where</p> $X1 = -3.585 + 0.8846 \frac{F_p}{D_c} + 2.677 \frac{P_t}{P_l},$ $Y1 = -0.0178 \frac{-246.678}{Re_{D_c}},$	<p>Dry Geometries = 12 $F_p = 1.21 \sim 2.48$ mm $D_c = 10.34$ mm $P_t = 25.4$ mm $P_l = 12.0$ mm $S_p = 2.2$ mm $S_h = 0.99$ mm $F_p = 0.12$ mm $N_{row} = 1 \sim 6$ Staggered tubes</p> <p>Uncertainty – j: 83.1% of the experimental data were correlated within error $\pm 10\%$. f: 92.8% of the experimental data were correlated within error $\pm 10\%$.</p> <p>[101]</p>

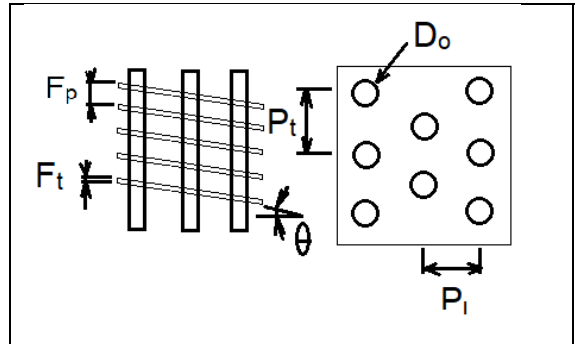
	$Z1 = -0.009 \ln(Re_{D_c})$.		
Louvered fin-tube,	<p>For $400 \leq Re_{D_c} \leq 3000$,</p> $j = 9.717 Re_{D_c}^X (N_{row})^{-0.543} \left(\frac{F_p}{D_c}\right)^Y \left(\frac{P_l}{P_t}\right)^Z \ln \left(3 - \frac{L_p}{F_p}\right)^{0.07162},$ <p>where</p> $X = -0.023634 - (N_{row})^{-0.18} \left(\frac{F_p}{D_c}\right)^{0.65} \left(\frac{P_l}{P_t}\right)^{0.2},$ $Y = 0.856 \exp(\tan(\theta)),$ $Z = 0.25 \ln(Re_{D_c}),$ <p>and</p> $f = 2.814 Re_{D_c}^{X1} (N_{row})^{0.04674} \left(\frac{F_p}{D_c}\right)^{Y1} \left(\frac{P_l}{P_t}\right)^{Z1} \left(\frac{P_l}{P_t} + 0.091\right)^{M1} \left(\frac{L_p}{F_p}\right)^{1.958},$ <p>where</p> $X1 = 1.223 - 2.857 \left(\frac{F_p}{D_c}\right)^{0.71} \left(\frac{P_l}{P_t}\right)^{-0.05},$ $Y1 = 0.8079 \ln(Re_{D_c}),$ $Z1 = 0.8932 \ln(Re_{D_c}),$ $M1 = -0.999 \ln\left(\frac{2\varphi}{\mu_w}\right),$ $\varphi = \text{condensate flow rate per tube row}, \quad \frac{\dot{m}}{W N_{row}},$ $D_c = D_o + 2F_t.$	<p>Wet Geometries = 10 $F_p = 1.2 \sim 2.5$ mm $D_c = 10.33$ mm $P_t = 25.4$ mm $P_l = 19 \sim 22$ mm $L_p/F_p = 0.8 \sim 1.94$ $F_p = 1.2 \sim 2.5$ mm $L_p = 2 \sim 2.35$ mm $\theta = 24.4 \sim 28.2^\circ$ $L_h = 1.07$ mm $F_t = 0.115$ mm $N_{row} = 1 \sim 2$ Staggered tubes</p> <p>Uncertainty – j: 80.5% of the experimental data were correlated within error $\pm 10\%$. f: 85.3% of the experimental data were correlated within error $\pm 10\%$.</p>	[115]
Louvered fin-tube,	<p>For $300 \leq Re_{D_c} \leq 1000$,</p> $j = 14.3117 Re_{D_c}^X \left(\frac{F_p}{D_c}\right)^Y \left(\frac{L_h}{L_p}\right)^Z \left(\frac{F_p}{P_t}\right)^M \left(\frac{P_l}{P_t}\right)^{-1.724},$ <p>where</p> $X = -0.991 - 0.1055 \left(\frac{P_l}{P_t}\right)^{3.1} \ln\left(\frac{L_h}{L_p}\right),$ $Y = -0.7344 + \frac{2.1059 (N_{row})^{0.55}}{\ln(Re_{D_c}) - 3.2},$ $Z = 0.08485 \left(\frac{P_l}{P_t}\right)^{-4.4} (N_{row})^{-0.68},$ $M = -0.1741 \ln(N_{row}).$ <p>For $1000 < Re_{D_c} \leq 7000$,</p> $j = 1.1373 Re_{D_c}^{X1} \left(\frac{F_p}{P_t}\right)^{Y1} \left(\frac{L_h}{L_p}\right)^{Z1} \left(\frac{P_l}{P_t}\right)^{M1} (N_{row})^{0.3545},$ <p>where</p>	<p>Dry Geometries = 49 $F_p = 1.21 \sim 2.49$ mm $D_c = 6.93 \sim 10.42$ mm $P_t = 17.7 \sim 25.4$ mm $P_l = 12.7 \sim 22.0$ mm $\theta = 13.5^\circ$ $L_h = 1.7 \sim 3.75$ mm $F_t = 0.115$ mm $N_{row} = 1 \sim 6$ Staggered tubes</p> <p>Uncertainty – j: 95.5% of the experimental data were correlated within error $\pm 10\%$. f: 90.8% of the experimental data were correlated within error $\pm 10\%$.</p>	[105]

	$X1 = -0.6027 + 0.02593 \left(\frac{P_l}{D_h} \right)^{0.52} (N_{row})^{-0.5} \ln \left(\frac{L_h}{L_p} \right),$ $Y1 = -0.4776 + \frac{0.40774 (N_{row})^{0.7}}{\ln(Re_{D_c}) - 4.4},$ $Z1 = -0.58655 \left(\frac{F_p}{D_h} \right)^{2.3} \left(\frac{P_l}{P_t} \right)^{-1.6} (N_{row})^{-0.65},$ $M1 = 0.0814 (\ln(Re_{D_c}) - 3.0).$ <p>For $1000 < Re_{D_c} \leq 7000$, and if $N_{row} = 1$,</p> $f = 0.00317 Re_{D_c}^{X2} \left(\frac{F_p}{P_l} \right)^{Y2} \left(\frac{D_h}{D_c} \right)^{Z2} \left(\frac{L_h}{L_p} \right)^{M2} \left(\ln \left(\frac{A_{tot}}{A_{tube}} \right) \right)^{-6.0483},$ <p>where</p> $X2 = 0.1691 + 4.4118 \left(\frac{F_p}{P_l} \right)^{-0.3} \left(\frac{L_h}{L_p} \right)^{-2} \ln \left(\frac{P_l}{P_t} \right) \left(\frac{F_p}{P_t} \right)^3,$ $Y2 = -2.6642 - \frac{14.3809}{\ln(Re_{D_c})},$ $Z2 = -0.6816 \ln \left(\frac{F_p}{P_t} \right),$ $M2 = 6.4668 \left(\frac{F_p}{P_t} \right)^{1.7} \ln \left(\frac{A_{tot}}{A_{tube}} \right).$ <p>If $N_{row} > 1$,</p> $f = 0.06393 Re_{D_c}^{X3} \left(\frac{F_p}{D_c} \right)^{Y3} \left(\frac{D_h}{D_c} \right)^{Z3} \left(\frac{L_h}{L_p} \right)^{M3} (N_{row})^{N3} (\ln(Re_{D_c}) - 4.0)^{-1.093},$ <p>where</p> $X3 = 0.1395 - 0.0101 \left(\frac{F_p}{P_l} \right)^{0.58} \left(\frac{L_h}{L_p} \right)^{-2} \ln \left(\frac{A_{tot}}{A_{tube}} \right) \left(\frac{P_l}{P_t} \right)^{1.9},$ $Y3 = -\frac{6.4367}{\ln(Re_{D_c})},$ $Z3 = 0.07191 \ln(Re_{D_c}),$ $M3 = -2.0585 \left(\frac{F_p}{P_t} \right)^{1.67} \ln(Re_{D_c}),$ $N3 = 0.1036 \ln \left(\frac{P_l}{P_t} \right),$ $D_c = D_o + 2F_t,$	
--	---	--

	$D_h = \frac{4A_{min}L_d}{A_{tot}}$, L_d is the core depth, and $L_h = L_p \tan(\theta)$.		
Plain fin-tube,	<p>For $400 \leq Re_{D_c} \leq 5000$,</p> $j = 0.4Re_{D_c}^{-0.468+0.4074N_{row}}(N_{row})^{-1.261}\left(\frac{A_{tot}}{A_{tube}}\right)^{0.159},$ $j_{N_{row}=4} = 0.29773Re_{D_c}^{-0.364}\left(\frac{A_{tot}}{A_{tube}}\right)^{-0.168},$ $f = 28.209 Re_{D_c}^{-0.5653}(N_{row})^{-0.1026}\left(\frac{F_p}{D_c}\right)^{-1.3305}\left(\frac{A_{tot}}{A_{tube}}\right)^{-1.3343}.$	Wet Geometries = 9 $F_p = 1.82 \sim 3.2$ mm $D_c = 10.23$ mm $P_t = 25.4$ mm $P_l = 22.0$ mm $F_t = 0.13$ mm $N_{row} = 2 \sim 6$ Water film = 0.127 mm Staggered tubes Uncertainty – j : 92.0% of the experimental data were correlated within error $\pm 10\%$. f : 91.0% of the experimental data were correlated within error $\pm 10\%$.	[111]
Wavy-staggered fin-tube,	<p>For $200 \leq Re_{D_h} \leq 6000$,</p> $j_{N_{row}=4} = Re_{D_h}^{-0.44}R_2^{-3.07}R_3^{0.37}R_4^{-6.14}\left(\frac{P_l}{D_0}\right)^{-2.13},$ $\frac{j_{N_{row}=4}}{j} = 0.87 + 0.0000143 Re_{D_h}^{0.55}(N_{row})^{-0.67}R_1^{-3.13}R_3^{4.95},$ $f = Re_{D_h}^{-0.25}R_2^{-1.43}R_3^{1.37}\left(\frac{F_p}{D_0}\right)^{1.65}\left(\frac{P_l}{D_0}\right)^{-3.05},$ <p>where</p> $R_1 = \frac{D_o}{D_i}\left(1 - \frac{F_t}{F_p}\right) + 2\frac{P_t P_l}{\pi D_i F_p} - \frac{D_o^2}{2 D_i F_p} + \frac{2 P_t F_t}{2 D_i F_p N_{row}},$ $R_2 = \frac{P_t F_p}{(P_t - D_o)(F_p - F_t)},$ $R_3 = \frac{1}{N_{row}}\left[\frac{\pi D_o N_{row}}{P_t}\left(1 - \frac{F_t}{F_p}\right) + \frac{N_{row}}{F_p}\left(2 P_l - \frac{\pi D_o^2}{2 P_t} + \frac{2 F_t}{N_{row}}\right)\right],$ $R_4 = \left[1 + \frac{2 \pi D_o (F_p - F_t)}{4 P_t P_l - \pi D_o^2 + \frac{4 P_t F_t}{N_{row}}}\right]^{-1},$ and	Dry Geometries = 15 $F_p = 1.64 \sim 2.65$ mm $D_o = 10.23$ mm $P_t = 19 \sim 25.4$ mm $P_l = 16.0 \sim 22.0$ mm $F_t = 0.12 \sim 0.13$ mm $N_{row} = 1 \sim 4$ $R_1 = 7.26 \sim 19.3$ $R_2 = 1.77 \sim 2.25$ $R_3 = 11.0 \sim 21.8$ $R_4 = 0.86 \sim 0.95$ $\frac{F_p}{D_0} = 0.16 \sim 0.27$ $\frac{P_l}{D_0} = 1.60 \sim 2.21$ Staggered tubes Uncertainty – j : 93.9% of the experimental data were correlated within error $\pm 3.6\%$. f : 98.7% of the experimental data were correlated within error $\pm 2.8\%$.	[99]

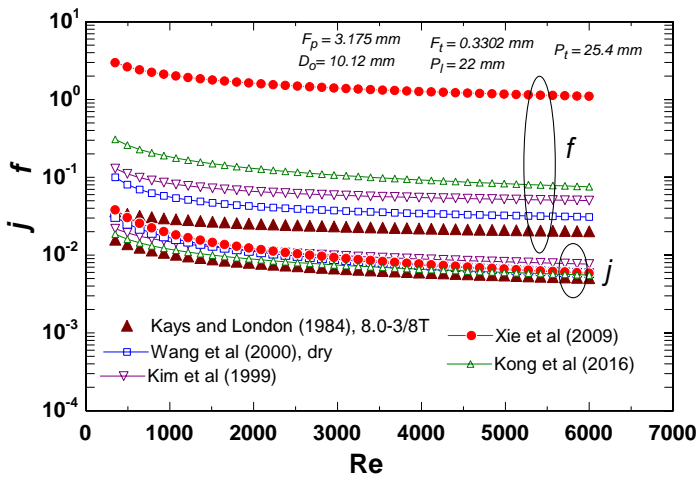
	$D_h = \frac{4A_{min}L}{A_{tot}}.$		
Individually finned tubes, helically wrapped or extruded, 	For $1100 \leq Re_{D_o} \leq 18000$, $j = 0.134 Re_{D_o}^{-0.319} \left(\frac{F_p - F_t}{F_l} \right)^{0.2} \left(\frac{F_p - F_t}{F_t} \right)^{0.11}.$	Geometries = not mentioned $0.13 \leq \left(\frac{F_p - F_t}{F_l} \right) \leq 0.63$ $1.01 \leq \left(\frac{F_p - F_t}{F_t} \right) \leq 7.62$ $0.09 \leq \frac{F_l}{D_o} \leq 0.69$ $0.011 \leq \frac{F_t}{D_o} \leq 0.15$ $1.54 \leq \frac{P_t}{D_o} \leq 8.23$ $D_o = 11.1 - 40.9 \text{ mm}$ $N_{fin} = 246 - 768 \text{ fins/m}$ Uncertainty – j : the standard deviation with experimental data is $\pm 5.1\%$.	[43, 124]
Individually finned tubes, helically wrapped or extruded,	For $2000 \leq Re_{D_o} \leq 50000$, $f = 9.465 Re_{D_o}^{-0.316} \left(\frac{P_t}{D_o} \right)^{-0.927} \left(\frac{P_t}{\sqrt{P_t^2 + P_l^2}} \right)^{0.515}.$	Geometries = not mentioned $F_p = 2.320 \sim 3.215$ $D_o = 18.6 \sim 40.9 \text{ mm}$ $0.15 \leq \left(\frac{F_p - F_t}{F_l} \right) \leq 0.19$	[44, 124]

	$3.75 \leq \left(\frac{F_p - F_t}{F_t}\right) \leq 6.03$ $0.35 \leq \frac{F_t}{D_o} \leq 0.56$ $0.011 \leq \frac{F_t}{D_o} \leq 0.025$ $1.86 \leq \frac{P_t}{D_o} \leq 4.6$ <p>Uncertainty – <i>j</i>: the standard deviation with experimental data is $\pm 7.8\%$.</p>	
Plain and slot finned tubes, 	For $800 \leq Re_{D_o} \leq 13000$, <p>Flat finned tube:</p> $Nu = 2.6653 Re_{D_o}^{0.3175} \left(\frac{P_t}{D_o}\right)^{-0.8732} \left(\frac{P_t}{D_o}\right)^{-0.5618},$ $f = 662.3561 Re_{D_o}^{0.6453} \left(\frac{P_t}{D_o}\right)^{-0.2801} \left(\frac{P_t}{D_o}\right)^{-0.3927},$ <p>Slotted finned tube:</p> $Nu = 4.8787 Re_{D_c}^{0.3173} \left(\frac{P_t}{D_o}\right)^{-0.8571} \left(\frac{P_t}{D_o}\right)^{-0.6648},$ $f = 324.0431 Re_{D_c}^{-0.4825} \left(\frac{P_t}{D_o}\right)^{-0.0258} \left(\frac{P_t}{D_o}\right)^{-0.2419},$	<p>Dry Geometries = 50 models</p> $1 \leq \frac{P_t}{D_c} \leq 1.8$ $1 \leq \frac{P_t}{D_c} \leq 1.8$ $D_o = 25 \text{ mm}$ $N_{row} = 4$ $F_t = 0.3 \text{ mm}$ $F_p = 3.2 \text{ mm}$ $S_{h1} = 1.1 \text{ mm}$ $S_{h2} = 0.5 \text{ mm}$ $S_w = 7 \text{ mm}$ $S_s = 2.75 \text{ mm}$ <p>Uncertainty – <i>Nu</i>: the data were correlated within error $\pm 6.5\%$. <i>f</i>: the data were correlated within error $\pm 8.2\%$.</p>
Plain finned tubes,	For $220 \leq Re_{D_o} \leq 5000$, $Nu = 0.3313 Re_{D_o}^{0.575} \left(1 - \theta \frac{\pi}{180}\right)^{-0.0522} \left(\frac{F_p - F_t}{D_h}\right)^{1.3204} \left(\frac{F_t}{D_h}\right)^{0.0351} \left(\frac{D_o}{D_h}\right)^{-0.1002},$ $f = 7.6551 Re_{D_o}^{-0.4927} \left(1 - \theta \frac{\pi}{180}\right)^{0.1441} \left(\frac{F_p - F_t}{D_h}\right)^{1.7383} \left(\frac{F_t}{D_h}\right)^{0.0004} \left(\frac{D_o}{D_h}\right)^{0.0922},$ <p>where θ, here, is the angle between flat plate and tubes – under assumption of inclined plates arrangements</p>	<p>Dry Geometries = 25</p> $0 \leq \theta \leq 30^\circ$ $0.5476 \leq \frac{F_p - F_t}{D_h} \leq 0.678$ $0.013 \leq \frac{F_t}{D_h} \leq 0.332$ $2.228 \leq \frac{D_o}{D_h} \leq 9.143$ <p>Uncertainty – <i>Nu</i>: the data were correlated within error $\pm 9.67\%$.</p>

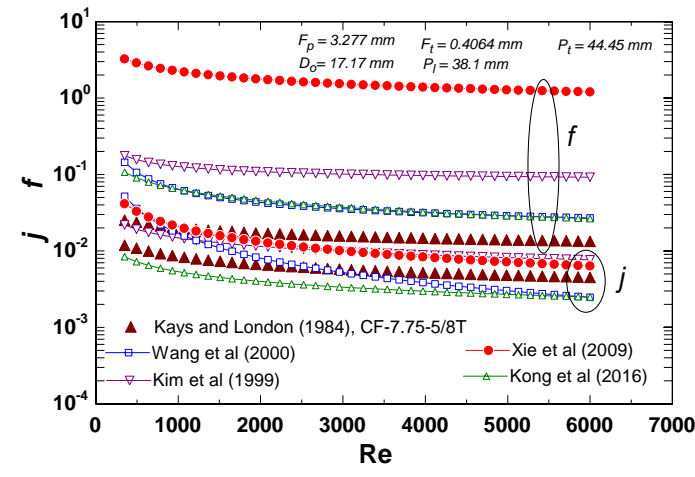


f. the data were correlated
within error $\pm 14.335\%$.

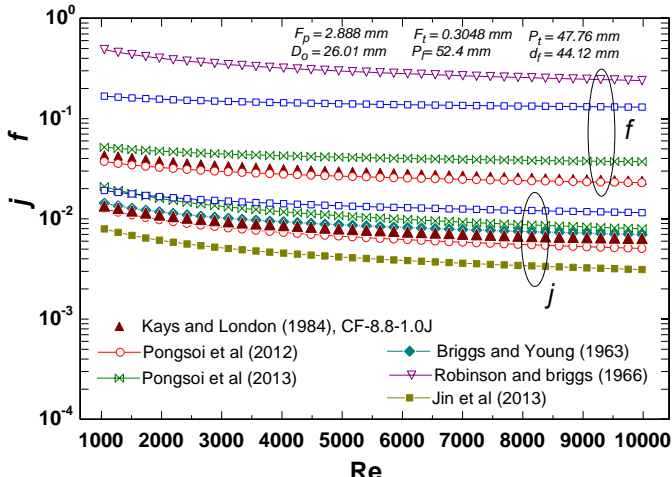
The limitations of tabulated correlations (Table 4) make some difficulty to compare them with the experimental reference (Kays and London [40]). However, we selected some experimental data that have close parameters to some correlations, from both spiral- and flat-fin tube heat exchangers, to explore the utilization of these correlation with different geometries as exhibited in Figure 11. For the flat-fin tube heat exchangers, the j - and f -factor values mismatch with those of experimental data of surfaces 8.0-3/8T (Figure 11 (a)) and CF-7.75-5/8T (Figure 11 (b)) [40]; the only addressed agreement is the f -factor correlations attained from the correlations reported by Kong et al. [1] and, to some extent, by Xie et al. and Wang et al, [103, 104] under high Reynolds number values. This demonstrates that the use of these correlations, out of their parameters limitations, should be used with caution. For spiral-fin tube heat exchanger, a similar caution can be recommended except the correlations reported by Briggs and Young [43], and Pongsoi et al. [109] that show an excellent agreement with the experimental data of surfaces CF-8.8-1.0J (Figure 11 (c)) and CF-8.72 (Figure 11 (d)).



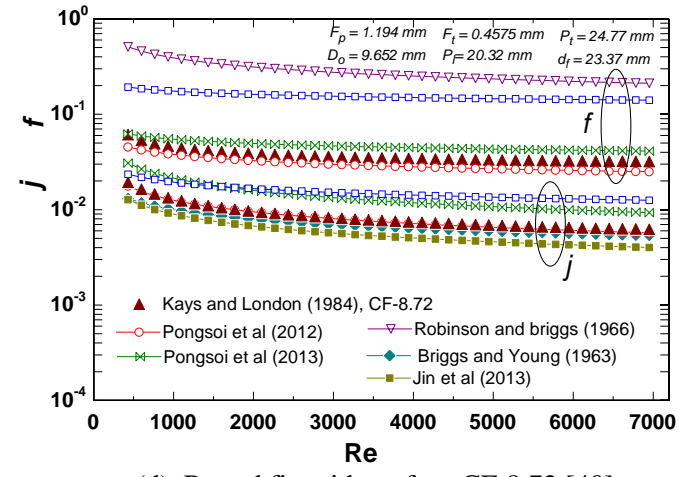
(a) Flat plate fin with surface 8.0-3/8T [40].



(b) Flat plate fin with surface CF-7.75-5/8T [40].



(c) Round fin with surface CF-8.8-1.0J [40].



(d) Round fin with surface CF-8.72 [40].

Figure 11. Comparison of experimental data (Kays and London [40]) and some correlations listed in Table 4 for both flat ((a) with the experimental surface 8.0-3/8T and (b) with the experimental surface CF-7.75-5/8T) and round ((c)with the experimental surface CF-8.8-1.0J and (d) with the experimental surface CF-8.72) finned tube compact heat exchangers.

2.6. Plain- and pin-fin compact and microchannel heat exchangers

Plain and circular pin fins, so-called extended surfaces, are commonly used as heat sink to cool different electronic devices, motors, and several devices. Some pin fins were experimentally and numerically investigated by Yang et al. [125] for microchannel heat sinks including five pin shapes: triangle, square, pentagon, hexagon, and circle. The circular pins showed the least pressure drop while triangular ones showed the highest flow blocking. Plain fins are desirable because of both higher heat transfer area and overall efficiency.

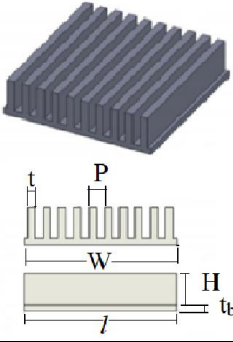
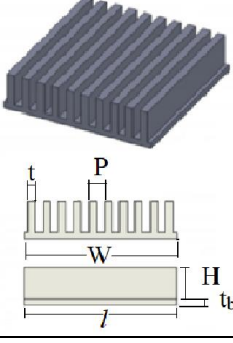
Despite the extended surfaces (fins and pins) have been used in many applications, the air-side heat transfer and fluid-flow correlations are so limited. The accurate prediction of heat transfer performance of pin finned tubes is not easy [126]. Teertstra et al. [20] developed a Nusselt number (Nu) correlation to calculate heat transfer rate for plain fins using analytical forced convection model. Interestingly, Jonsson and Moshfegh [127] studied heat and flow performances for different types of extended surfaces including plate-fin, inline strip-fin, staggered strip-fin, inline circular-pin, staggered circular-pin, inline square-pin, and staggered square-pin. They correlated heat transfer and fluid-flow performances in terms of Nusselt number and dimensionless pressure

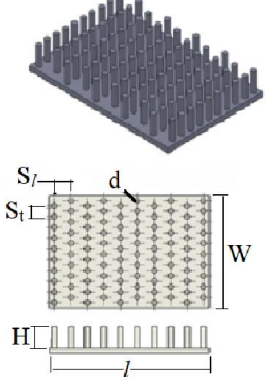
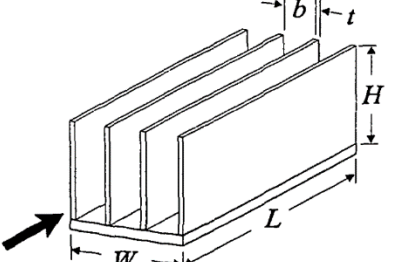
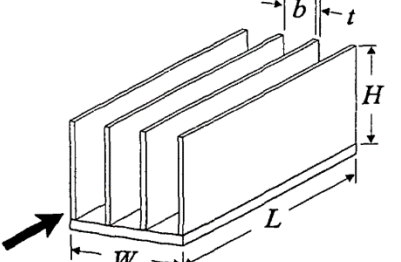
drop (ΔP^*) coefficients. Sahiti [128] investigated seventeen pin-fin geometries to obtain heat transfer and fluid-flow characteristics denoted by Nusselt number and Euler number, respectively. They proposed correlations for both inline and staggered pin arrangements. Diani et al. [129] carried out an extensive simulation modeling (108 simulations for fins and 63 for pins) to obtain good correlations for such heat exchangers.

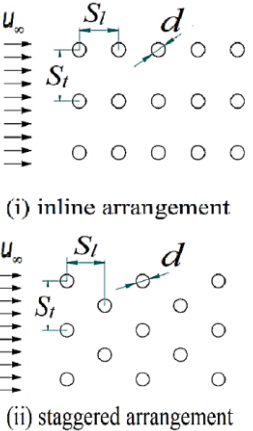
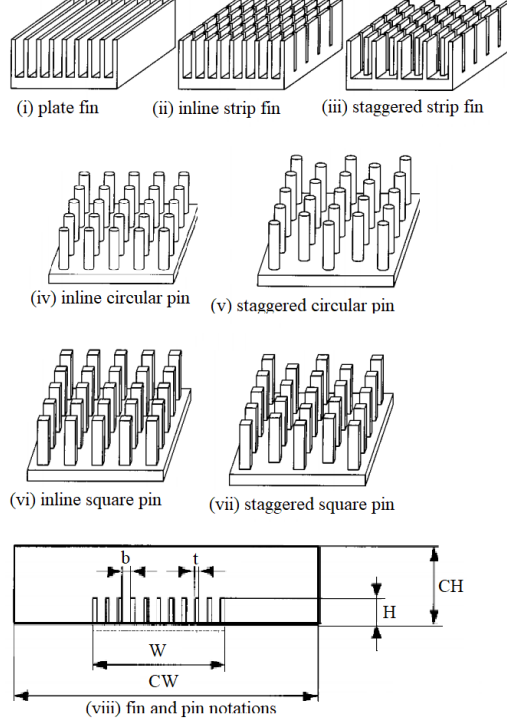
The suggested heat and flow correlations for different geometries of fins and pins are summarized in Table 5. More details about the geometrical parameter limitations, operating range of Reynolds number, and the fitting uncertainties, are also tabulated.

It is difficult to compare the correlations values (Table 5) with those of experimental data reported by Kays and London [40] as a result of a big difference existing between the geometrical parameters. Moreover, the method of representing the listed correlations in Table 5 are inconsistent with each other (e.g., f -factor, ΔP^* , Eu are different expressions reported for representing fluid-flow performances).

Table 5. Summary of reported thermal-hydraulic performance correlations using plain- and pin-fin geometries.

Geometry	Correlations	Conditions and limitations	Ref.
Plain-fin,	<p>For $2700 \leq Re_{D_h} \leq 10100$,</p> $j = 0.233 Re_{D_h}^{-0.48} \left(\frac{t}{H}\right)^{-0.208} \left(\frac{P}{H}\right)^{0.192},$ $f = 0.029 Re_{D_h}^{-0.09} \left(\frac{t}{H}\right)^{-0.034} \left(\frac{P}{H}\right)^{-0.169}.$ 	<p>Dry Geometries = not mentioned (108 simulations including geometries and Re)</p> <p>$0.1 \leq \frac{t}{H} \leq 0.6$ $0.33 \leq \frac{P}{H} \leq 1.11$ $N_{fin} = 9 \sim 15$ $h = 10 \sim 20.0 \text{ mm}$ $t = 2 \sim 6 \text{ mm}$</p> <p>Uncertainty – j: standard deviation $\pm 5.3\%$. f: standard deviation $\pm 3.4\%$.</p>	[129]
Plain fin,	<p>For $2700 \leq Re_{D_h} \leq 10100$,</p> $j = 0.609 Re_{D_h}^{-0.493} \left(\frac{t}{H}\right)^{-0.011} \left(\frac{P}{H}\right)^{-0.071} \left(\frac{l}{D_h}\right)^{-0.298},$ $f = 0.059 Re_{D_h}^{-0.117} \left(\frac{t}{H}\right)^{0.118} \left(\frac{P}{H}\right)^{-0.253} \left(\frac{l}{D_h}\right)^{-0.147}.$ 	<p>Dry Geometries = not mentioned (updated work in regard to [129])</p> <p>$0.1 \leq \frac{t}{H} \leq 0.6$ $0.33 \leq \frac{P}{H} \leq 1.11$ $8 \leq \frac{l}{D_h} \leq 15$</p> <p>Uncertainty – j: standard deviation $\pm 3\%$. f: standard deviation $\pm 8\%$.</p>	[130]
Pin-fin,	<p>For $1000 \leq Re_d \leq 4200$,</p> $j = 0.327 Re_d^{-0.45} \left(\frac{S_t}{d}\right)^{0.037} \left(\frac{S_t}{d}\right)^{-0.397} \left(\frac{H}{d}\right)^{0.201},$ $f = 0.277 Re_d^{-0.04} \left(\frac{S_t}{d}\right)^{-1.307} \left(\frac{S_t}{d}\right)^{-0.692} \left(\frac{H}{d}\right)^{0.107}.$	<p>Dry Geometries = not mentioned (63 simulations including geometries and Re)</p> <p>$1.8 \leq \frac{S_t}{d} \leq 3.0$ $2.5 \leq \frac{S_t}{d} \leq 5.0$</p>	[129, 130]

	$3.0 \leq \frac{H}{d} \leq 7.0$ $d = 2.5 \text{ mm}$ $N_{fin} = 9 \sim 15$ $S_t = 2.5 \sim 5 \text{ mm}$ $S_t = 1.8 \sim 3 \text{ mm}$	Uncertainty – <i>j</i> : standard deviation $\pm 8\%$. <i>f</i> : standard deviation $\pm 14\%$.	
Plain-fin, 	For $0.1 \leq Re_b \leq 100$, $Nu = \frac{\tanh \sqrt{2Nu^* \frac{k_f}{k} \frac{H}{t} \frac{H}{b} \left(\frac{t}{l} + 1 \right)}}{\sqrt{2Nu^* \frac{k_f}{k} \frac{H}{t} \frac{H}{b} \left(\frac{t}{l} + 1 \right)}} Nu^*,$ where $Nu^* = \left[\left(\frac{Re_b Pr}{2} \right)^{-3} + \left(0.664 \sqrt{Re_b} Pr^{1/3} \sqrt{1 + \frac{3.65}{Re_b}} \right)^{-3} \right]^{-1/3},$ $Re_b = \frac{Ub^2}{l \nu}, b = P-t,$ $j = \frac{Nu}{Re_{D_h} Pr^{1/3}}.$	Dry Geometries = not mentioned $B \ll H$ Parallel plate channels Uncertainty – the experimental data were correlated within error $\pm 2.1\%$.	[20]
Pin-fin, 	For $50 \leq Re_{D_h} \leq 800$, Staggered arrangements: $Nu = 2.12 Re_{D_h}^{0.57} \left(\frac{S_t}{d} \right)^{-0.83} \left(\frac{S_t}{d} \right)^{-0.94} \left(\frac{H}{d} \right)^{0.71},$ $Eu = 17.22 Re_{D_h}^{-0.38} \left(\frac{S_t}{d} \right)^{-0.32} \left(\frac{S_t}{d} \right)^{-0.21} \left(\frac{H}{d} \right)^{-0.14}.$ Inline arrangements: $Nu = 1.62 Re_{D_h}^{0.54} \left(\frac{S_t}{d} \right)^{-1.53} \left(\frac{S_t}{d} \right)^{-0.48} \left(\frac{H}{d} \right)^{0.78},$ $Eu = 12.11 Re_{D_h}^{-0.43} \left(\frac{S_t}{d} \right)^{-1.84} \left(\frac{S_t}{d} \right)^{0.68} \left(\frac{H}{d} \right)^{-0.18}.$	Dry Geometries = 17 $1.5 \leq \frac{S_t}{d} \leq 4.5$ $1.5 \leq \frac{S_t}{d} \leq 4.5$ $2.5 \leq \frac{H}{d} \leq 15$ Uncertainty – <i>Nu</i> and <i>Eu</i> standard errors for staggered arrangements are 0.102 and 0.137, respectively. <i>Nu</i> and <i>Eu</i> standard errors for inline arrangements are 0.074 and 0.102, respectively.	[128]

 <p>(i) inline arrangement</p> <p>(ii) staggered arrangement</p>																																																																																										
<p>Different pin and fin arrangements,</p>  <p>(i) plate fin (ii) inline strip fin (iii) staggered strip fin</p> <p>(iv) inline circular pin (v) staggered circular pin</p> <p>(vi) inline square pin (vii) staggered square pin</p> <p>(viii) fin and pin notations</p>	<p>For $1950 \leq Re_{D_h} \leq 16500$, the heat and flow characteristics can be obtain from:</p> $Nu_t = C_1 \left(\frac{Re_{D_h}}{1000} \right)^{m1} \left(\frac{CW}{W} \right)^{m2} \left(\frac{CH}{H} \right)^{m3} \left(\frac{b}{H} \right)^{m4} \left(\frac{t}{H} \right)^{m5},$ $\Delta P^* = C_2 \left(\frac{Re_{D_h}}{1000} \right)^{n1} \left(\frac{CW}{W} \right)^{n2} \left(\frac{CH}{H} \right)^{n3} \left(\frac{b}{H} \right)^{n4} \left(\frac{t}{H} \right)^{n5},$ <p>where</p> $\Delta P^* = \frac{\Delta P}{\frac{1}{2} \rho \omega^2},$ $Nu_t = \frac{h l}{k},$ $\omega = \frac{\dot{Q}}{CW \cdot CW - A_{front}},$ $W = (N_{fin} - 1)b + N_{fin}t,$ $D_h = \frac{2CH \cdot CW}{CH + CW},$ $CW = W + 2b \quad \text{for zero bypass duct,}$ $CH = H \quad \text{for zero bypass duct,}$ <p>and</p> <table border="1"> <thead> <tr> <th>Nu_L</th> <th>C1</th> <th>m1</th> <th>m2</th> <th>m3</th> <th>m4</th> <th>m5</th> <th>R²</th> </tr> </thead> <tbody> <tr> <td>Plate fin</td> <td>88.28</td> <td>0.6029</td> <td>-0.1098</td> <td>-0.5632</td> <td>0.08713</td> <td>0.4139</td> <td>0.9782</td> </tr> <tr> <td>Inline strip fin</td> <td>90.88</td> <td>0.7065</td> <td>-0.07122</td> <td>-0.6485</td> <td>0.04164</td> <td>0.4700</td> <td>0.9742</td> </tr> <tr> <td>Staggered strip fin</td> <td>105.4</td> <td>0.7210</td> <td>-0.08695</td> <td>-0.6558</td> <td>0.03624</td> <td>0.7327</td> <td>0.9783</td> </tr> <tr> <td>Inline circular pin</td> <td>169.3</td> <td>0.6422</td> <td>-0.1528</td> <td>-0.6382</td> <td>0.2626</td> <td>0.2772</td> <td>0.9793</td> </tr> <tr> <td>Staggered circular pin</td> <td>219.6</td> <td>0.6432</td> <td>-0.1793</td> <td>-0.6410</td> <td>0.1119</td> <td>0.4500</td> <td>0.9810</td> </tr> <tr> <td>Inline square pin</td> <td>108.3</td> <td>0.6642</td> <td>-0.1713</td> <td>-0.6434</td> <td>0.3537</td> <td>0.1045</td> <td>0.9807</td> </tr> <tr> <td>Staggered square pin</td> <td>153.1</td> <td>0.6736</td> <td>-0.1943</td> <td>-0.6677</td> <td>0.2075</td> <td>0.3102</td> <td>0.9819</td> </tr> </tbody> </table> <table border="1"> <thead> <tr> <th>ΔP^*</th> <th>C2</th> <th>n1</th> <th>n2</th> <th>n3</th> <th>n4</th> <th>n5</th> <th>R²</th> </tr> </thead> <tbody> <tr> <td>Plate fin</td> <td>4.783</td> <td>-0.4778</td> <td>-0.6874</td> <td>-0.5979</td> <td>-0.7184</td> <td>0.6736</td> <td>0.9637</td> </tr> <tr> <td>Inline strip fin</td> <td>4.027</td> <td>-0.3599</td> <td>-0.5754</td> <td>-0.6750</td> <td>-0.6232</td> <td>0.6286</td> <td>0.9602</td> </tr> </tbody> </table>	Nu_L	C1	m1	m2	m3	m4	m5	R ²	Plate fin	88.28	0.6029	-0.1098	-0.5632	0.08713	0.4139	0.9782	Inline strip fin	90.88	0.7065	-0.07122	-0.6485	0.04164	0.4700	0.9742	Staggered strip fin	105.4	0.7210	-0.08695	-0.6558	0.03624	0.7327	0.9783	Inline circular pin	169.3	0.6422	-0.1528	-0.6382	0.2626	0.2772	0.9793	Staggered circular pin	219.6	0.6432	-0.1793	-0.6410	0.1119	0.4500	0.9810	Inline square pin	108.3	0.6642	-0.1713	-0.6434	0.3537	0.1045	0.9807	Staggered square pin	153.1	0.6736	-0.1943	-0.6677	0.2075	0.3102	0.9819	ΔP^*	C2	n1	n2	n3	n4	n5	R ²	Plate fin	4.783	-0.4778	-0.6874	-0.5979	-0.7184	0.6736	0.9637	Inline strip fin	4.027	-0.3599	-0.5754	-0.6750	-0.6232	0.6286	0.9602	<p>[127]</p> <p>Dry Geometries = 42 (6 for each type)</p> $1.2 \leq \frac{CW}{W} \leq 3.1$ $1.5 \leq \frac{CH}{H} \leq 3.0$ $0.15 \leq \frac{b}{H} \leq 0.5$ $0.075 \leq \frac{t}{H} \leq 0.15$ <p>Uncertainty –</p> <p>Nu_t: the experimental data were correlated within error $\pm 10\%$.</p> <p>ΔP^*: the experimental data were correlated within error $\pm 20\%$.</p>
Nu_L	C1	m1	m2	m3	m4	m5	R ²																																																																																			
Plate fin	88.28	0.6029	-0.1098	-0.5632	0.08713	0.4139	0.9782																																																																																			
Inline strip fin	90.88	0.7065	-0.07122	-0.6485	0.04164	0.4700	0.9742																																																																																			
Staggered strip fin	105.4	0.7210	-0.08695	-0.6558	0.03624	0.7327	0.9783																																																																																			
Inline circular pin	169.3	0.6422	-0.1528	-0.6382	0.2626	0.2772	0.9793																																																																																			
Staggered circular pin	219.6	0.6432	-0.1793	-0.6410	0.1119	0.4500	0.9810																																																																																			
Inline square pin	108.3	0.6642	-0.1713	-0.6434	0.3537	0.1045	0.9807																																																																																			
Staggered square pin	153.1	0.6736	-0.1943	-0.6677	0.2075	0.3102	0.9819																																																																																			
ΔP^*	C2	n1	n2	n3	n4	n5	R ²																																																																																			
Plate fin	4.783	-0.4778	-0.6874	-0.5979	-0.7184	0.6736	0.9637																																																																																			
Inline strip fin	4.027	-0.3599	-0.5754	-0.6750	-0.6232	0.6286	0.9602																																																																																			

	Staggered strip fin	4.139	-0.3366	-0.6362	-0.7026	-0.6423	0.6320	0.9591		
	Inline circular pin	5.357	-0.1759	-0.7161	-0.8230	-0.5401	0.5990	0.9698		
	Staggered circular pin	6.967	-0.1556	-0.8533	-0.9592	-0.7740	0.7838	0.9631		
	Inline square pin	3.209	-0.1551	-0.7790	-0.8169	-0.5306	0.3408	0.9494		
	Staggered square pin	4.857	-0.1617	-0.8921	-0.9773	-0.6890	0.5097	0.9658		

2.7. Manifold microchannel heat exchangers

Manifold microchannel heat exchangers are recently introduced to solve the high pressure drop on the air-side by using microchannel heat exchangers. The high pressure drop in microchannel heat exchangers is mainly caused by two issues; the maldistribution of flow in the microchannels and the small flow area along the flow-path [5]. The manifolds can solve these issues by reducing the flow misdistribution and distributing the flow along entire length of the microchannel *via* dividing the flow-path into smaller flow regions, as shown in Figure 12, while the general construction of integrated manifold-microchannel is shown in Figure 13.

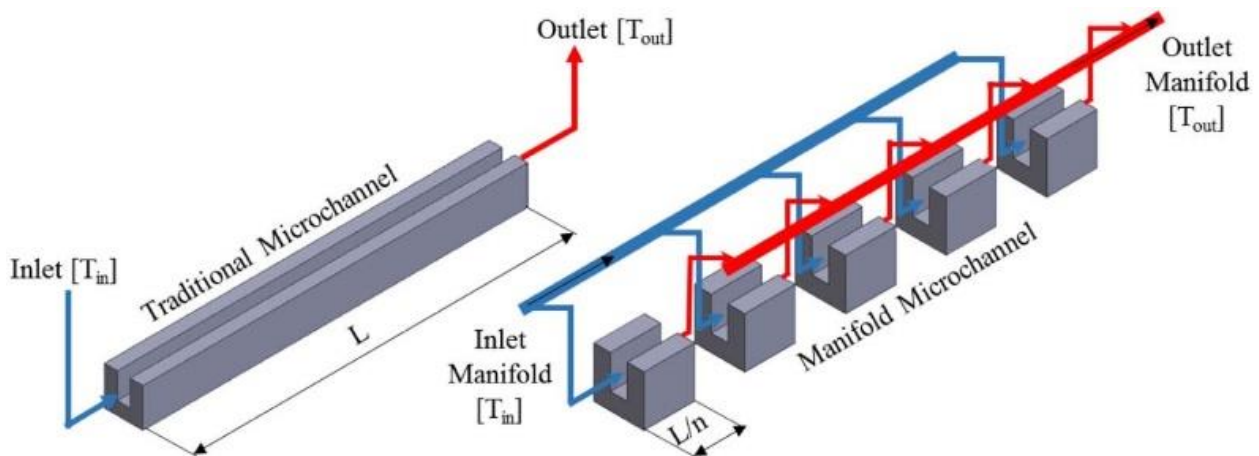


Figure 12. Distribution of the flow along microchannel [5].

Arie et al. [131] investigated different geometries of manifold microchannel heat exchangers. For calculating air-side fluid-flow and heat transfer, they used the same *f*- and *j*-factor correlations of the compact heat exchangers [40]. No new correlations are derived for such types of heat exchanger. Some researchers used water as working fluid instead of air for manifold microchannel heat exchangers [5, 131]. Using air as a cooling medium is employed early [17], but without obtaining thermal-hydraulic performance correlations. Most of the correlations obtained for manifold microchannel heat exchangers are for water or refrigerants as the main working fluids inside the microchannels. Air-side thermal-hydraulic correlations are not available. More details about these new promising candidates (manifold microchannel) of heat exchangers can be found in Ref [132].

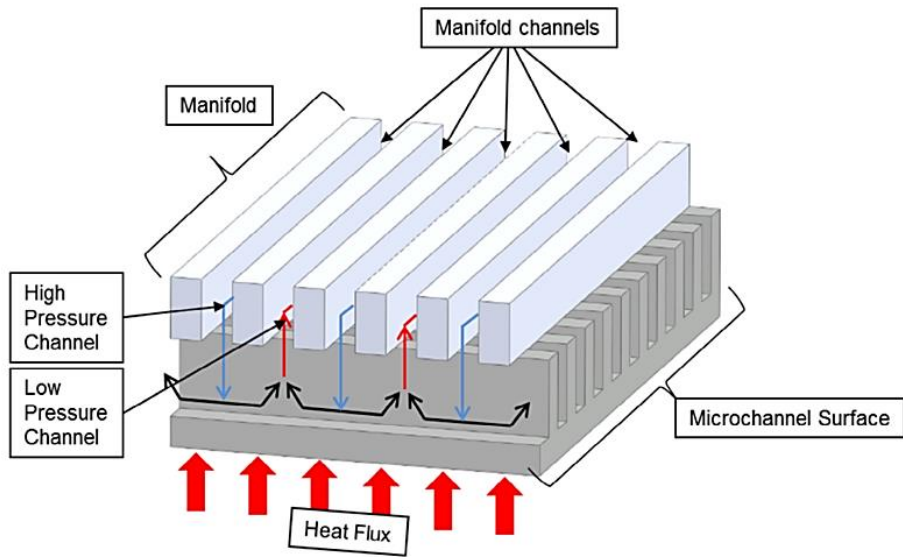


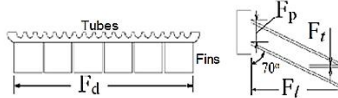
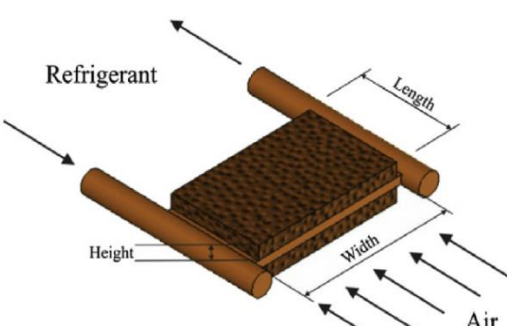
Figure 13. Manifold microchannel heat exchanger [5].

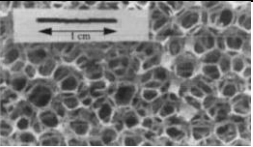
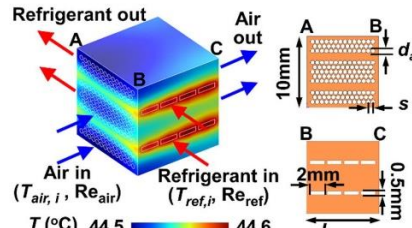
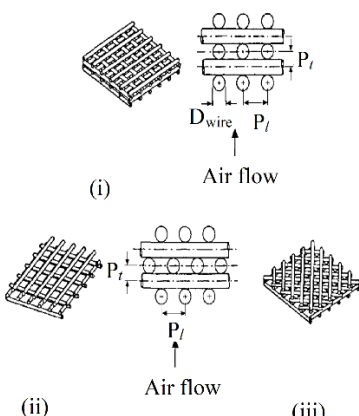
2.8. Other types of compact and microchannel heat exchangers

Air as a cheap medium is exploited to investigate thermal-hydraulic performance enhancements in different heat exchangers. One slab holding some microchannels cooled by some inclined fins was investigated by Li et al. [24, 25]. They suggested fluid-flow and heat-transfer correlations by testing eleven geometries. Metal-foam showed a good candidate to replace traditional fins; however, they are still expensive attributable to the low production of such materials [133]. Some correlations of thermal-hydraulic performances were reported/derived for a wet metal-foam to represent the air-side of the microchannel and compact heat exchangers [134, 135]. Another way to use air for cooling purposes is that by high-power density air passes inside microchannels in cross-flow arrangements with a refrigerant. We have fitted heat transfer and fluid-flow correlations from plotted data reported by Kwon et al. [136] for hydraulic diameter, $D_h = 0.52$ mm, in pursuit of representing these types of heat exchangers. Cross rod heat exchangers are also utilized in cooling purposes; many arrangements could be constructed such as inline, staggered, and random. Kays and London [40] reported some experimental heat and flow characteristic data for cross-rod heat exchangers. These data were used to formulate new thermal-hydraulic correlations [124].

The corresponding heat-transfer and fluid-flow correlations, of all these aforementioned heat exchangers, are summarized in Table 6 that explains the geometrical parameter limitations, Reynolds number operating ranges, and fitting uncertainties.

Table 6. Summary of reported heat-transfer and fluid-flow performance correlations used for some heat exchangers.

Geometry	Correlations	Conditions and limitations	Ref.
Integrated fins over one slab of microchannel tubes,  	For $200 \leq Re_{D_c} \leq 1730$, $j = 0.2162Re_{D_c}^{0.351} \left(\frac{F_d}{D_c}\right)^{-0.875} \left(\frac{F_p}{D_c}\right)^{-0.543} \left(\frac{F_l}{D_c}\right)^{0.426} \left(\frac{F_t}{D_c}\right)^{0.12}$, $f = 0.4183Re_{D_c}^{-0.506} \left(\frac{F_d}{D_c}\right)^{0.69} \left(\frac{F_p}{D_c}\right)^{-1.837} \left(\frac{F_l}{D_c}\right)^{1.382} \left(\frac{F_t}{D_c}\right)^{0.062}$. Here, $D_c = D_o + 2F_t$.	Dry Geometries = 11 $F_p = 1.0 \sim 1.4$ mm $F_i = 4.2 \sim 6.6$ mm $\theta = 70^\circ$ $F_d = 26 \sim 51$ mm $F_t = 0.1 \sim 0.14$ mm Uncertainty – j : 96% of experimental data were correlated within error 10%. f : 92% of the experimental data were correlated within 12%.	[25]
Metal foams, 	For $1920 \leq Re_H \leq 4380$, $j^* = 0.5924Re_H^{-0.404}$, $f^* = 15.835 - 0.0014 Re_H$.	Wet Geometries = 3 (we obtained the correlations from the optimal geometry) L_d (Length) = 35 mm W (width) = 48 mm H (Height) = 7 mm P_d = 10 pores per inch (PPI) ε = 0.947 β = 624 m ² /m ³ K = 3.26×10^{-8} C = 241 1/m K_{Dukhan} = 1.29×10^{-7} m ² C_{Dukhan} = 23 1/m Uncertainty – j : R ² = 0.9965 f : R ² = 0.9950	[135]
Metal foams,	For forced convection, $Nu = 0.52Re_{df}^{0.5} Pr^{0.37}$,	Wet Geometries = 5 P_d = 5 – 40 pores per inch (PPI) ε = 0.94 – 0.97 K = $0.61 - 2.70 \times 10^{-7}$	[137]

		$dp(\text{pore dia}) = 0.18 - 0.402 \text{ cm}$ $df(\text{fiber dia}) = 0.025 - 0.55 \text{ cm}$	
<p>High power density air cooling cross-flow microchannel heat exchanger,</p> 	<p>For $12000 \leq Re_{D_h} \leq 20500$,</p> $j^* = 0.033122 Re_{D_h}^{-0.225},$ $f^* = 2.4344 Re_{D_h}^{-0.332}.$	<p>Dry Geometries = 1 $D_h = 0.52 \text{ mm}$</p> <p>Uncertainty – $j: R^2 = 0.9834$ $f: R^2 = 0.9914$</p>	[136]
<p>Cross rod geometries,</p> 	<p>For thermal entrance turbulent flow,</p> $Nu = 0.535 [\varepsilon (1 - \varepsilon)^{-0.25} f Re_{D_h}^2 Pr]^{1/3},$ $f = \begin{cases} 0.603 Re_{D_h}^{-0.104} \left(\frac{P_t}{D_{\text{wire}}} \right)^{0.136} & \text{for inline arrangement} \\ 0.728 Re_{D_h}^{-0.188} \left(\frac{P_t}{D_{\text{wire}}} \right)^{0.913} & \text{for staggered arrangement} \\ 0.475 Re_{D_h}^{-0.108} \left(\frac{P_t}{D_{\text{wire}}} \right)^{0.458} & \text{for random arrangement,} \end{cases}$ <p>where,</p> $D_h = \frac{4P_t}{\pi} - D_{\text{wire}},$ $\varepsilon = 1 - \frac{\pi D_{\text{wire}}}{4P_t}.$	<p>Geometries = not mentioned</p> <p>$1.571 \leq \frac{P_t}{D_{\text{wire}}} \leq 4.675$ $0.5 \leq \varepsilon \leq 0.832$ $D_{\text{wire}} = 9.53 \text{ mm}$</p> <p>Uncertainty – j is accurate with error $\pm 4.8\%$. f is accurate with error $\pm 7.8, 6.7$, and 7.1% for inline, staggered, and random arrangements; the experimental data were taken from [40].</p>	[124]

* We fitted the j - and f -factor correlations from plotted experimental data.

2.9. Assessments of reliable correlations used for different air-side geometries

Amongst all correlations described above, in this section, we suggest some correlations to represent different types of air-side arrangement. These suggestions are made by the authors' investigations based on some advantages summarized in Table 7. In this regard, some aspects are considered such as the number of fins per inch (FPI), number of investigated geometries upon with the correlation were fitted, a comparison with the experimental data [40], and representing the entire fin arrangements in generalized correlations. Based on these aspects, more than one correlation for each f - and j - correlations are recommended to give a credit for the more useful correlations. It is found that many correlations were obtained for louvered fin and fin-and-tube geometries, and some are carried out for strip-fin and wavy-fin geometries, while limited correlations were reported for other arrangements. Therefore, the selection of recommended correlations is also restricted by the availability of reported correlations.

Table 7. Some suggested correlations for the air-side geometries of compact and micro-channel heat exchangers.

Air-side geometry	Correlations*	Advantages
Louver-fin Table 1	j and f -factor [58, 59]	<ul style="list-style-type: none"> - Generalized j- and f-factor correlations for all types of louvered fin heat exchangers. - No. of geometries tested to obtain the correlations is 91. - Valid over a wide range of geometries; for example, FPI = 4 – 49. - The best agreement with the experimental data, refer to Figure 6. - Used frequently in the literature.
	j -factor [62]	<ul style="list-style-type: none"> - Generalized j-factor correlations for all types of louvered fin heat exchangers. - No. of geometries tested to obtain the correlations is 104. - Valid over a wide range of geometries; for example, FPI = 5 – 49. - In good agreement with the experimental data, refer to Figure 6.
	j - and f -factor [41]	<ul style="list-style-type: none"> - Generalized j- and f-factor correlations for all types of louvered fin heat exchangers.

		<ul style="list-style-type: none"> - No. of geometries tested to obtain the correlations is 126. - Valid over a wide range of geometries; for example, FPI = 5 – 49. - In good agreement with the experimental data, refer to Figure 6.
Wavy-fin Table 2	No generalized correlations are available for all geometries of wavy-fin.	
	<i>j</i> - and <i>f</i> -factor [75]	<ul style="list-style-type: none"> - Flow cross-sectional area is rectangular - No. of geometries tested to obtain the correlations is 18. - Valid over a wide range of geometries; for example, FPI = 12 – 30. - In excellent agreement with the experimental data, refer to Figure 7.
	<i>j</i> - and <i>f</i> -factor [76]	<ul style="list-style-type: none"> - Flow cross-sectional area is non-perfectly or perfectly rectangular. - No. of geometries tested to obtain the correlations is 15. - Valid over a range of geometries of FPI = 10 – 13. - In excellent agreement with the experimental data [76].
	<i>j</i> - and <i>f</i> -factor [74]	<ul style="list-style-type: none"> - Flow cross-sectional area is non-perfectly rectangular. - No. of geometries tested to obtain the correlations is 11. - Valid over a range of geometries as FPI = 10 – 12. - In good agreement with the experimental data, refer to Figure 7.
Strip-fin Table 3	All the correlations presented in Table 3 show a good accuracy with the experimental data, refer to Figure 9.	
	<i>j</i> - and <i>f</i> -factor [89]	<ul style="list-style-type: none"> - Generalized <i>j</i>- and <i>f</i>-factor correlations for offset strip fin. - No. of geometries tested to obtain the correlations is 55. - In excellent agreement with the experimental data, refer to Figure 9.
	<i>j</i> - and <i>f</i> -factor [85]	<ul style="list-style-type: none"> - Used frequently in the literature. - No. of geometries tested to obtain the correlations is 18. - In excellent agreement with the experimental data, refer to Figure 9.
Plate-fin tube(round) Table 4	No generalized correlations are available for all arrangements of plate-fin tube.	
	<i>j</i> - and <i>f</i> -factor [103]	<ul style="list-style-type: none"> - No. of geometries tested to obtain the correlations is 74. - Valid over a wide range of geometries; for example, FPI = 2 – 21.
	<i>j</i> - and <i>f</i> -factor [105]	<ul style="list-style-type: none"> - Specified for plate-fin having louvers

		<ul style="list-style-type: none"> - No. of geometries tested to obtain the correlations is 49. - Valid over a wide range of geometries; for example, FPI = 8 – 21.
	j- and f-factor [100]	<ul style="list-style-type: none"> - Used for wet air-side conditions. - Specified for plate-fin having slits. - Coated and uncoated surfaces. - No. of geometries tested to obtain the correlations is 22. - Valid over a range of geometries as FPI = 19 – 21.
	j- and f-factor [111]	<ul style="list-style-type: none"> - Used for wet air-side conditions. - No. of geometries tested to obtain the correlations is 9. - Valid over a wide range of geometries as FPI = 7 – 14.
Spiral-fin tube(round) Table 4	No generalized correlations are available for all arrangements of spiral-fin tube.	
	j- and f-factor [110]	<ul style="list-style-type: none"> - Valid over a range of geometries as FPI = 4 – 7. - The best agreement with the experimental data at different geometries, refer to Figure 11.
	j-factor by [43, 124]	<ul style="list-style-type: none"> - Valid over a wide range of geometries as FPI = 6 – 19. - One of the best agreement with the experimental data at different geometries, refer to Figure 11.
Plain fin and pin Table 5	No generalized correlations are available for all arrangements of plain fins and pins. Different methods were used to evaluate the correlations so that a comparison among them is not appropriate. The tabulated correlation could be used under the given limitations.	
	Nu and ΔP^* by [127]	<ul style="list-style-type: none"> - No. of geometries tested to obtain the correlations is 42. - Providing correlations for the most fins and pins arrangements. - Used mainly for heat sink applications.
Integrated manifold-microchannels	No new correlation was proposed for air-side of such heat exchangers.	
Cross-rod geometries Table 6	Nu and f-factor [124]	<ul style="list-style-type: none"> - Valid for different cross rod geometries arranged in inline, staggered, and random.

*The correlations were referred to the involving tables and the citation number, which can be easily picked up in the proper table.

2.10. Comparison between different air-side geometries

Compact heat exchangers are used in different applications depending upon different criteria including heat transfer enhancements, friction power, and compactness. Improving heat transfer

by interrupting the airflow and regenerating a turbulence result in a high friction power. The issue of dust accumulation and blockage also plays an important role for the selection of air-side arrangements in different applications. A general comparison of different air-side geometries is illustrated in Table 8 based on the heat transfer enhancement, friction power, compactness, dust accumulation, and appropriate applications. The plain-fin arrangement might be considered as a reference for such comparisons.

Table 8. Advantages and disadvantages of different air-side arrangements.

Air-side geometry	Advantages	Disadvantages	Applications
Plain-fin	- Low friction power. - Low dust accumulation. - Compactness could be high (for low hydraulic diameters).	- Low heat transfer.	Transformer air cooler, air cooled heat exchangers, Air-preheaters [138], and heat sink [127].
Pin-fin	- High heat transfer.	- High friction power. - Dust accumulation could be high for small space between pins, due to interrupting the flow. - Low compactness.	Power plant industry, electronic industry, and hot water boilers of central heating systems [138], and heat sink [127].
Louver-fin	- High heat transfer (higher than plate-fin and strip fin [138]). - Very good compactness.	- High friction power. - High dust accumulation and blockage [71].	Automotive industry, radiators, heaters, evaporators [65].
Wavy-fin	High heat transfer (depending mainly on wavy length and amplitude, and then on fin length, height and pitch [71]). - Low dust accumulation and blockage [71]. - Good compactness.	- High friction power (air flows in wavy path).	Off-road vehicles including agricultural vehicles, loading machines, excavators, and engineering machinery [71]. It can be also used in refrigeration and air conditioning, process industry [138].
Offset strip-fin	- High heat transfer (higher than plain-fin	- High friction power (flow is interrupted	Aircraft, cryogenic, small industries

	<p>by 1.5 to 4 times [138]).</p> <ul style="list-style-type: none"> - Good compactness. 	<p>several times along a flow path).</p> <ul style="list-style-type: none"> - Susceptible to dust accumulations (specially at flow interrupters) 	[138], and aircraft applications [139].
Fin and tube (round)	<ul style="list-style-type: none"> - High heat transfer (the plate can be flat, louver-fin, wavy, slit, or spiral fin). - Dust accumulation could be high (e.g. for louvered plates) or low (e.g. for plain plates). - Good compactness. 	<ul style="list-style-type: none"> - High friction power, especially for non-plain plates. 	Motivation application [99], refrigeration and air conditioning [117], boilers, waste heat recovery [140], and dry cooling systems in power plants [113].
Microchannel	<ul style="list-style-type: none"> - High heat transfer. - Ultra-compactness. 	<ul style="list-style-type: none"> - Very high friction power(due to very low hydraulic diameter) [5]. - Susceptible to fouling (liquids are frequently used). 	Aerospace, automotive, bioengineering, cooling of gas turbine blades, process industries, refrigeration and air conditioning, infrared detectors, and powerful laser mirrors and superconductors [141].
Integrated manifold-microchannel	<ul style="list-style-type: none"> - High heat transfer. - Low friction (manifold distributes the flow). - Excellent compactness. 	<ul style="list-style-type: none"> - Susceptible to fouling (liquids are frequently used). 	Generally used in electronics; particularly, in microchips cooling [142], also in the same applications of microchannel heat exchangers.

To compare the air-side thermal-hydraulic performance of different arrangements, Kays and London [40] reported a comparison method by plotting heat-transfer coefficient vs. friction power. The heat transfer coefficient and friction power as a function of f and j factors are [40]:

$$h_e = \frac{c_p \mu}{Pr^{2/3}} \frac{j \cdot Re}{D_h}, \quad (10)$$

$$E = \frac{\mu^3}{2 \rho^2} \left(\frac{1}{D_h} \right)^3 f \cdot Re^3, \quad (11)$$

where h_e (in $\text{W/m}^2\cdot\text{K}$) is the heat transfer coefficient, E (in W/m^2) is the friction power per unit of surface area, c_p (in $\text{J/kg}\cdot\text{K}$) is the air specific heat capacity, μ (in $\text{Pa}\cdot\text{s}$) is the air dynamic viscosity, D_h (m) is the hydraulic diameter, ρ (in kg/m^3) is the air density, Re is Reynolds number, and Pr is Prandtl number.

Furthermore, some performance indices were suggested in the literature such as a surface area goodness factor (j/f) [62, 136, 143, 144]. However, j/f does not take account of the effect of several primary parameters such as heat transfer area, fin efficiency, and heat exchanger compactness. Another index (volume goodness factor) can be driven from Eqs. (10) and (11) by eliminating Re as:

$$\frac{j}{f^{1/3}} = \frac{Pr^{2/3}}{2^{1/3} \rho^{2/3} c_p} \frac{h}{E^{1/3}}. \quad (12)$$

Similar to j/f , this index ($j/f^{1/3}$) did not consider the heat transfer area, fin efficiency, and heat exchanger compactness. To a degree, plotting $j/f^{1/3}$ vs. Re could be used alternatively instead of plotting h vs. E . Moreover, it is recommended for a good heat transfer to pressure loss performance [3, 67, 91]. It was also used to compare the extended surfaces performance to that of plain surfaces ($(j/j_p)/(f/f_p)^{1/3}$) having the same hydraulic diameters [144, 145].

The above formulations of performance indices do not consider the effect of compactness of heat exchangers, heat transfer area and efficiency, as well as they imply the use of same hydraulic diameter for all (compared) geometries [144]. As a result, Shah and Sekulić [144] and Webb and Kim [145] reported more reliable core volume goodness factor to compare compact heat exchangers performance by adding overall heat transfer efficiency as well as the heat exchanger compactness to Eqs. (10) and (11). The resulting equations are written as:

$$\eta_o h_e \beta = \frac{c_p \mu}{Pr^{2/3}} \eta_o \frac{4\sigma}{D_h^2} j \cdot Re, \quad (13)$$

$$E \beta = \frac{\mu^3}{2 \rho^2} \frac{4\sigma}{D_h^4} f \cdot Re^3. \quad (14)$$

Here, β ($= 4\sigma/D_h$) is the compactness, η_o ($= 1 - (A_f/A_{tot}) (1 - \eta_f)$) is the overall heat transfer efficiency, σ is the ratio of the minimum flow area over the frontal area. The air properties in Eqs.

(3) and (4) are estimated at any preferred "standard condition" [145]. Therefore, plotting ' $\eta_0 h_e \beta$ ' vs. ' $E \beta$ ' can efficiently predict the best heat transfer and fluid-flow performance from the viewpoint of heat exchanger volume.

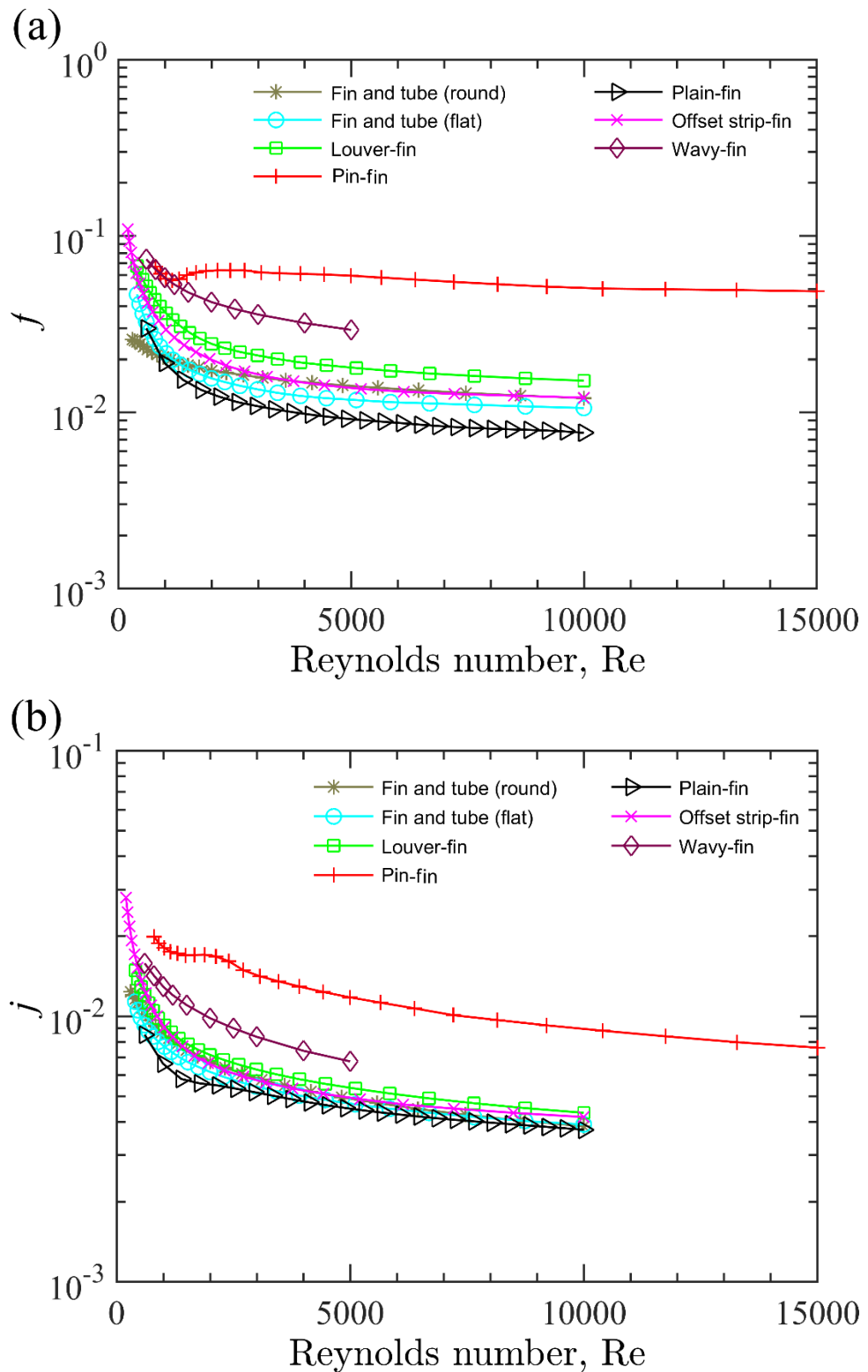
We have conducted the typical geometries of Kays and London [40] to compare the performance of different air-side arrangements. About 72 geometries have been pre-evaluated to select geometries having an optimal j/f , $j/f^{d/3}$, and $(\eta_0 h_e \beta)$ vs. $(E \beta)$ from each air-side type (louver-fin, offset strip-fin, wavy-fin, fin and tube (round), fin and tube (flat), plain-fin, and pin-fin). These geometries are listed in Table 9. It is noticed that, two indices may have the optimal values form the same geometry in the same air-side type (for example, louvered plate-fin, surface 1/4(b)-11.1 shows optimal j/f and $(\eta_0 h_e \beta)$ vs. $(E \beta)$ amongst all louver-fin arrangements). To evaluate these indices, the reported f and j factors [40, 146] are used, and the materials properties are taken at 330 K and 101.3 kPa.

Table 9. Geometrical parameters of optimal typical air-side arrangements [40].

Arrangement	Geometrical parameters (the units are in mm)
Set # 1: The optimal typical geometries for j/f	
Louvered plate-fin, surface 1/4(b)-11.1	$F_p = 2.288, L_p = 3.084, F_l = 6.35, \theta = 30^\circ, T_d = 40, F_t = 0.152, L_h = 0.7735, T_p = 9.434$
Offset strip-fin, surface 1/8-16.00(D)	$F_p = 1.588, h = 6.4777, L = 3.175, t = 0.152, L_d = 40$
Wavy-fin, surface 11.5-3/8W	$F_p = 2.21, h = 9.525, L = 9.525, t = 0.254, L_d = 40, 2A = 1.981$
Fin and tube (flat), surface 9.29-0.737-SR	$F_p = 2.732, P_l = 20.07, P_t = 13.97, F_t = 0.102, N_{row} = 3, L_d = 40, D_o = 2.54$
Fin and tube (round), surface CF-7.0-5/8J	$F_p = 3.623, P_l = 34.29, P_t = 31.29, F_t = 0.254, N_{row} = 3, L_d = 40, D_o = 16.38, d_f = 30.73$ (spiral fin)
Plain-fin, surface 5.30	$P = 9.58, H = 11.94, t = 0.152, l = 63.29, D_h = 6.145$
Pin-fin, surface PF-9(F)	$d = 1.651, S_t = 6.045, S_l = 4.775, H = 12.95, D_h = 9.042$
Set # 2: The optimal typical geometries for $j/f^{d/3}$	
Louvered plate-fin, surface 3/4-11.1	$F_p = 2.288, L_p = 2.344, F_l = 6.35, \theta = 30^\circ, T_d = 40, F_t = 0.152, L_h = 0.586, T_p = 6.502$
Offset strip-fin, surface 1/2-11.94(D)	$F_p = 2.129, h = 3.01, L = 12.7, t = 0.152, L_d = 40$
Wavy-fin, surface 17.8-3/8W	$F_p = 1.427, h = 10.45, L = 9.525, t = 0.152, L_d = 40, 2A = 1.969$
Fin and tube (flat), surface 9.68-0.87	$F_p = 2.624, P_l = 22.1, P_t = 11.07, F_t = 0.102, N_{row} = 3, L_d = 40, D_o = 3.048$
Fin and tube (round), surface 7.75-5/8T	$F_p = 3.623, P_l = 44.45, P_t = 38.1, F_t = 0.4064, N_{row} = 3, L_d = 40, D_o = 17.18$ (flat fin)
Plain-fin, surface 5.30	$P = 9.58, H = 11.94, t = 0.152, l = 63.29, D_h = 6.145$
Pin-fin, surface PF-10(F)	$d = \text{elliptic } (1.6, 0.533), S_t = 2.886, S_l = 2.794, H = 11.18, D_h = 4.343$

Set # 3: The optimal typical geometries for $(\eta_0 h_e \beta)$ vs. $(E \beta)$	
Louvered plate-fin, surface 1/4(b)-11.1	$F_p = 2.288, L_p = 3.084, F_l = 6.35, \theta = 30^\circ, T_d = 40, F_t = 0.152, L_h = 0.7735, T_p = 9.434$
Offset strip-fin, surface 1/10-27.03	$F_p = 20.9398, h = 6.35, L = 2.54, t = 0.152, L_d = 40$
Wavy-fin, surface 17.8-3/8W	$F_p = 1.427, h = 10.45, L = 9.525, t = 0.152, L_d = 40, 2A = 1.969$
Fin and tube (flat), surface 11.32-0.737-SR	$F_p = 2.227, P_l = 18.72, P_t = 13.97, F_t = 0.102, N_{row} = 3, L_d = 40, D_o = 2.54$
Fin and tube (round), surface CF-8.72	$F_p = 2.915, P_l = 20.32, P_t = 24.77, F_t = 0.4572, N_{row} = 3, L_d = 40, D_o = 9.652, d_f = 23.37$ (spiral fin)
Plain-fin, surface 46.45T	$P = 1.095, H = 2.54, t = 0.051, l = 66, D_h = 0.805$
Pin-fin, surface PF-9(F)	$d = 1.651, S_t = 6.045, S_l = 4.775, H = 12.95, D_h = 9.042$

Figure 14 shows the thermal-hydraulic performance of different air-side arrangements (see Set #1, Table 9) based on the optimal j/f index. Figure 14(a) exhibits the f -factor values of different air-side arrangements against Re values. The highest f -factor values, which mean high pressure drop, are obtained by pin-fin (surface PF-9(F)) while the lowest values are shown for the plain-fin (surface 5.30). This is because the plain-fin has no flow interruptions along the flow path. The values of j -factor are shown in Figure 14(b). Also, the pin-fin surface shows the highest j values (which may refer to high heat transfer) while the lowest values are associated with the plain-fin. The performance index (j/f) values are shown in Figure 14(c). Noticeably, j/f gives some discriminants to the surfaces that have lower f -factor values. The values of f -factor are mostly smaller than j -factor; thus, low values of f directly increase j/f values. Therefore, the best j/f values (for $Re > 1800$) are obtained by the plain-fin arrangement followed by flat-tube plate-fin.



(c)

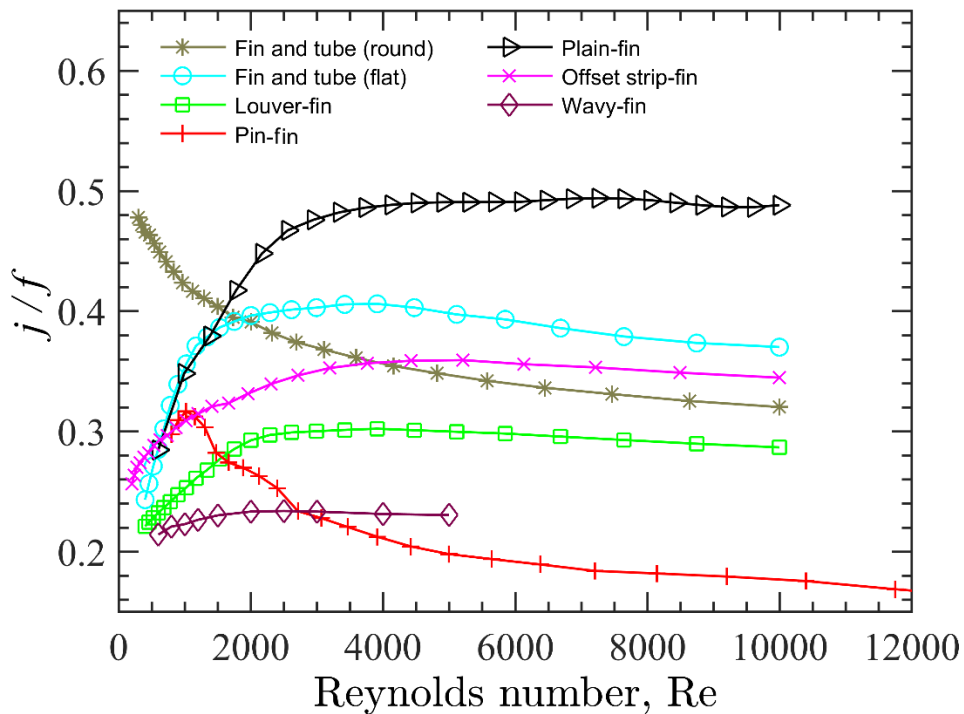
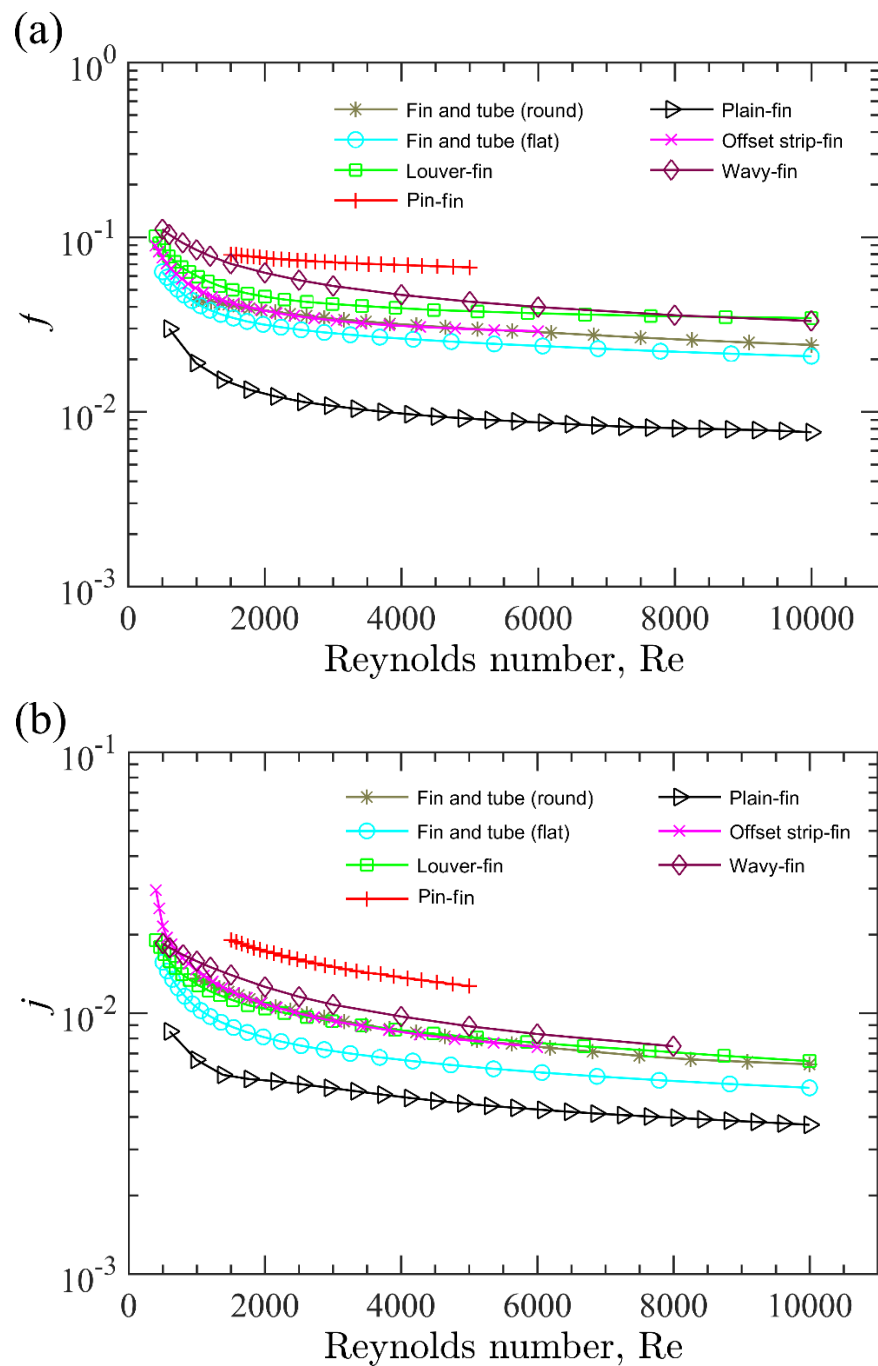


Figure 14. Comparison of different air-side arrangements (refer to Set #1, Table 9) based on j/f performance index; (a) f -factor, (b) j -factor, and (c) j/f .

Concerning $j/f^{d/3}$ index, Figure 15 shows the thermal-hydraulic performances of different air-side arrangements (see Set #2, Table 9). The f - and j -factor values (Figure 15(a and b)) of the Set #2 have similar order to those of Set #1 (see Figure 14(a and b)); the highest f - and j -factor values are obtained by pin-fin (surface PF-10(F)) while the lowest values are shown for the plain-fin (surface 530). Figure 15(c) shows the performance index ($j/f^{d/3}$) values against Reynolds number. Unlike j/f index, the $j/f^{d/3}$ gives a little discriminant to the surfaces that have higher j -factor values. The pin-fin surface has the highest j and $j/f^{d/3}$ values while the lowest are obtained by the plain-fin surface. The surfaces offset strip-fin and fin-and-tube (round) show good performances in terms of both the j/f (see Figure 14(c)) and the $j/f^{d/3}$ (see Figure 15(c)). It may refer from the j/f and the $j/f^{d/3}$ values that, the first one (j/f) might be used when the pumping power is the primary factor for the heat exchanger design, whereas the second ($j/f^{d/3}$) is important when the heat transfer enhancements are the main factor.



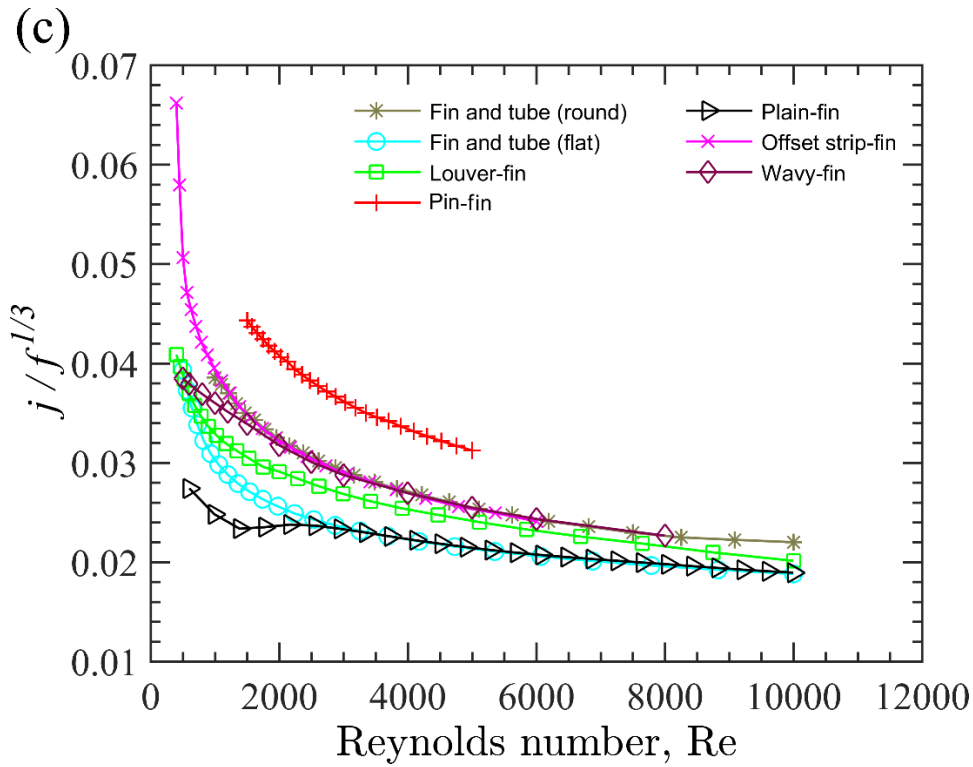
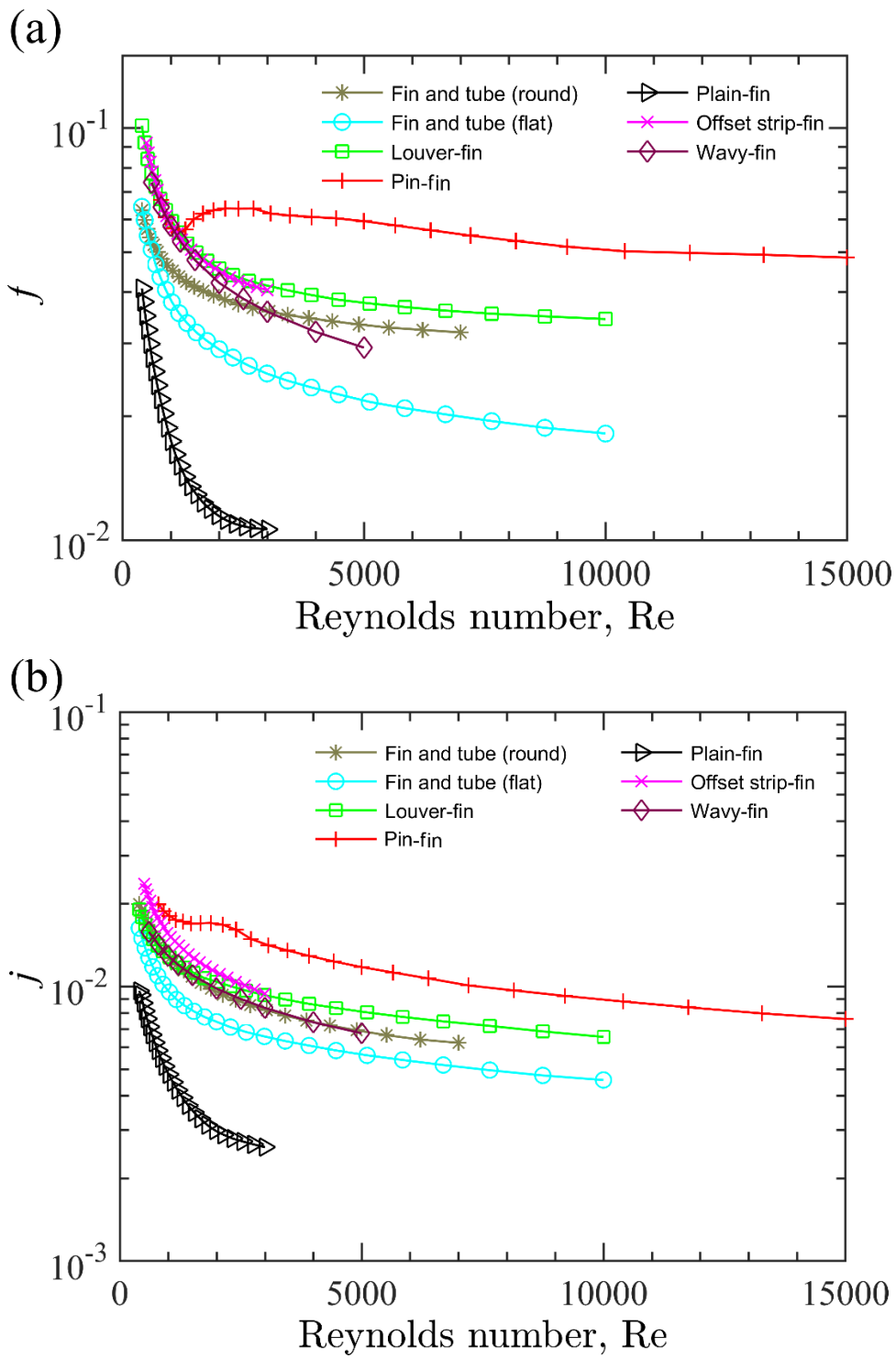


Figure 15. Comparison of different air-side arrangements (refer to Set #2, Table 9) based on $j/f^{d/3}$ performance index; (a) f -factor, (b) j -factor, and (c) $j/f^{d/3}$.

The results shown in Figure 14 and Figure 15 are direct functions of f - and j -factor with neglecting the heat transfer area, fin efficiency, and heat exchanger compactness. Thus, the air-side heat transfer ($\eta_0 h_e \beta$) vs. power fraction ($E \beta$) plots represent more robust method to compare air-side arrangements. Set # 3 listed in Table 9 are selected geometries for each type of air-side compact heat exchanger, that have the optimal values of $\eta_0 h_e \beta$ vs. $E \beta$ from the 72 typical geometries of Kays and London [40]. The f - and j -factor values vs Reynolds number for this set (Set # 3) are shown in Figure 16 (a and b). In a similar behavior to Set #1 and Set # 2, the highest values of f and j are obtained by the pin-fin arrangement while the lowest are with the plain-fin.

Figure 16(c) shows the heat transfer index $\eta_0 h_e \beta$ against $E \beta$ values. The offset strip-fin (surface 1/10-27.03) has the highest heat transfer values at constant friction power values. For instance, at 100 kW/m^3 friction power (per unit volume of heat exchanger), the heat transfer index is about 287, 208, 174, 183, 112, 110, and 108 $\text{kW}/\text{m}^3 \cdot \text{K}$ for offset strip-fin, plain-fin, fin and tube

(flat), louver-fin, fin and tube (round), wavy-fin, and pin-fin, respectively. The lowest values of pin-fin (surface, PF-9(F)) might be explained by its high values of f -factor and a low compactness (e.g. $D_h = 9.04$ mm and $\beta = 322 \text{ m}^2/\text{m}^3$); whereas, plain-fin (surface 46.45T) shows an excellent heat transfer to friction power performance due to low f -values and high compactness (e.g. $D_h = 0.805$ mm $\beta = 1568 \text{ m}^2/\text{m}^3$). It may be believed that, the plain-fin arrangements have the lowest performance; however, Figure 16(c) confirms that a proper design of plain-fin can be competitive in the heat transfer/friction power performance to other arrangements. The offset strip-fin arrangement has, in general, good compactness (e.g. $D_h = 1.42$ mm and $\beta = 1068 \text{ m}^2/\text{m}^3$) beside a low friction power and good heat transfer).



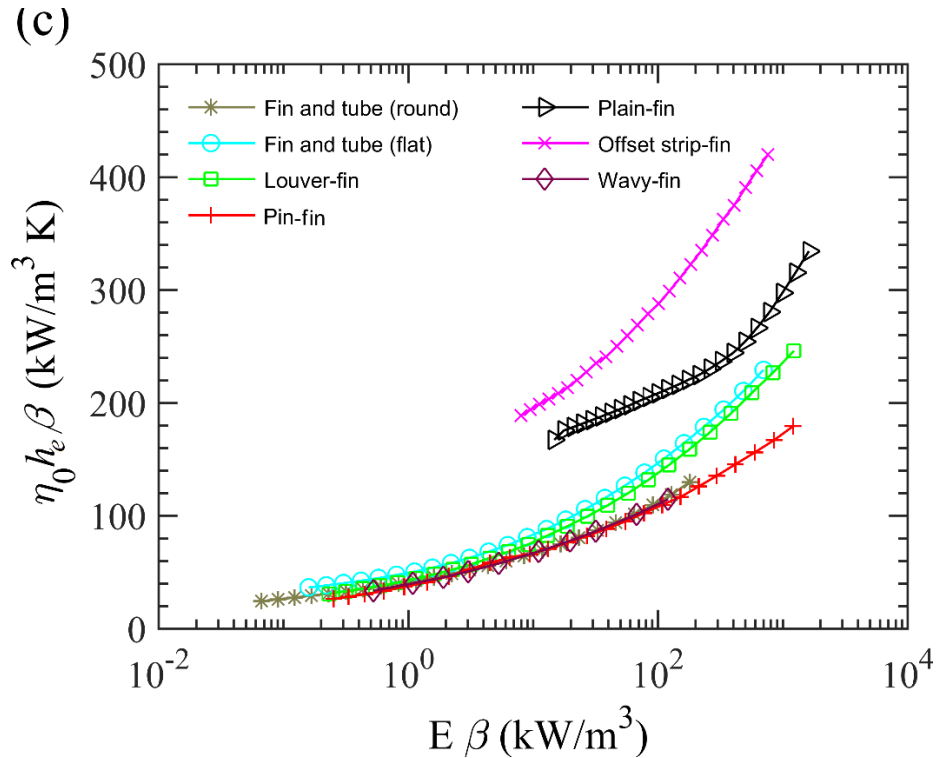


Figure 16. Comparison of different air-side arrangements (refer to Set # 3, Table 9) based on heat transfer index vs. friction with considering the compactness; (a) f -factor, (b) j -factor, and (c) $(\eta_0 h \beta)$ vs. $(E \beta)$.

Based on j and f values of the three investigated sets (Set #1, 2, and 3; as shown in Figure 14(a and b), Figure 15(a and b), and Figure 16(a and b))) and $\eta_0 h_e \beta$ of the Set # 3 (Figure 16(c)), we summarize the heat and flow performance of different air-side geometries in Figure 17. The order of the optimal j and f is assigned based on the average values of the three figures (Figure 14(a and b), Figure 15(a and b), and Figure 16(a and b)). This summary ends up with giving a credit to offset strip-fin (surface 1/10-27.03) as an optimal air-side arrangement when the heat transfer, friction power, and compactness are the critical criteria for the compact heat exchanger selection. Again, it is worth mentioning here that, this optimization method is only relied on the typical geometries of Kays and London [40], which are the most practical arrangements.

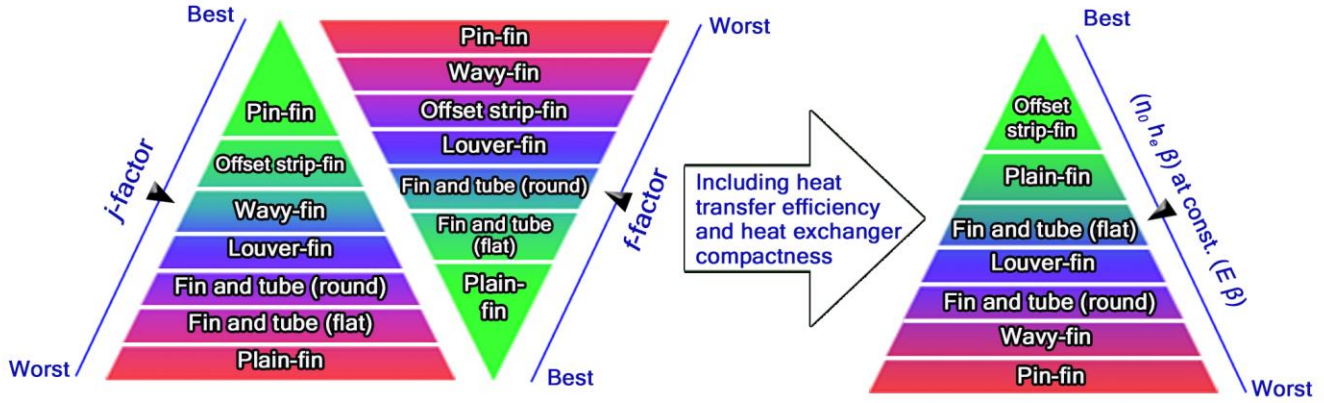


Figure 17. Air-side thermal-hydraulic performance optimization charts in terms of *j*-factor, *f*-factor, and $\eta_0 h_e \beta$ values for the typical geometries of Kays and London [40].

3. Conclusion and recommendations

This study review the existing thermal-hydraulic performance correlations, mainly in terms of Colburn *j*-factor and fanning friction factor (*f*) that are typically used to evaluate heat transfer rate and pressure drop for the air-side of compact and micro-channel heat exchangers. The *j*- and *f*-factor correlations of louver-fin, wavy-fin, offset strip-fin arrangements, plain fins and pins could be used in most applications of both types of heat exchangers (compact and microchannel), whereas those used for finned tube (round) heat exchangers are only valid for compact heat exchangers as a result of large tube diameters (> 6 mm).

The thermal-hydraulic correlations are listed in tables based on the fin arrangement type, Reynolds number range, geometrical parameter limits, and fitting uncertainties. Furthermore, we compared some correlations representing different types of fin arrangements to the experimental data reported by Kays and London [40]. It is found that the most correlations were devoted to the louver-fin and the finned tube (round) heat exchangers. In contrast, the heat and flow performance correlations of the air-side of manifold-microchannal heat exchangers are scarce. Some researchers introduced generalized correlations such as those obtained by [41, 58, 59, 62] for representing all types of louver-fin arrangements. Furthermore, some researchers included more than 50 different geometries in pursuit of introducing accurate correlations (e.g. 126 louver-fin geometries by Park and Jacobi [41], 55 offset strip-fin geometries by Yang and Li [89], and 74 of fin-and-tube geometries by Wang et al. [103]). The heat-transfer and fluid-flow correlations driven for wet and frost surfaces are limited. The most obtained wet surfaces correlations were proposed for fin-and-tube heat exchangers, and only few were carried out for louver-fin heat exchangers, because these types

are typically used in the refrigeration and air conditioning applications. The parameters influencing the heat transfer and flow for the wet surfaces were not satisfactorily addressed such as evaporation/condensation rate, variation of water film thickness on fin surfaces, thermal resistance of water film, contraction of the flow cross-section, wet contact angle, and evaporation/condensation latent heat.

A comparison between different geometries based on the optimal j -factor, f -factor, and heat transfer/friction power performances are also investigated.

According to this review, we found some gaps related to thermal-hydraulic performance correlations. Therefore, we suggest the following recommendations:

- Generalized thermal-hydraulic performance correlations using a wide range of different geometries, under same fin type, are needed for the air-side of wavy-fin, offset strip-fin, plain fin and pin arrangements.
- Performance correlations related to wet surfaces or humid air applications should be widely explored for microchannel and compact heat exchangers – especially for louver-fin, wavy-fin, offset strip-fin and plain fin and pin arrangements. The effect of water evaporation and condensation (including their latent heats) on the heat transfer and flow should be explored. Moreover, the additional thermal resistance of a water film on surfaces and the corresponding contraction of air flow cross-section should be studied. The coated, hydrophobic, and hydrophilic surfaces should be investigated for all fin types under different humid conditions.
- Frost surfaces result in high-pressure drop; the existing correlations are not valid for such conditions. The accumulated ice acts, moreover, as an additional resistance to heat transfer. The need to obtain correlations to be valid under these conditions, including accumulation and removal of ice, are important for thermal-hydraulic design and performance applications.
- Manifold-microchannel heat exchangers are expected to be the future of heat exchangers; however, no correlations obtained for air-side heat-transfer and fluid-flow performances. The research should immensely introduce new correlations for integrated manifolds and microchannels.
- Computational Fluid Dynamics (CFD) as a cost and time effective tool could be used to produce reasonably accurate thermal-hydraulic correlations, including wide range of geometrical parameters, to generalize correlations for each type of compact and microchannel heat exchangers.
- Involving all geometrical parameters as independent variables to the correlation equations will result in more accuracy and less uncertainty.
- Metal-foam microchannel heat exchangers as promising candidates of heat exchangers need more investigations.

Acknowledgements

The authors acknowledge the support provided by King Fahd University of Petroleum & Minerals through the project IN151001.

References

- [1] Kong, Y.Q., et al., *Impacts of geometric structures on thermo-flow performances of plate fin-tube bundles*. International Journal of Thermal Sciences, 2016. **107**: p. 161-178.
- [2] Song, R., M. Cui, and J. Liu, *A correlation for heat transfer and flow friction characteristics of the offset strip fin heat exchanger*. International Journal of Heat and Mass Transfer, 2017. **115**(Part B): p. 695-705.
- [3] Kim, J.H., J.H. Yun, and C.S. Lee, *Heat-Transfer and Friction Characteristics for the Louver-Fin Heat Exchanger*. Journal of Thermophysics and Heat Transfer, 2004. **18**(1): p. 58-64.
- [4] Kharati-Koopaei, M. and M.R. Akhtari, *Numerical study of fluid flow and heat transfer phenomenon within microchannels comprising different superhydrophobic structures*. International Journal of Thermal Sciences, 2018. **124**(Supplement C): p. 536-546.
- [5] Andhare, R.S., et al., *Heat transfer and pressure drop characteristics of a flat plate manifold microchannel heat exchanger in counter flow configuration*. Applied Thermal Engineering, 2016. **96**(Supplement C): p. 178-189.
- [6] Dixit, T. and I. Ghosh, *Review of micro- and mini-channel heat sinks and heat exchangers for single phase fluids*. Renewable and Sustainable Energy Reviews, 2015. **41**: p. 1298-1311.
- [7] Okbaz, A., et al., *An experimental, computational and flow visualization study on the air-side thermal and hydraulic performance of louvered fin and round tube heat exchangers*. International Journal of Heat and Mass Transfer, 2018. **121**: p. 153-169.
- [8] Ryu, K., S.-J. Yook, and K.-S. Lee, *Optimal design of a corrugated louvered fin*. Applied Thermal Engineering, 2014. **68**(1): p. 76-79.
- [9] Singh, S.K., M. Mishra, and P.K. Jha, *Nonuniformities in compact heat exchangers—scope for better energy utilization: A review*. Renewable and Sustainable Energy Reviews, 2014. **40**: p. 583-596.
- [10] Sheik Ismail, L., R. Velraj, and C. Ranganayakulu, *Studies on pumping power in terms of pressure drop and heat transfer characteristics of compact plate-fin heat exchangers—A review*. Renewable and Sustainable Energy Reviews, 2010. **14**(1): p. 478-485.
- [11] Kakaç, S., H. Liu, and A. Pramanjaroenkij, *Heat Exchangers: Selection, Rating, and Thermal Design, Second Edition*. 2002: Taylor & Francis. p. 615.
- [12] Khan, M.G. and A. Fartaj, *A review on microchannel heat exchangers and potential applications*. International Journal of Energy Research, 2011. **35**(7): p. 553-582.
- [13] Luo, L., Y. Fan, and D. Tondeur, *Heat exchanger: from micro- to multi-scale design optimization*. International Journal of Energy Research, 2007. **31**(13): p. 1266-1274.
- [14] Escher, W., et al., *Experimental Investigation of an Ultrathin Manifold Microchannel Heat Sink for Liquid-Cooled Chips*. Journal of Heat Transfer, 2010. **132**(8): p. 081402-081402-10.
- [15] Fedorov, A.G. and R. Viskanta, *Three-dimensional conjugate heat transfer in the microchannel heat sink for electronic packaging*. International Journal of Heat and Mass Transfer, 2000. **43**(3): p. 399-415.

- [16] Ghani, I.A., et al., *Heat transfer enhancement in microchannel heat sink using hybrid technique of ribs and secondary channels*. International Journal of Heat and Mass Transfer, 2017. **114**(Supplement C): p. 640-655.
- [17] Kim, Y.H., et al., *Forced air cooling by using manifold microchannel heat sinks*. KSME International Journal, 1998. **12**(4): p. 709-718.
- [18] Mudawar, I., *Two-Phase Microchannel Heat Sinks: Theory, Applications, and Limitations*. Journal of Electronic Packaging, 2011. **133**(4): p. 041002-041002-31.
- [19] Silvério, V., et al., *Design, fabrication and test of an integrated multi-microchannel heat sink for electronics cooling*. Sensors and Actuators A: Physical, 2015. **235**(Supplement C): p. 14-27.
- [20] Teertstra, P., et al. *Analytical forced convection modeling of plate fin heat sinks*. in *Fifteenth Annual IEEE Semiconductor Thermal Measurement and Management Symposium (Cat. No.99CH36306)*. 1999. p. 34-41.
- [21] Wang, G.-L., et al., *Heat Transfer and Friction Characteristics of the Microfluidic Heat Sink with Variously-Shaped Ribs for Chip Cooling*. Sensors (Basel, Switzerland), 2015. **15**(4): p. 9547-9562.
- [22] Alfaryjat, A.A., et al., *Numerical investigation of heat transfer enhancement using various nanofluids in hexagonal microchannel heat sink*. Thermal Science and Engineering Progress, 2018. **5**: p. 252-262.
- [23] Huang, L., V. Aute, and R. Radermacher, *A model for air-to-refrigerant microchannel condensers with variable tube and fin geometries*. International Journal of Refrigeration, 2014. **40**(Supplement C): p. 269-281.
- [24] Li, J., et al., *Numerical study on air-side performance of an integrated fin and micro-channel heat exchanger*. Applied Thermal Engineering, 2010. **30**(17): p. 2738-2745.
- [25] Li, J., S. Wang, and W. Zhang, *Air-side thermal hydraulic performance of an integrated fin and micro-channel heat exchanger*. Energy Conversion and Management, 2011. **52**(2): p. 983-989.
- [26] Ling, L., et al., *Study on thermal performance of micro-channel separate heat pipe for telecommunication stations: Experiment and simulation*. International Journal of Refrigeration, 2015. **59**(Supplement C): p. 198-209.
- [27] Moallem, E., et al., *Effects of frost growth on louvered folded fins of microchannel heat exchangers on the time-dependent air side convective heat transfer coefficient*. Experimental Thermal and Fluid Science, 2017. **88**(Supplement C): p. 326-335.
- [28] Sedrez, P.C., J.R.B. Jr., and G.B. Ribeiro. *Experimental Evaluation of Compact Microchannel Heat Exchangers with Louver Fins* in *22nd International Congress of Mechanical Engineering (COBEM 2013)*. 2013. Ribeirão Preto, SP, Brazil. p. 4569-4577.
- [29] Türkakar, G., T. Okutucu-Özyurt, and S.G. Kandlikar, *Entropy generation analysis of a microchannel-condenser for use in a vapor compression refrigeration cycle*. International Journal of Refrigeration, 2016. **70**(Supplement C): p. 71-83.
- [30] Yin, X.-W., et al., *Evaluation of microchannel condenser characteristics by numerical simulation*. International Journal of Refrigeration, 2015. **54**(Supplement C): p. 126-141.
- [31] Bell, I.H. and E.A. Groll, *Air-side particulate fouling of microchannel heat exchangers: Experimental comparison of air-side pressure drop and heat transfer with plate-fin heat exchanger*. Applied Thermal Engineering, 2011. **31**(5): p. 742-749.
- [32] Hrnjak, P. and A.D. Litch, *Microchannel heat exchangers for charge minimization in air-cooled ammonia condensers and chillers*. International Journal of Refrigeration, 2008. **31**(4): p. 658-668.
- [33] Siddiqui, F.A., E.S. Dasgupta, and A. Fartaj, *Experimental investigation of air side heat transfer and fluid flow performances of multi-port serpentine cross-flow mesochannel heat exchanger*. International Journal of Heat and Fluid Flow, 2012. **33**(1): p. 207-219.
- [34] Xia, Y., et al., *Frost, defrost, and refrost and its impact on the air-side thermal-hydraulic performance of louvered-fin, flat-tube heat exchangers*. International Journal of Refrigeration, 2006. **29**(7): p. 1066-1079.

- [35] Asadi, M., G. Xie, and B. Sundén, *A review of heat transfer and pressure drop characteristics of single and two-phase microchannels*. International Journal of Heat and Mass Transfer, 2014. **79**: p. 34-53.
- [36] Kim, M.-H., et al., *Microchannel Heat Exchanger Design for Evaporator and Condenser Applications*, in *Advances in Heat Transfer*. 2003, Elsevier. p. 297-429.
- [37] Mohammed, H.A., et al., *Heat transfer and fluid flow characteristics in microchannels heat exchanger using nanofluids: A review*. Renewable and Sustainable Energy Reviews, 2011. **15**(3): p. 1502-1512.
- [38] Siddiqui, O.K. and S.M. Zubair, *Efficient energy utilization through proper design of microchannel heat exchanger manifolds: A comprehensive review*. Renewable and Sustainable Energy Reviews, 2017. **74**: p. 969-1002.
- [39] Garimella, S., A. Agarwal, and J.D. Killion, *Condensation Pressure Drops in Circular Microchannels*, in *ASME 2nd International Conference on Microchannels and Minichannels*ASME: New York. 2004. p. 649-656.
- [40] Kays, W.M. and A.L. London, *Compact Heat Exchangers*. Vol. 3rd. 1984: Krieger, Malabar, FL. p. 336.
- [41] Park, Y.-G. and A.M. Jacobi, *Air-Side Heat Transfer and Friction Correlations for Flat-Tube Louver-Fin Heat Exchangers*. Journal of Heat Transfer, 2008. **131**(2): p. 021801-021801-12.
- [42] Kays, W.M. and A.L. London, *Heat Transfer and Flow Friction Characteristics of Some Compact Heat-Exchanger Surfaces, Part I. Test System and Procedure*. Trans. ASME, 1950. **72**: p. 1075-1085.
- [43] Briggs, D.E. and E.H. Young, *Convection Heat Transfer and Pressure Drop of Air Flowing across Triangular Pitch Banks of Finned Tubes*. Chemical Engineering Progress Symposium Series, 1963. **59**(41): p. 1-10.
- [44] Robinson, K.K. and D.E. Briggs, *Pressure drop of air flowing across triangular pitch banks of finned tubes*. Chem. Eng. Prog. Symp. Series, 1966. **64**(62): p. 177-184.
- [45] Rich, D.G., *The Effect of Fin Spacing on the Heat Transfer and Friction Performance of Multi-Row, Smooth Plate Fin-and-Tube Heat Exchangers*. ASHRAE Transactions, 1973. **79**(2): p. 137-145.
- [46] Rich, D.G., *The effect of the number of tubes rows on heat transfer performance of smooth plate fin-and-tube heat exchangers*. ASHRAE Transactions, 1975. **81**(1): p. 307-317.
- [47] Wieting, A.R., *Empirical Correlations for Heat Transfer and Flow Friction Characteristics of Rectangular Offset-Fin Plate-Fin Heat Exchangers*. Journal of Heat Transfer, 1975. **97**(3): p. 488-490.
- [48] Davenport, C.J., *Correlation for heat transfer and flow friction characteristics of louvered fin*. AIChE Syrup. Ser., 1983. **79**: p. 19-27.
- [49] Shinde, P. and C.-X. Lin, *A heat transfer and friction factor correlation for low air-side Reynolds number applications of compact heat exchangers (1535-RP)*. Science and Technology for the Built Environment, 2017. **23**(1): p. 192-210.
- [50] Saleem, A. and M.-H. Kim, *Air-side thermal hydraulic performance of microchannel heat exchangers with different fin configurations*. Applied Thermal Engineering, 2017. **125**: p. 780-789.
- [51] Jang, J.-Y. and C.-C. Chen, *Optimization of louvered-fin heat exchanger with variable louver angles*. Applied Thermal Engineering, 2015. **91**: p. 138-150.
- [52] Leu, J.-S., et al., *A numerical investigation of louvered fin-and-tube heat exchangers having circular and oval tube configurations*. International Journal of Heat and Mass Transfer, 2001. **44**(22): p. 4235-4243.
- [53] Achaichia, A. and T.A. Cowell, *Heat transfer and pressure drop characteristics of flat tube and louvered plate fin surfaces*. Experimental Thermal and Fluid Science, 1988. **1**(2): p. 147-157.
- [54] Sundén, B. and J. Svantesson, *Correlation of j- and f-factors for Multilouvered Heat Transfer Surfaces*, in *Proc. of the 3rd UK National Conference on Heat Transfer*. 1992. p. 805-811.

- [55] Dillen, E.R. and R.L. Webb, *Rationally Based Heat Transfer and Friction Correlations for the Louver Fin Geometry*, SAE International. 1994. p. 600-607.
- [56] Webb, R.L., Y. Chang, and C. Wang, *Heat Transfer and Friction Correlations for the Louver Fin Geometry*, in *Vehicle Thermal Management Systems Conference Proc.* 1995. p. 533-541.
- [57] Chang, Y.-J. and C.-C. Wang, *Air Side Performance of Brazed Aluminum Heat Exchangers*. 1996. **3**(1): p. 15-28.
- [58] Chang, Y.-J., et al., *A generalized friction correlation for louver fin geometry*. *International Journal of Heat and Mass Transfer*, 2000. **43**(12): p. 2237-2243.
- [59] Chang, Y.-J. and C.-C. Wang, *A generalized heat transfer correlation for louver fin geometry*. *International Journal of Heat and Mass Transfer*, 1997. **40**(3): p. 533-544.
- [60] Kim, M.H. and C.W. Bullard, *Air-Side Thermal Performance of Micro-Channel Heat Exchangers Under Dehumidifying Conditions*, in *International Refrigeration and Air Conditioning Conference*. 2000. p. 119-126.
- [61] Kim, M.-H. and C.W. Bullard, *Air-side thermal hydraulic performance of multi-louvered fin aluminum heat exchangers*. *International Journal of Refrigeration*, 2002. **25**(3): p. 390-400.
- [62] Jacobi, M., et al., *High Performance Heat Exchangers for Air-Conditioning and Refrigeration Applications (Non-Circular Tubes)*: Air-Conditioning and Refrigeration Technology Institute. University of Illinois, Urbana, IL. ARTI-21CR/605-20021-01. 2005. p. 288.
- [63] Deng, J., *Improved correlations of the thermal-hydraulic performance of large size multi-louvered fin arrays for condensers of high power electronic component cooling by numerical simulation*. *Energy Conversion and Management*, 2017. **153**: p. 504-514.
- [64] Saleem, A. and M.-H. Kim, *Air-side thermal hydraulic performance of microchannel heat exchangers with different fin configurations*. *Applied Thermal Engineering*, 2017. **125**(Supplement C): p. 780-789.
- [65] Cowell, T.A., M.R. Heikal, and A. Achaichia, *Flow and heat transfer in compact louvered fin surfaces*. *Experimental Thermal and Fluid Science*, 1995. **10**(2): p. 192-199.
- [66] Xia, Y. and A.M. Jacobi, *A model for predicting the thermal-hydraulic performance of louvered-fin, flat-tube heat exchangers under frosting conditions*. *International Journal of Refrigeration*, 2010. **33**(2): p. 321-333.
- [67] Dong, J., et al., *Heat transfer and pressure drop correlations for the multi-louvered fin compact heat exchangers*. *Energy Conversion and Management*, 2007. **48**(5): p. 1506-1515.
- [68] Webb, R.L. and S.H. Jung, *Air-Side Performance of Enhanced Brazed Aluminum Heat Exchangers*. *ASHRAE Transactions*, 1992. **98**(2): p. 391-401.
- [69] Rugh, J.P., J.T. Pearson, and S. Ramadhyani, *A study of a very compact heat exchanger used for passenger compartment heating in automobiles*. *ASME HTD*, 1992. **201**: p. 15-24.
- [70] Tanaka, T., et al., *Improvement of Compact Heat Exchangers with Inclined Louvered Fins*. *Bulletin of JSME*, 1984. **27**(224): p. 219-226.
- [71] Dong, J., et al., *Experimental study on thermal-hydraulic performance of a wavy fin-and-flat tube aluminum heat exchanger*. *Applied Thermal Engineering*, 2013. **51**(1): p. 32-39.
- [72] Lotfi, B., et al., *3D numerical investigation of flow and heat transfer characteristics in smooth wavy fin-and-elliptical tube heat exchangers using new type vortex generators*. *Energy*, 2014. **73**: p. 233-257.
- [73] Zhang, J., J. Kundu, and R.M. Manglik, *Effect of fin waviness and spacing on the lateral vortex structure and laminar heat transfer in wavy-plate-fin cores*. *International Journal of Heat and Mass Transfer*, 2004. **47**(8): p. 1719-1730.
- [74] Junqi, D., et al., *Heat transfer and pressure drop correlations for the wavy fin and flat tube heat exchangers*. *Applied Thermal Engineering*, 2007. **27**(11): p. 2066-2073.
- [75] Ismail, L.S. and R. Velraj, *Studies on Fanning Friction (f) and Colburn (j) Factors of Offset and Wavy Fins Compact Plate Fin Heat Exchanger-A CFD Approach*. *Numerical Heat Transfer, Part A: Applications*, 2009. **56**(12): p. 987-1005.

- [76] Aliabadi, M.K., et al., *3D-CFD simulation and neural network model for the j and f factors of the wavy fin-and-flat tube heat exchangers*. Brazilian Journal of Chemical Engineering, 2011. **28**: p. 505-520.
- [77] Aliabadi, M.K., F. Hormozi, and H. Elham, *New correlations for wavy plate-fin heat exchangers: different working fluids*. International Journal of Numerical Methods for Heat & Fluid Flow, 2014. **24**(5): p. 1086-1108.
- [78] Duan, F., et al., *Numerical study of laminar flow and heat transfer characteristics in the fin side of the intermittent wavy finned flat tube heat exchanger*. Applied Thermal Engineering, 2016. **103**(Supplement C): p. 112-127.
- [79] Dasgupta, E.S., et al., *Air cooling by multiport slabs heat exchanger: An experimental approach*. Experimental Thermal and Fluid Science, 2012. **42**(Supplement C): p. 46-54.
- [80] Peng, H., X. Ling, and J. Li, *Performance investigation of an innovative offset strip fin arrays in compact heat exchangers*. Energy Conversion and Management, 2014. **80**: p. 287-297.
- [81] Norris, R.H. and W.A. Spofford, *High-performance fins for heat transfer*. Trans. ASME, 1942. **64**: p. 489-496.
- [82] Briggs, D.C. and A.L. London, *THE HEAT TRANSFER AND FLOW FRICTION CHARACTERISTICS OF FIVE OFFSET RECTANGULAR AND SIX PLAIN TRIANGULAR PLATE-FIN HEAT TRANSFER SURFACES*. Technical Report No. 49, ; Stanford Univ., Calif. 1960. p. Medium: X; Size: Pages: 76.
- [83] Joshi, H.M. and R.L. Webb, *Heat transfer and friction in the offset stripfin heat exchanger*. International Journal of Heat and Mass Transfer, 1987. **30**(1): p. 69-84.
- [84] Mochizuki, S., Y. Yagi, and W.-J. Yang, *TRANSPORT PHENOMENA IN STACKS OF INTERRUPTED PARALLEL-PLATE SURFACES*. Experimental Heat Transfer, 1987. **1**(2): p. 127-140.
- [85] Manglik, R.M. and A.E. Bergles, *Heat transfer and pressure drop correlations for the rectangular offset strip fin compact heat exchanger*. Experimental Thermal and Fluid Science, 1995. **10**(2): p. 171-180.
- [86] Dong, J., et al., *Air-side thermal hydraulic performance of offset strip fin aluminum heat exchangers*. Applied Thermal Engineering, 2007. **27**(2): p. 306-313.
- [87] Kim, M.-S., et al., *Correlations and optimization of a heat exchanger with offset-strip fins*. International Journal of Heat and Mass Transfer, 2011. **54**(9): p. 2073-2079.
- [88] Chennu, R. and P. Paturu, *Development of heat transfer coefficient and friction factor correlations for offset fins using CFD*. International Journal of Numerical Methods for Heat & Fluid Flow, 2011. **21**(8): p. 935-951.
- [89] Yang, Y. and Y. Li, *General prediction of the thermal hydraulic performance for plate-fin heat exchanger with offset strip fins*. International Journal of Heat and Mass Transfer, 2014. **78**: p. 860-870.
- [90] Peng, H. and X. Ling, *Neural networks analysis of thermal characteristics on plate-fin heat exchangers with limited experimental data*. Applied Thermal Engineering, 2009. **29**(11): p. 2251-2256.
- [91] Bhowmik, H. and K.-S. Lee, *Analysis of heat transfer and pressure drop characteristics in an offset strip fin heat exchanger*. International Communications in Heat and Mass Transfer, 2009. **36**(3): p. 259-263.
- [92] kuchhadiya, B.B. and P.P. Rathod, *Experimental Investigation of Thermal Behavior of Cross Flow Plate-fin Heat Exchanger with Offset Strip Fin*. Procedia Technology, 2016. **23**: p. 423-430.
- [93] Fernández-Seara, J. and R. Díz, *Thermo-hydraulic behavior of ice slurry in an offset strip-fin plate heat exchanger*. International Journal of Refrigeration, 2014. **41**: p. 171-180.
- [94] Saad, S.B., et al., *Experimental distribution of phases and pressure drop in a two-phase offset strip fin type compact heat exchanger*. International Journal of Multiphase Flow, 2011. **37**(6): p. 576-584.

- [95] Yujie, Y., et al., *Performance Evaluation of Heat Transfer Enhancement in Plate-fin Heat Exchangers with Offset Strip Fins*. Physics Procedia, 2015. **67**: p. 543-550.
- [96] Qian, S.W., *Heat Exchanger Design Handbook*. 2002: Chemical Industry Press, Beijing. p. 1122
- [97] Liu, X., J. Yu, and G. Yan, *A numerical study on the air-side heat transfer of perforated finned-tube heat exchangers with large fin pitches*. International Journal of Heat and Mass Transfer, 2016. **100**: p. 199-207.
- [98] Wang, C.C., W.L. Fu, and C.T. Chang, *Heat transfer and friction characteristics of typical wavy fin-and-tube heat exchangers*. Experimental Thermal and Fluid Science, 1997. **14**(2): p. 174-186.
- [99] Abu Madi, M., R.A. Johns, and M.R. Heikal, *Performance characteristics correlation for round tube and plate finned heat exchangers: Equations relatives aux performances d'échangeurs de chaleur constitués de tubes ronds et de plaques à ailettes*. International Journal of Refrigeration, 1998. **21**(7): p. 507-517.
- [100] Kim, G.J. and A.M. Jacobi, *Condensate Accumulation Effects on the Air-Side Thennal Perfonnance of Slit-Fin Surfaces*: University of Illinois at Urbana-Champaign, IL. 2000. p. 123.
- [101] Wang, C.-C., W.-H. Tao, and C.-J. Chang, *An investigation of the airside performance of the slit fin-and-tube heat exchangers*. International Journal of Refrigeration, 1999. **22**(8): p. 595-603.
- [102] Kim, N.H., B. Youn, and R.L. Webb, *Air-Side Heat Transfer and Friction Correlations for Plain Fin-and-Tube Heat Exchangers With Staggered Tube Arrangements*. Journal of Heat Transfer, 1999. **121**(3): p. 662-667.
- [103] Wang, C.-C., K.-Y. Chi, and C.-J. Chang, *Heat transfer and friction characteristics of plain fin-and-tube heat exchangers, part II: Correlation*. International Journal of Heat and Mass Transfer, 2000. **43**(15): p. 2693-2700.
- [104] Xie, G., Q. Wang, and B. Sundén, *Parametric study and multiple correlations on air-side heat transfer and friction characteristics of fin-and-tube heat exchangers with large number of large-diameter tube rows*. Applied Thermal Engineering, 2009. **29**(1): p. 1-16.
- [105] Wang, C.C., et al., *Heat transfer and friction correlation for compact louvered fin-and-tube heat exchangers*. International Journal of Heat and Mass Transfer, 1999. **42**(11): p. 1945-1956.
- [106] Tang, L.H., M. Zeng, and Q.W. Wang, *Experimental and numerical investigation on air-side performance of fin-and-tube heat exchangers with various fin patterns*. Experimental Thermal and Fluid Science, 2009. **33**(5): p. 818-827.
- [107] Jin, Y., et al., *Parametric study and field synergy principle analysis of H-type finned tube bank with 10 rows*. International Journal of Heat and Mass Transfer, 2013. **60**(Supplement C): p. 241-251.
- [108] Kiatpachai, P., S. Pikulkajorn, and S. Wongwises, *Air-side performance of serrated welded spiral fin-and-tube heat exchangers*. International Journal of Heat and Mass Transfer, 2015. **89**(Supplement C): p. 724-732.
- [109] Pongsoi, P., et al., *Effect of fin pitches on the air-side performance of L-footed spiral fin-and-tube heat exchangers*. International Journal of Heat and Mass Transfer, 2013. **59**(Supplement C): p. 75-82.
- [110] Pongsoi, P., et al., *Effect of number of tube rows on the air-side performance of crimped spiral fin-and-tube heat exchanger with a multipass parallel and counter cross-flow configuration*. International Journal of Heat and Mass Transfer, 2012. **55**(4): p. 1403-1411.
- [111] Wang, C.-c., Y.-c. Hsieh, and Y.-t. Lin, *Performance of Plate Finned Tube Heat Exchangers Under Dehumidifying Conditions*. Journal of Heat Transfer, 1997. **119**(1): p. 109-117.
- [112] Wang, C.-C., et al., *Airside performance of herringbone fin-and-tube heat exchangers in wet conditions*. The Canadian Journal of Chemical Engineering, 1999. **77**(6): p. 1225-1230.
- [113] Kong, Y.Q., et al., *Air-side flow and heat transfer characteristics of flat and slotted finned tube bundles with various tube pitches*. International Journal of Heat and Mass Transfer, 2016. **99**: p. 357-371.
- [114] Kong, Y.Q., et al., *Effects of continuous and alternant rectangular slots on thermo-flow performances of plain finned tube bundles in in-line and staggered configurations*. International Journal of Heat and Mass Transfer, 2016. **93**: p. 97-107.

- [115] Wang, C.-C., Y.-T. Lin, and C.-J. Lee, *Heat and momentum transfer for compact louvered fin-and-tube heat exchangers in wet conditions*. International Journal of Heat and Mass Transfer, 2000. **43**(18): p. 3443-3452.
- [116] Kim, Y. and Y. Kim, *Heat transfer characteristics of flat plate finned-tube heat exchangers with large fin pitch*. International Journal of Refrigeration, 2005. **28**(6): p. 851-858.
- [117] Bhuiyan, A.A. and A.K.M.S. Islam, *Thermal and hydraulic performance of finned-tube heat exchangers under different flow ranges: A review on modeling and experiment*. International Journal of Heat and Mass Transfer, 2016. **101**(Supplement C): p. 38-59.
- [118] Tahseen, T.A., M. Ishak, and M.M. Rahman, *An overview on thermal and fluid flow characteristics in a plain plate finned and un-finned tube banks heat exchanger*. Renewable and Sustainable Energy Reviews, 2015. **43**(Supplement C): p. 363-380.
- [119] Seshimo, Y. and M. Fujii. *An experimental study on the performance of plate fin and tube heat exchangers at low Reynolds numbers*. 1991. United States: American Society of Mechanical Engineers. p. 449-454.
- [120] Wang, C.C., J.Y. Chang, and N.F. Chiou, *Effects of waffle height on the air-side performance of wavy fin-and-tube heat exchangers*. Heat Transfer Engineering, 1999. **20**(3): p. 45-56.
- [121] Wang, C.-C., et al., *Sensible heat and friction characteristics of plate fin-and-tube heat exchangers having plane fins*. International Journal of Refrigeration, 1996. **19**(4): p. 223-230.
- [122] Wang, C.-C., et al., *Some Aspects of Plate Fin-and-Tube Heat Exchangers: With and Without Louvers*. 1999. **6**(5): p. 357-368.
- [123] Wang, C.-C., Y.-T. Lin, and C.-J. Lee, *An airside correlation for plain fin-and-tube heat exchangers in wet conditions*. International Journal of Heat and Mass Transfer, 2000. **43**(10): p. 1869-1872.
- [124] Shah, R.K. and D.P. Sekulić, *Surface Basic Heat Transfer and Flow Friction Characteristics*, in *Fundamentals of Heat Exchanger Design*. 2007, John Wiley & Sons, Inc. p. 425-562.
- [125] Yang, D., et al., *Numerical and experimental analysis of cooling performance of single-phase array microchannel heat sinks with different pin-fin configurations*. Applied Thermal Engineering, 2017. **112**: p. 1547-1556.
- [126] Huang, L., Q. Li, and H. Zhai, *Experimental study of heat transfer performance of a tube with different shaped pin fins*. Applied Thermal Engineering, 2018. **129**: p. 1325-1332.
- [127] Jonsson, H. and B. Moshfegh, *Modeling of the thermal and hydraulic performance of plate fin, strip fin, and pin fin heat sinks-influence of flow bypass*. IEEE Transactions on Components and Packaging Technologies, 2001. **24**(2): p. 142-149.
- [128] Sahiti, N., *Thermal and Fluid Dynamic Performance of Pin Fin Heat Transfer Surfaces* University of Erlangen-Nuremberg: Erlangen, Germany. 2006. p. 173.
- [129] Diani, A., et al., *Experimental and numerical analyses of different extended surfaces*. Journal of Physics: Conference Series, 2012. **395**(1): p. 012045.
- [130] Diani, A., et al., *An assessment on air forced convection on extended surfaces: Experimental results and numerical modeling*. International Journal of Thermal Sciences, 2013. **67**: p. 120-134.
- [131] Arie, M.A., et al., *Air-Side Heat Transfer Enhancement Utilizing Design Optimization and an Additive Manufacturing Technique*. Journal of Heat Transfer, 2016. **139**(3): p. 031901-031901-12.
- [132] Ohadi, M.M., et al., *Next Generation Micro Channel Heat Exchangers*. 2013: Springer Publishing Co. p. 124.
- [133] Han, X.-H., et al., *A Review of Metal Foam and Metal Matrix Composites for Heat Exchangers and Heat Sinks*. Heat Transfer Engineering, 2012. **33**(12): p. 991-1009.
- [134] Dai, Z., et al., *A Comparison of Metal-Foam Heat Exchangers to Compact Multilouver Designs for Air-Side Heat Transfer Applications*. Heat Transfer Engineering, 2012. **33**(1): p. 21-30.

- [135] Ribeiro, G.B., J.R. Barbosa, and A.T. Prata, *Performance of microchannel condensers with metal foams on the air-side: Application in small-scale refrigeration systems*. Applied Thermal Engineering, 2012. **36**(Supplement C): p. 152-160.
- [136] Kwon, B., et al., *High power density air-cooled microchannel heat exchanger*. International Journal of Heat and Mass Transfer, 2018. **118**(Supplement C): p. 1276-1283.
- [137] Calmidi, V.V. and R.L. Mahajan, *Forced Convection in High Porosity Metal Foams*. Journal of Heat Transfer, 2000. **122**(3): p. 557-565.
- [138] Kashyap, P. and p. jhavar, *Enhancement of Heat Exchanger Performance by the Extended Surfaces-Fins*. International Journal of Engineering Trends and Technology, 2016. **34** (6): p. 260-265.
- [139] VYAS, A. and A.B. Agrawal, *Offset-Strip Fin Heat Exchangers A Conceptual Review Study*. International Journal of Engineering Research and applications, 3 (1), 2013: p. 1306-1312.
- [140] Chen, H., et al., *Experimental Investigation of Heat Transfer and Pressure Drop Characteristics of H-type Finned Tube Banks*. Energies, 2014. **7**(11): p. 7094.
- [141] Ohadi, M., et al., *Emerging Applications of Microchannels*, in *Next Generation Microchannel Heat Exchangers*, M. Ohadi, et al., Editors. 2013, Springer New York: New York, NY. p. 67-105.
- [142] Poh, S.T. and E.Y.K. Ng. *Heat transfer and flow issues in manifold microchannel heat sinks: a CFD approach*. in *Proceedings of 2nd Electronics Packaging Technology Conference (Cat. No.98EX235)*. 1998. p. 246-250.
- [143] Ruiz, M. and V.P. Carey, *Experimental Study of Single Phase Heat Transfer and Pressure Loss in a Spiraling Radial Inflow Microchannel Heat Sink*. Journal of Heat Transfer, 2015. **137**(7): p. 071702-071702-8.
- [144] Shah, R.K. and D.P. Sekulić, *Selection of Heat Exchangers and Their Components*, in *Fundamentals of Heat Exchanger Design*. 2007, John Wiley & Sons, Inc. p. 673-734.
- [145] Webb, R.L. and N.-H. Kim, *Principles of enhanced heat transfer*. 2nd ed ed. 2005: Taylor & Francis. p. 795.
- [146] *EES: Engineering Equation Solver / F-Chart Software : Engineering Software*. 2018; Available from: <http://www.fchart.com/ees/>.